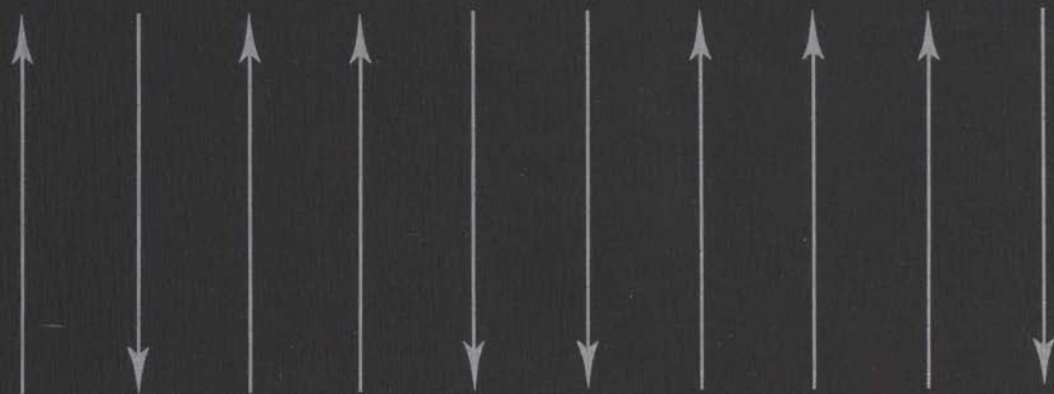


An experimental study on the behaviour of
magnetic moments
in
concentrated and diluted compounds
at very low temperatures



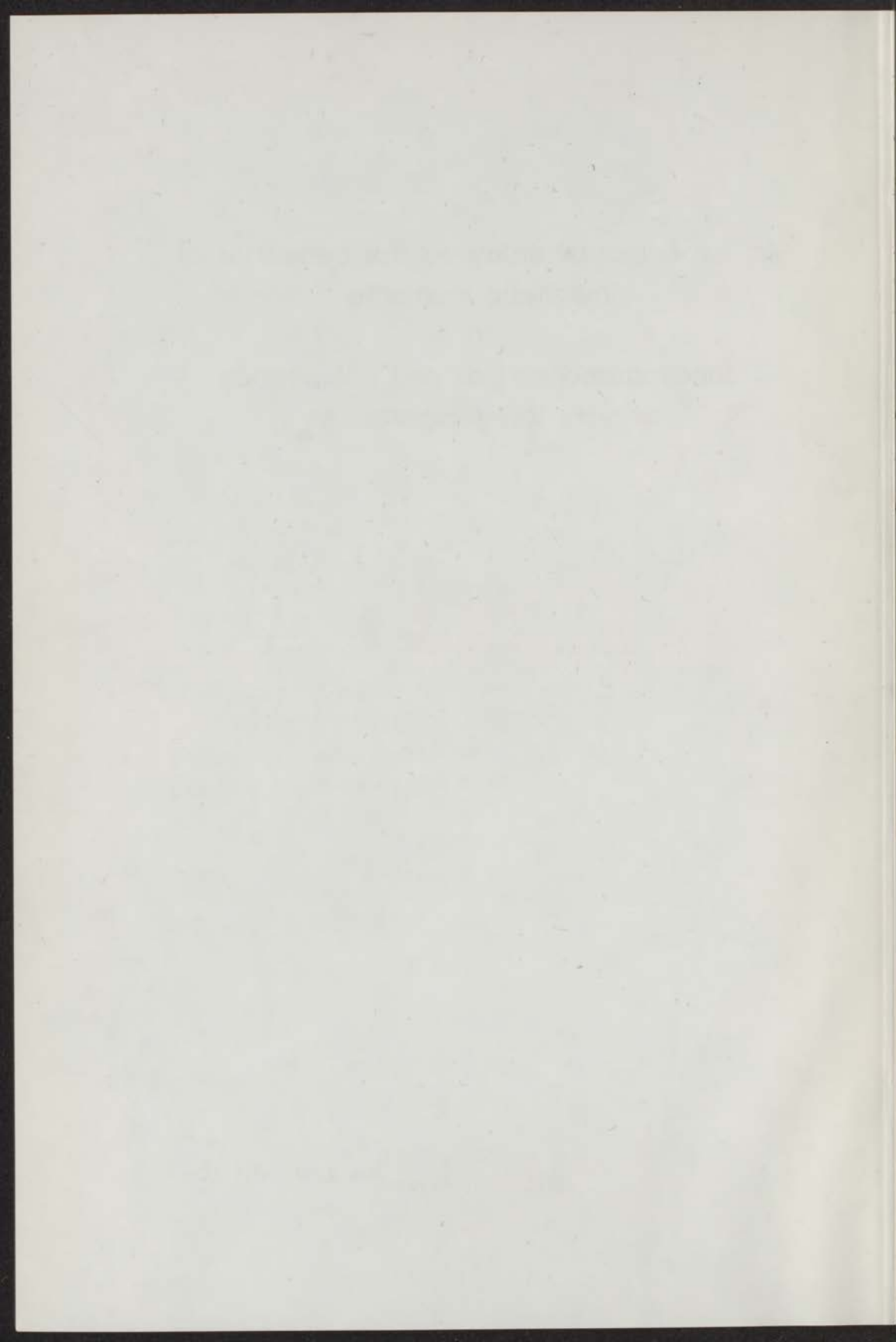
E. Lagendijk

12 APR 1972

An experimental study on the behaviour of
magnetic moments
in
concentrated and diluted compounds
at very low temperatures

INSTITUUT-LORENTZ
voor theoretische natuurkunde
Huisvesting 18-Loeben-Nederland

kast dissertaties



An experimental study on the behaviour of
magnetic moments
in
concentrated and diluted compounds
at very low temperatures

PROEFSCHRIFT

TER VERKRIJGING VAN DE GRAAD VAN DOCTOR
IN DE WISKUNDE EN NATUURWETENSCHAPPEN AAN
DE RIJKSUNIVERSITEIT TE LEIDEN, OP GEZAG VAN
DE RECTOR MAGNIFICUS DR. W.R.O. GOSLINGS, HOOG-
LERAAR IN DE FACULTEIT DER GENEESKUNDE,
VOLGENS BESLUIT VAN HET COLLEGE VAN DEKANEN
TE VERDEDIGEN OP WOENSDAG 26 APRIL 1972 TE
KLOKKE 15.15 UUR

DOOR

ERIK LAGENDIJK

GEBOREN TE AMSTERDAM IN 1942

DRUK: cv elve/labor vincit

An experimental study on the behaviour of
magnetic moments
in
concentrated and diluted compounds
at very low temperatures

PROMOTOR: PROF. DR. W.J. HUISKAMP

PROF. DR. W.J. HUISKAMP
TER VERKRIJGING VAN DE GRAAD VAN DOCTOR
IN DE WISKUNDE EN NATUURWETENSCHAPPEN AAN
DE RIJSCHE UNIVERSITEIT TE LEIDEN OP GEZAG VAN
DE RECTOR-MAGISTRUS DR. W. G. G. O. DE VRIES
LEZEND IN DE FACULTEIT DER WETENSCHAPPEN
NOLLENSRECHT VAN HET COLLEGE VAN DEKANS
TE VERVOLGEN OP WOENSDAG 25 APRIL 1953 TE
ELF OER 15.15 UUR

DOOR

ERIC J. VAN DER WOUDE

DE WETENSCAPPELIJK OORDEEL

The author is a member of the scientific staff of the 'Stichting voor Fundamenteel Onderzoek der Materie (F.O.M.)', financially supported by the 'Organisatie voor Zuiver Wetenschappelijk Onderzoek (Z.W.O.)'.

STELLINGEN

behorende bij het proefschrift van E. LAGENDIJK

- II
Met zijn studie over de voorlopige veranderingen in de viscositeit van $\text{CaCl}_2 \cdot 6\text{H}_2\text{O}$ en $\text{CaCl}_2 \cdot 4\text{H}_2\text{O}$ heeft de auteur een belangrijke bijdrage geleverd aan de kennis van de viscositeit van kristallijne zouten.
- III
De studie van McCoy en Wu over de viscositeit van oplossingen van CaCl_2 in water heeft belangrijke inzichten gegeven in de viscositeit van oplossingen van zouten in water.
- IV
De studie van McCoy, B.M. en Wu, T.T., *Phys. Rev. Letters* 27 (1951) 519, over de viscositeit van oplossingen van CaCl_2 in water heeft belangrijke inzichten gegeven in de viscositeit van oplossingen van zouten in water.
- V
In veel gevallen kan de Koppes-waarde bij temperatuur van vloeibare helium worden beschouwd als de warmtegeleidingscoëfficiënt van een amorfe stof.
- Chen, J.D.N., *J. Phys. (Paris)* 37 (1970) C3-128.
Zellin, R.G. en Pohl, R.O., *Phys. Rev. B* 4 (1971) 2029.
- VI
De studie van Pohl, R.O., Collins, H.K., Erickson, G.L. en Ginzburg, V.V., *J. Low Temp. Phys.* 6 (1972) 351, over de viscositeit van oplossingen van CaCl_2 in water heeft belangrijke inzichten gegeven in de viscositeit van oplossingen van zouten in water.
- VII
De studie van Pohl, R.O., Collins, H.K., Erickson, G.L. en Ginzburg, V.V., *J. Low Temp. Phys.* 6 (1972) 351, over de viscositeit van oplossingen van CaCl_2 in water heeft belangrijke inzichten gegeven in de viscositeit van oplossingen van zouten in water.
- VIII
De studie van Pohl, R.O., Collins, H.K., Erickson, G.L. en Ginzburg, V.V., *J. Low Temp. Phys.* 6 (1972) 351, over de viscositeit van oplossingen van CaCl_2 in water heeft belangrijke inzichten gegeven in de viscositeit van oplossingen van zouten in water.
- IX
De studie van Pohl, R.O., Collins, H.K., Erickson, G.L. en Ginzburg, V.V., *J. Low Temp. Phys.* 6 (1972) 351, over de viscositeit van oplossingen van CaCl_2 in water heeft belangrijke inzichten gegeven in de viscositeit van oplossingen van zouten in water.

I

Het verdient aanbeveling na te gaan in hoeverre de waargenomen oriëntatie van kernen van tweewaardige $3d$ overgangsmetalen in cerium magnesium nitraat (CMN) kan worden verklaard door te veronderstellen dat CMN beneden het overgangspunt *ferromagnetisch* geordend is.

Daniels, J.M. en Felsteiner, J., *Can. J. Phys.* **42** (1964) 1469.

Dit proefschrift, hoofdstuk I.

II

Metingen van de soortelijke warmte van ellipsoidaal gevormde éénkristallen van $DyCl_3 \cdot 6H_2O$ en $ErCl_3 \cdot 6H_2O$ in een uitwendig magnetisch veld kunnen belangrijke informatie geven over het magnetisch gedrag, in het bijzonder over de spontane magnetisatie.

Griffiths, R.B., *J. Appl. Phys.* **40** (1969) 1542.

Dit proefschrift, hoofdstuk II.

III

De suggestie van McCoy en Wu dat lukraak ingevroren onzuiverheden de oorzaak zijn van de waargenomen afrondingsverschijnselen bij magnetische faseovergangen, is in zijn algemeenheid onjuist.

McCoy, B.M. en Wu, T.T., *Phys. Rev. Letters* **21** (1968) 549.

Dit proefschrift, hoofdstuk III.

IV

Het gebruik van ^{54}Mn in goud als kernoriëntatie-thermometer bij zeer lage temperaturen verdient aanbeveling boven het gebruik van ^{54}Mn in koper of in ferromagnetische metalen.

Pratt, W.P., Schermer, R.I. en Steyert, W.A., *J. Low Temp. Phys.* **1** (1969) 469.

Berglund, P.M., Collan, H.K., Ehnholm, G.J., Gylling, R.G. en Lounasmaa, O.V., *J. Low Temp. Phys.* **6** (1972) 357.

Dit proefschrift, hoofdstuk IV.

V

In veel gevallen kan de Kapitza-weerstand bij temperaturen van vloeibaar helium worden beschouwd als de warmteweerstand van een amorfe laag.

Cheeke, J.D.N., *J. Phys. (Paris)* **31** (1970) c3-129.

Zeller, R.C. en Pohl, R.O., *Phys. Rev. B* **4** (1971) 2029.

VI

De conclusies van Begemann over de positie waar Cu zich bij voorkeur vastzet bij opdampen op een NaCl oppervlak, zijn zeer aanvechtbaar.

Begemann, S.H.A., proefschrift, Groningen (1972).

VII

Het gebruik van de begrippen 'samengestelde kern' en 'vangsttoestand' bij de beschrijving van (n, γ) reacties heeft er toe bijgedragen dat interferentieverschijnselen tot voor kort werden genegeerd.

Mellema, J., proefschrift, Groningen (1970).

VIII

De interpretatie van de waargenomen anisotropie van de α -emissie van uranium-verbindingen wordt bemoeilijkt doordat de quadrupool-koppelingsconstante P niet voldoende nauwkeurig bekend is. Magnetisatie-metingen met een SQUID magnetometer kunnen hier uitkomst brengen, in het bijzonder wat betreft het teken van P .

Kuiken, R., proefschrift, Leiden (1971).

Giffard, R.P., Webb, R.A. en Wheatley, J.C., *J. Low Temp. Phys.* 6 (1972) 533.

IX

Voor de meeste natuurkundige laboratoria verdient het gebruik van één of meer (kleine) computersystemen ter plaatse de voorkeur boven het uitsluitend gebruik maken van een grote computerinstallatie op afstand. Het inschakelen van terminals biedt in dit verband geen afdoende oplossing.

X

De didactische en pedagogische waarde van de huidige televisieprogramma's bestemd voor jonge kinderen is in het algemeen niet groot. Aan deze waarde wordt verder ernstig afbreuk gedaan doordat in een vreemde taal gesproken programma's als regel niet worden nagesynchroniseerd.

In the beginning there was an exponent and the exponent was fixed.

M.E. Fisher

E. Lagendijk, thesis, Leiden (1972)

List of errors, 10-4-1977

Note: references to sections are by number only, e.g. p. 41 line 1 from below

- 11A.6¹ should read "section 6.4.6"
- 16 formula 1.2.1: \dots should read \dots
- 17 formula 1.2.2: \dots should read \dots
- 20 line 14 from above: "the spin sites of a Bravais lattice" should read "the spin sites into the sites of a Bravais lattice"
line 8 from below: "the spheres surrounding" should read "the larger spheres surrounded by"
- 23 table 1.4, row 1, column 2: "W" should read "W"
row 1, column 4: "y" should read "dy"
table 1.5, row 10, column 4: "0.259" should read "0.259"
row 8, column 8: "0.42" should read "0.40"
- 27 caption of fig. 1.2: "0.0131" should read "0.0121"
- 30 table 1.7, row 2, column 6: "-0.0017" should read "0.0017"
row 6, column 7: "0.248" should read "0.0348"
- 33 ref. 1: "9810" should be inserted
- 37 line 1 from below: "P₁₂" should read "P₂₁₂"
- 42 table 11.2: \dots should be omitted at $T=$
- 44 table 11.4, row 4, column 1: " \dots " should read " \dots "
column 5: numbers headed "spolar" should be shifted one row upwards
line 25.7 from below: " \dots " should be inserted before "long"
see labelled "x" and "y" should be omitted
- 47 fig. 11.6: dots in H_1 should be omitted.
- 51 line 6 from below: "fig. 11.2" should read "fig. 11.7"
- 55 ref. 20: "Transition" should read "or Transition here"
ref. 7: "10" should read "10, 8"
- 74 line 15 from above: "D₁₂" should read "D₁₂"
- 81 ref. 20: "125" should read "125"
- 85 line 21 from above: "matrix density" should read "density matrix"
- 110 table A.1: the formula for δ should read as in line 16 from below

Aan mijn ouders

Aan Minca

CONTENTS

SAMENVATTING		8
GENERAL INTRODUCTION		11
CHAPTER I	Caloric and magnetic study of five rare-earth ionic compounds having predominantly magnetic dipole-dipole interaction	
1.1	Introduction	15
1.2	The Van Vleck moment method	16
1.3	The Luttinger and Tisza method	19
1.4	Calculations	20
1.5	Comparison with existing calculations and experimental data	25
1.5-1	CMN	25
1.5-2	DyES	26
1.5-3	ErES	28
1.5-4	DyCl ₃ ·6H ₂ O, ErCl ₃ ·6H ₂ O	29
1.6	Conclusions	32
	References	33
CHAPTER II	Caloric and magnetic properties of two compounds having predominantly magnetic dipole-dipole interactions: DyCl₃·6H₂O and ErCl₃·6H₂O	
II.1	Introduction	34
II.2	Experimental	36
II.3	Crystallographic and magnetic data, sample preparation	37
II.4	Specific heat in zero applied field	41
II.4-1	General behaviour, energy and entropy	41
II.4-2	Energy, compared to calculations	44
II.4-3	Dipolar fields	46
II.4-4	Critical behaviour	48
II.4-5	Analysis of specific-heat curve near T_c	49
II.4-6	DyCl ₃ ·6H ₂ O	49
II.4-7	ErCl ₃ ·6H ₂ O	52
II.4-8	Low-temperature behaviour	53
II.5	Specific heat in an applied field	54
II.6	Specific heat of Y-diluted samples	56
II.7	Susceptibility	57
II.8	Magnetothermal effect	60
II.9	Discussion of the critical behaviour	61
II.10	Conclusions	64
	References	65

CHAPTER III	Calorimetric study of a random Ising spin system: $\text{Co}_p\text{Zn}_{1-p}\text{Cs}_3\text{Cl}_5$	
III.1	Introduction	67
III.2	Preparation	69
III.3	Experimental	69
III.4	Specific heat	70
III.4-1	General behaviour, theory	70
III.4-2	General behaviour, experiment	71
III.4-3	Critical behaviour, theory	75
III.4-4	Critical behaviour, experiment	76
III.5	Susceptibility	78
III.6	Conclusions	80
	References	81
CHAPTER IV	Nuclear orientation study on the behaviour of 3d transition metal elements dissolved in a non-magnetic metal (the Kondo problem)	
IV.1	Introduction	83
IV.2	Hyperfine interaction	85
IV.3	Nuclear orientation, slow and fast relaxation	86
IV.4	The relaxation problem	91
IV.5	Experimental	92
IV.6	Preparation of the samples	93
IV.7	AuMn	94
IV.8	AuCr	96
IV.9	ZnMn	97
IV.10	AuCo	99
IV.11	Concluding remarks	99
	References	101
APPENDIX	Carbon resistance thermometry below 1 K	
A.1	Introduction	103
A.2	Calibration	104
A.3	Numerical procedures	107
A.4	Low parameter fit	108
A.5	Multi parameter fit	110
A.6	Reproducibility	112
A.7	Use of the carbon resistor	113
A.8	Conclusions	113
	References	115
VERANTWOORDING		117
CURRICULUM VITAE		118

SAMENVATTING

In dit proefschrift worden onderzoeken beschreven, verricht met behulp van calorimetrische en kernoriëntatie technieken aan een aantal verbindingen die qua samenstelling sterk variëren. De overeenkomst is gelegen in het optreden van coöperatieve verschijnselen ten gevolge van magnetische wisselwerkingen bij temperaturen beneden 1 Kelvin. Deze temperaturen zijn bereikt door toepassing van de methode van de adiabatische demagnetisatie. Hierbij werd de 'grote' magneet van het Kamerlingh Onnes Laboratorium gebruikt. Na een 40-jarige periode van intensief gebruik is deze magneet nu in het bezit gekomen van het Rijksmuseum voor de Geschiedenis der Natuurwetenschappen te Leiden.

In hoofdstuk I wordt een aantal ionische verbindingen besproken waarvan mag worden aangenomen dat de voornaamste wisselwerking tussen de magnetische momenten, afkomstig van ionen van de $4f$ groep (de zeldzame aardmetalen), van dipolaire aard is. Aan de hand van een groot aantal berekeningen volgens de methoden van Van Vleck en Luttinger en Tisza wordt aangetoond dat calorische experimenten deze aanname bevestigen.

In het tweede hoofdstuk wordt op een tweetal van deze verbindingen, $DyCl_3 \cdot 6H_2O$ en $ErCl_3 \cdot 6H_2O$, nader ingegaan. Uit de metingen volgt dat deze verbindingen ferromagnetisch ordenen, respectievelijk bij 0.289 K en 0.356 K. Het gedrag van de soortelijke warmte dicht bij het overgangspunt (het kritisch gedrag) is nauwkeurig onderzocht en vertoont frappante verschillen tussen de twee verbindingen. De soortelijke warmte van de Dy verbinding divergeert sterk in het beschouwde temperatuur gebied. De metingen suggereren een hoge waarde van de kritische exponent, $a_{\pm} \approx 0.5$. De soortelijke warmte van de Er verbinding lijkt eindig te blijven, maar de afgeleide naar de temperatuur divergeert bij het overgangspunt ('cusp', $a_{\pm} = 0$). Een vergelijking met de theorie kan niet worden gemaakt zolang niet meer berekeningen bekend zijn betreffende het kritisch gedrag in dipolaire roosters. De lange dracht en de ingewikkelde hoekafhankelijkheid van de wisselwerking zijn hierbij ernstige complicaties.

Het derde hoofdstuk behandelt calorische en magnetische metingen aan een magnetisch systeem met voornamelijk plaatsruil (exchange) wisselwerking: $CoCs_3Cl_5$. Een deel van de Co ionen is *lukraak* (random) vervangen door diamagnetische Zn ionen. Zoals verwacht daalt daardoor de overgangstemperatuur. Het gedrag van het overgangspunt als functie van de concentratie bevestigt de veronderstelling dat de magnetische wisselwerking in $CoCs_3Cl_5$ sterk anisotroop is wat betreft het aantal spincomponenten dat bij de wisselwerking is betrokken, maar isotroop in drie dimensies wat betreft de sterkte van de wisselwerking,

afgezien van het teken. Door extrapolatie van de curve die het gemeten verband tussen de overgangstemperatuur en de concentratie van de magnetische ionen weergeeft, volgt een kritische concentratie die in redelijke overeenstemming is met de voorspelde waarde voor een drie dimensionaal Ising systeem met alleen naaste burens wisselwerking.

Bestudering van het kritisch gedrag toont aan dat de substitutie van Zn nauwelijks invloed heeft op de afronding van de soortelijke warmte piek. Dit staat in tegenstelling tot eerder gedane suggesties dat onzuiverheden de oorzaak zijn van de veelvuldig waargenomen afrondingsverschijnselen in soortelijke warmte metingen dicht bij het overgangspunt van magnetische kristallen. De suggestie dat het lukraak verbreken van magnetische koppelingen in het rooster overeenkomt met het effectief verlagen van de ruimtelijke dimensie van de ordening, wordt door onze metingen niet bevestigd.

De oriëntatie van radioactieve kernen van chroom, mangaan en cobalt in goud en van mangaan in zink in zeer lage concentraties (≤ 1 ppm) wordt beschouwd in hoofdstuk IV. Men neemt aan dat in zeer verdunde legeringen niet de interacties tussen de magnetische momenten onderling de oorzaak zijn van de waargenomen anomalieën, maar de interacties tussen de magnetische momenten en de geleidingselektronen van het niet-magnetische gastheer metaal. Benaderende berekeningen tonen aan dat vele van de waargenomen verschijnselen zoals een minimum in de elektrische weerstand bij lage temperaturen en een Curie-Weiss gedrag van de susceptibiliteit bij hoge temperaturen kunnen worden verklaard indien men veronderstelt dat het magnetisch moment van het overgangsmetaal (als onzuiverheid aanwezig) lokaal en statisch van aard is. Aangenomen wordt dat tussen dit lokale moment en de geleidingselektron dichtheid ter plaatse van de onzuiverheid een isotrope exchange wisselwerking bestaat (s-d exchange model). Indien de exchange koppeling het antiferromagnetische teken heeft, kan anomaal gedrag worden verwacht bij lage temperaturen. Dit is voor het eerst door J. Kondo aangetoond.

De kernspinoriëntatie methode bepaalt de mate van gerichtheid van radioactieve atoomkernen door de anisotropie in de intensiteitsverdeling van de uitgezonden gammastraling te meten. Een waarneembaar effect wordt bereikt door een combinatie van een lage temperatuur (< 0.1 K) en een groot magneetveld (> 100 kOe). In de door ons onderzochte systemen wordt gebruik gemaakt van de wisselwerking tussen de momenten van de elektronen en het moment van de kern (hyperfijn wisselwerking) om velden van voldoende sterkte te verkrijgen. De gemeten anisotropie kan dus informatie verschaffen omtrent de elektron toestand in de omgeving van de kern. Zolang de hyperfijn wisselwerking relatief zwak is kunnen op deze wijze gegevens worden verkregen over effecten van elektron-elektron wisselwerkingen, zoals de s-d exchange interactie. Kernspinoriëntatie metingen hebben het voordeel boven calorische metingen dat met zeer lage concentraties van magnetische atomen kan worden volstaan.

De metingen tonen aan dat Mn in Au zich tot zeer lage temperaturen paramagnetisch gedraagt met een spinwaarde die gelijk is aan die van het vrije ion, waarbij men aanneemt dat de elektronspin relaxatietijden lang zijn vergeleken met de kernspin precessietijd. De metingen suggereren een soortgelijk resultaat voor Cr in Au. De kernoriëntatie van ^{54}Mn in Zn

kan niet met een vrije elektronspin worden beschreven, ook niet indien men snelle elektronspin relaxatie veronderstelt. Dit wordt geweten aan de effecten van de s-d interactie. Voor ^{60}Co in Au hebben wij in ons temperatuur- en veldgebied geen kernspinoriëntatie effecten waargenomen, hetgeen waarschijnlijk wordt veroorzaakt door een overgang naar niet-magnetisch gedrag bij hoge temperaturen. Het is niet duidelijk of het s-d exchange model op deze legering van toepassing is.

In een appendix wordt het gebruik van koolweerstanden als thermometers bij zeer lage temperaturen beschreven. Bijzondere nadruk is gelegd op het aanpassen van reeksen aan het gemeten weerstands-temperatuur verband met kleinste kwadraten methoden. Het weergeven van de weerstandsvariatie als functie van de temperatuur door een analytische uitdrukking maakt nauwkeurige interpolatie tussen de gemeten punten mogelijk. Dergelijke interpolaties zijn noodzakelijk indien calorische metingen met een hoog temperatuur oplossend vermogen worden verricht.

GENERAL INTRODUCTION

Interactions among magnetic moments can be studied by a variety of experimental methods. In particular, measurements on bulk properties such as the specific heat and the susceptibility provide an important source of information. The interpretation of such measurements is facilitated if only the magnetic interactions of interest appreciably contribute to the measured quantity. In this respect, low temperatures are often quite advantageous. In the present thesis we describe caloric and magnetic experiments at very low temperatures on a number of ionic compounds. A microscopic technique, nuclear orientation, has been applied to study the interactions in some very dilute alloys.

Pair interactions among localized magnetic moments may give rise to phase transitions from an unordered, paramagnetic state to states in which the magnetic moments are ordered, *e.g.* ferromagnetically or antiferromagnetically. At the phase transition temperature, large anomalies occur in various physical quantities, for instance the specific heat, and these so called critical phenomena have received a great deal of interest, both from experimental and from theoretical side. Most calculations start from a specific assumption on the pair interaction among magnetic moments μ_j , which are located in a periodic lattice structure. In many cases, the interaction is written in terms of the associated spins S_j , which are coupled to the magnetic moments via the \mathbf{g} tensor, *viz.* $\mu_j = \mu_B \mathbf{g} \cdot S_j$, where μ_B is the Bohr magneton. Here we use the word 'spin' rather loosely to indicate any angular momentum operator. If S_j represents a true spin, the \mathbf{g} tensor is isotropic and the corresponding g value is $g_j=2$.

It is found that calculations on phase transitions are much easier to perform if it is assumed that only one spatial component of the spin interacts. The number of interacting spin components will be designated as the spin dimensionality. If the spin dimensionality is less than three, the interaction is called anisotropic. However, within a given spin dimensionality, the interaction is called anisotropic if the strength depends on the direction of the pair bond with respect to the crystal axes. Interactions with spin dimensionality one are designated as Ising interactions:

$$\mathcal{H}_{ij}^I = J_{ij} S_i^z S_j^z \quad (\text{I.1})$$

This hamiltonian has been studied extensively on lattices of various lattice dimensionalities and symmetries¹). The eigenvalue problem being trivial, only the statistical problem of the calculation of the partition function remains. This problem can be further simplified by the assumption of short-ranged interactions. From the calculations on the Ising problem,

Onsager's exact solution of the two-dimensional Ising model with nearest neighbour interactions is the highlight²). The Onsager solution clearly shows that approximate closed-form calculations generally fail to make quantitatively correct predictions on the critical behaviour.

For a long time it was believed that a model like eq. (I.1), exhibiting extreme anisotropy, is physically unrealistic and that interactions among spins are isotropic. The pair interaction would then be given by:

$$\mathcal{H}_{ij}^C = J_{ij} S_i \cdot S_j \quad (I.2)$$

This hamiltonian has been derived by Heisenberg for a pair of *s*-electrons with overlapping wavefunctions. The coupling constant depends on the overlap, and is called the exchange integral. Since wavefunctions of electrons which are localized on ions rapidly diminish with increasing radial distance from the nucleus, (direct) exchange interactions are usually confined to near neighbours. The same applies to the exchange interactions which are transferred by the surrounding diamagnetic ligands (superexchange). If the magnetic moment is due to spin only, eq. (I.2) is expected to be a reasonable approximation. However, in the case of the 4*f* transition elements (the rare earths), and also in the case of Co, which belongs to the 3*d* transition elements, the orbital moment is not completely quenched, which can lead to anisotropy of the *g* tensor, and hence to reduction of the spin dimensionality. The orbital moment contribution may give rise to other non-classical interactions among magnetic moments. These have been reviewed recently by Baker³).

An interaction which is often neglected in studies on systems containing magnetic moments is the inevitable magnetic dipole-dipole interaction, *viz.*

$$\mathcal{H}_{ij}^{MDD} = \frac{\mu_i \cdot \mu_j}{r_{ij}^3} - 3 \frac{(\mu_i \cdot r_{ij})(\mu_j \cdot r_{ij})}{r_{ij}^5} \quad (I.3)$$

where r_{ij} is the vector connecting the *i*-th and *j*-th lattice site. The spin dimensionality is determined by the symmetry of the *g* tensor. Within a given spin dimensionality, this interaction is anisotropic, which complicates the calculations. Moreover, the dipolar interaction is of a long range. As pointed out already by Weiss, this interaction is much too weak to account for ferromagnetism at room temperature, such as observed in Fe and Ni. However, even in these cases it has an important effect, since it causes domain formation.

Calculations on the properties of a dipolar lattice close to the critical point have not yet been performed. Formally, even the *existence* of a critical point has not been derived in general. Also, the ground-state spin configuration remains a problem. Experimental information on dipolar coupled systems is scarce, due to the low temperatures needed, and because exchange interactions dominate in many magnetic materials.

We have studied a number of compounds which are believed to be good examples of dipolar lattices. This is substantiated by the comparison of results of calculations on the caloric behaviour with experimental results (see chapter I). The critical behaviour and the magnetic properties of the ordered state of two of these compounds, DyCl₃·6H₂O and ErCl₃·6H₂O,

have been studied extensively. The results are collected in chapter II. They are compared with theories on phase transitions⁴), often expressed as beliefs, such as the one by Fisher, which is the motto of this thesis.

It turns out that interesting information on the nature of the interactions can be obtained from measurements as a function of the concentration of magnetic ions. Starting from an undiluted magnetic compound, we expect the critical temperature to decrease on random substitution of a diamagnetic species in a rigid lattice. Calculations show the curve which represents the critical point *versus* concentration to depend on the range and the spin dimensionality of the interaction, and on the lattice dimensionality. In chapter III, measurements are discussed on $\text{Co}_p\text{Zn}_{1-p}\text{Cs}_3\text{Cl}_5$. The results can be explained by the random spin model⁵), assuming short-ranged Ising interactions in a three-dimensional lattice, which confirms the picture obtained from measurements on the undiluted compound. In particular, the experimental results indicate the existence of a critical concentration of magnetic ions, below which no cooperative phenomena occur at any temperature. The disappearance of such phenomena is verified by calculations which were undertaken in connection with experiments on metallic diluted systems, *i.e.* alloys. Due to the band structure of metals, the magnetic moment may contain contributions from non-localized electronic states, and the hamiltonians of eqs. (I.1) to (I.3) may be poor approximations. Nonetheless, the magnetic behaviour of a large number of metallic systems is strongly reminiscent of the behaviour of systems containing only localized moments, such as ionic crystals. Accordingly, at very low concentrations, we expect paramagnetic behaviour down to very low temperatures. However, a large number of experiments on non-magnetic metals containing transition metal impurities have shown the existence of anomalies in various physical properties, such as a minimum and a subsequent logarithmic increase in the electrical resistivity, and a giant thermoelectric power. These anomalies are observed at relatively high temperatures, and are clearly not related to impurity-impurity interactions. An explanation has been given by Kondo⁶), on the assumption of a (static) localized impurity spin S , which interacts with the host conduction electron spin density s at the impurity site according to:

$$\mathcal{H}_{s-d} = J s \cdot S \quad (\text{I.4})$$

After Kondo's explanation of the resistivity minimum, a great deal of attention has been paid to the dilute alloy problem⁷). It appears that the formation of a local moment is closely related to its interaction with the surrounding sea of conduction electrons. In this connection, dynamical problems arise, which have led to the concept of a localized spin fluctuation.

The deviations from pure host behaviour are proportional to the concentration of transition metal elements, hence at very low concentrations such deviations are difficult to detect by bulk measurements. But very low concentrations are needed to study the effects of isolated impurities, in particular at low temperatures. We have applied the method of nuclear orientation to the study of dilute alloys, because nuclear orientation measurements can be performed on a relatively small assembly of radioactive nuclei ($\approx 10^{10}$). When the nuclear

spins are oriented in space, the emitted gamma radiation will have an anisotropic directional distribution with respect to the axis of alignment. If the transition metal impurity carries a local moment, nuclear orientation can be achieved via magnetic hyperfine interaction by polarizing the local moment in an applied external field. In this way, the nucleus may probe the electronic state at or near the impurity. It will be shown that an analysis of the dynamical behaviour of the local moment is important for describing thermal equilibrium nuclear orientation measurements, even in the absence of *s-d* interaction effects. Chapter IV describes nuclear-orientation experiments on a number of very diluted alloys, *viz.* AuMn, AuCr, AuCo, and ZnMn.

The use of carbon resistors in very low temperature thermometry is discussed in an appendix, which concentrates on fitting the measured resistance *versus* temperature data by analytical expressions. Such expressions can be used for extrapolation purposes outside the fitted region, if the expression has a limited number of terms. Expressions containing a large number of terms have been utilized for interpolation purposes in the analysis of calorimetric experiments requiring a high temperature resolution, such as described in chapters II and III.

References

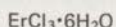
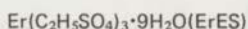
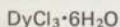
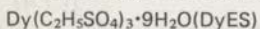
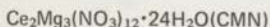
- 1) Domb, C., *Adv. Phys.* **9** (1960) 170.
- 2) Onsager, L., *Phys. Rev.* **65** (1944) 117.
- 3) Baker, J.M., *Rep. Progr. Phys.* **34** (1971) 109.
- 4) Fisher, M.E., *Rep. Progr. Phys.* **30** (1967) 615.
- 5) Griffiths, R.B. and Lebowitz, J.L., *J. Math. Phys.* **9** (1968) 1284.
- 6) Kondo, J., *Progr. Theor. Phys. (Kyoto)* **32** (1964) 37.
- 7) Heeger, A.J., in 'Solid State Physics', eds. F. Seitz, D. Turnbull and H. Ehrenreich (Academic Press, New York, 1969) vol. 23, p. 283.

CHAPTER I

CALORIC AND MAGNETIC STUDY OF FIVE RARE-EARTH IONIC COMPOUNDS HAVING PREDOMINANTLY MAGNETIC DIPOLE-DIPOLE INTERACTION

Synopsis

Calculations on the ground-state energy, the ground-state spin configuration, the high-temperature specific heat, and the Curie-Weiss constant of dipolar-coupled spin systems are presented. Numerical results have been obtained on the following substances:



using the method of Van Vleck, extended by Daniels, and Wong, Dembinski and Opechowski, and the method of Luttinger and Tisza. The results have been compared with existing experimental data and with new data obtained for ErES and the rare-earth trichloride hexahydrates.

1.1 Introduction

Dipolar coupling is always present when magnetic moments μ_i are localized at the sites i of a crystal lattice:

$$\mathcal{H}^{\text{MDD}} = \sum_{i < j} \left(\frac{\mu_i \cdot \mu_j}{r_{ij}^3} - \frac{3(\mu_i \cdot r_{ij})(\mu_j \cdot r_{ij})}{r_{ij}^5} \right), \quad (1.1.1)$$

where r_{ij} is the vector connecting the i -th and j -th lattice sites. We will assume that the magnetic moments are associated with spinvectors S_i according to

$$\mu_i = \mu_B g_i \cdot S_i \quad (1.1.2)$$

We will not discuss here which factors determine the components g_i^{ab} of the g tensor and how they are measured. The magnetic moment is considered to be temperature independent in the range of interest.

It has been realized long ago¹⁾ that eq. (1.1.1) alone could not account for magnetic ordering effects above 1K. Because many substances are known which order at temperatures much

higher than 1 K, other interactions have been introduced. The corresponding hamiltonians are approximations in most cases, unlike eq. (1.1.1). However, they contain only short-range forces, and are therefore theoretically more tractable. It should be remarked that due to its very long range, the dipolar interaction can give rise to macroscopic effects in the ordered region (*e.g.* demagnetization by domain formation). The hamiltonian (1.1.1) is exact for point dipoles and it is a very good approximation for the real case, when the magnetic moments are due to the unfilled electron shells of ions of the transition elements. Calculations on this hamiltonian for ideal (perfect and rigid) lattices have been done, among others, by Van Vleck²), Luttinger and Tisza³), Daniels⁴), Peverley and Meijer⁵), and Meijer and O'Keeffe⁶). We have used their formalisms to calculate the high-temperature specific heat:

$$c/R = \sum_{n=2}^{\infty} b_n/T^n, \quad (1.1.3)$$

and the Curie-Weiss constants $\Delta^{a\beta}$ in

$$\chi^{a\beta} = \frac{C_1^{a\beta}}{T - \Delta^{a\beta}} \quad (\text{no sum}) \quad (1.1.4)$$

from the high-temperature expansion of the free energy; the ground-state energy E/R and the corresponding spin configuration have also been calculated according to the eigenvalue method of Luttinger and Tisza (LT). We shall discuss an iterative method which also solves the ground-state problem while avoiding some of the difficulties of the LT method. A number of these results have already been obtained by other authors. Nowadays, many compounds are known which order at temperatures in the liquid-helium region or below⁷), but only few of them have dominant dipolar coupling. We will discuss five compounds which are expected to be nearly purely dipolar, *viz.* CMN, DyES, ErES, DyCl₃·6H₂O and ErCl₃·6H₂O. A comparison will be made with the existing experimental data and with new data obtained for ErES and the trichloride hexahydrates. Except for ErES, there is experimental evidence that these compounds are ferromagnets or metamagnets with very low transition fields.

1.2 The Van Vleck moment method

In the Van Vleck moment expansion²) the partition function is expressed in powers of $1/kT$:

$$Z = \text{Tr} \sum_{n=0}^{\infty} \frac{(\tilde{\chi}_D/kT)^n}{n!} \quad (1.2.1)$$

From this we can derive to second order in $1/T$:

$$\frac{C}{R} = \frac{b_2}{T^2}, \text{ and} \quad (1.2.2)$$

$$\chi_o^{a\beta} = \frac{C_{1o}^{a\beta}}{T} + \frac{C_{2o}^{a\beta}}{T^2} \quad (1.2.3)$$

for the specific heat and the susceptibility tensor for the reference ion (o) respectively, where

$$b_2 = \frac{1}{18k^2} S^2 (S+1)^2 \sum_j P_{oj}^{a\beta} P_{oj}^{a\beta}, \quad (1.2.4)$$

$$C_{1o}^{a\beta} = \frac{N}{3k} S(S+1) \mu_B^2 g_o^{a\gamma} g_o^{\beta\gamma}, \text{ and} \quad (1.2.5)$$

$$C_{2o}^{a\beta} = -\frac{N}{9k^2} S^2 (S+1)^2 \mu_B^2 \sum_j P_{oj}^{\gamma\delta} g_o^{a\gamma} g_j^{\beta\delta} \quad (1.2.6)$$

(the dummy suffix summation convention is applied for Greek suffices).

We have used the notation of Daniels⁴):

$$P_{ij}^{a\beta} = \mu_B^2 \left(\frac{g_i^{\sigma\alpha} g_j^{\sigma\beta}}{r_{ij}^3} - \frac{3g_i^{\alpha\lambda} g_j^{\beta\nu} r_{ij}^{\lambda\nu}}{r_{ij}^5} \right). \quad (1.2.7)$$

It may be remarked that inclusion of another type of interaction in the calculation is easily performed by adding terms to $P_{ij}^{a\beta}$. Writing eq. (1.2.3) in the form

$$\chi_o^{a\beta} = \frac{C_{1o}^{a\beta}}{T - \Delta_o^{a\beta}} \quad (\text{no sum}) \quad (1.2.8)$$

which is the Curie-Weiss relation for the high-temperature susceptibility, we get in this approximation

$$\Delta_o^{a\beta} = C_{2o}^{a\beta} / C_{1o}^{a\beta} \quad (\text{no sum}). \quad (1.2.9)$$

Whereas both $C_{1o}^{a\beta}$ and $C_{2o}^{a\beta}$ are tensors, the $\Delta_o^{a\beta}$ may not have tensorial transformation properties. It is easy to include the effects of an external field on the specific heat eq. (1.2.2). As is well known²), the sum (1.2.6) is only conditionally convergent, and its value depends on the shape of the sample. We have followed the usual method of taking an ellipsoidal sample shape with the reference ion in its centre. A sphere of radius R is taken within the sample, centred at the reference ion, and eq. (1.2.6) is calculated within the sphere. This sum will converge for sufficiently large R . The convergence can be improved by the use of the weighting function method of Peverley and Meijer^{5,8}), or the Ewald method^{8,9}) can be

employed. The contribution to the local field on the reference ion due to the dipoles outside the sphere is approximated by taking a continuous volume distribution of magnetization. The field of such a volume magnetization follows simply from the demagnetizing tensors $D^{\alpha\beta}$ of the inner (spherical) and outer (ellipsoidal) surfaces. Hence we can write

$$C_{2o}^{\alpha\beta} = C_{2oR}^{\alpha\beta} + d_{2o}^{\alpha\beta} \quad (1.2.10)$$

where $C_{2oR}^{\alpha\beta}$ is given by expression (1.2.6), calculated for $r_{oj} < R$ and for sufficiently large R , and where

$$d_{2o}^{\alpha\beta} = \frac{1}{N\nu} C_{1o}^{\alpha\epsilon} \left(\frac{4\pi}{3} \delta^{\epsilon\gamma} - D^{\epsilon\gamma} \right) C_{1c}^{\gamma\beta}. \quad (1.2.11)$$

N is Avogadro's number, ν is the volume of the unit cell, and the $C_{1c}^{\alpha\beta}$ are the components of the 'Curie tensor' evaluated for the whole unit cell. If the demagnetization tensors can be replaced by scalars, eq. (1.2.11) becomes:

$$d_{2o}^{\alpha\beta} = \frac{1}{N\nu} C_{1o}^{\alpha\gamma} C_{1c}^{\gamma\beta} \left(\frac{4\pi}{3} - D \right). \quad (1.2.12)$$

Explicit formulas for b_2 and the next higher coefficient b_3 in the specific heat expansion have been given by Wong *et al.*¹⁰⁾ in terms of a number of lattice sums S_1, \dots, S_{13} .

$$b_2 = \frac{1}{18k^2} \mu_B^4 S^2 (S+1)^2 [(5g_{\perp}^4 + g_{\parallel}^4) S_1 - 6(g_{\perp}^2 - g_{\parallel}^2)(2g_{\perp}^2 - g_{\parallel}^2) S_2 + 9(g_{\perp}^2 - g_{\parallel}^2)^2 S_3] \quad (1.2.13)$$

$$b_3 = -\frac{1}{6k^3} S^2 (S+1)^2 g_{\perp}^4 g_{\parallel}^2 \mu_B^6 S_4 - \frac{1}{3k^3} S^3 (S+1)^3 \mu_B^6 \left\{ \frac{1}{3} (-7g_{\perp}^6 + g_{\parallel}^6) S_5 + 3(g_{\perp}^6 - g_{\parallel}^6) S_6 + 9[g_{\perp}^6 (S_7 - S_{10}) + g_{\perp}^4 g_{\parallel}^2 (S_8 - 3S_{11}) + g_{\perp}^2 g_{\parallel}^4 (S_8 - 3S_{12}) + g_{\parallel}^6 (S_9 - S_{13})] \right\}. \quad (1.2.14)$$

The ions are assumed to be magnetically equivalent, having an axial \mathbf{g} tensor. The z axis of the coordinate system in which the sums S_1, \dots, S_{13} are calculated is along the g_{\parallel} direction. The sums are:

$$S_1 = \sum_i \frac{1}{r_{ij}^6}, \quad S_2 = \sum_i \frac{z_{ij}^2}{r_{ij}^8}, \quad S_3 = \sum_i \frac{z_{ij}^4}{r_{ij}^{10}}, \quad S_4 = \sum_i \frac{1}{r_{ij}^9}, \quad S_5 = \sum_{jk} \frac{1}{r_{ij}^3 r_{jk}^3 r_{ki}^3},$$

$$S_6 = \sum_{jk} \frac{z_{ki}^2}{r_{ij}^3 r_{jk}^3 r_{ki}^5}, \quad S_7 = \sum_{jk} \frac{(x_{jk} x_{ki} + y_{jk} y_{ki})^2}{r_{ij}^3 r_{jk}^5 r_{ki}^5}, \quad S_8 = \sum_{jk} \frac{(x_{jk} x_{ki} + y_{jk} y_{ki}) z_{jk} z_{ki}}{r_{ij}^3 r_{jk}^5 r_{ki}^5},$$

$$\begin{aligned}
S_9 &= \sum_{jk} \frac{z_{jk}^2 z_{ki}^2}{r_{ij}^3 r_{jk}^5 r_{ki}^5}, \quad S_{10} = \sum_{jk} \frac{(x_{ij}^x x_{jk}^y + y_{ij}^y y_{jk}^x)(x_{jk}^x x_{ki}^y + y_{jk}^y y_{ki}^x)(x_{ki}^x x_{ij}^y + y_{ki}^y y_{ij}^x)}{r_{ij}^5 r_{jk}^5 r_{ki}^5}, \\
S_{11} &= \sum_{jk} \frac{(x_{ij}^x x_{jk}^y + y_{ij}^y y_{jk}^x)(x_{jk}^x x_{ki}^y + y_{jk}^y y_{ki}^x) z_{ki} z_{ij}}{r_{ij}^5 r_{jk}^5 r_{ki}^5}, \quad S_{12} = \sum_{jk} \frac{(x_{ij}^x x_{jk}^y + y_{ij}^y y_{jk}^x) z_{jk} z_{ki}^2 z_{ij}}{r_{ij}^5 r_{jk}^5 r_{ki}^5}, \\
S_{13} &= \sum_{jk} \frac{z_{ij}^2 z_{jk}^2 z_{ki}^2}{r_{ij}^5 r_{jk}^5 r_{ki}^5}. \tag{1.2.15}
\end{aligned}$$

These expressions can be numerically evaluated on a fast digital computer to a precision of a few percent within a reasonable time.

1.3 The Luttinger and Tisza method*

If the magnetic unit cell of the ordered state at $T=0$ is given, energy calculations can be performed as a function of the spin directions of the ions in the unit cell. In the method of Luttinger and Tisza³) these spin direction variables are combined into a vector in multidimensional space. The components of the field at the various lattice sites, produced by a certain spin configuration, can be represented by a vector in the same space. The two vectors are linearly dependent. The lowest eigenvalue of the corresponding matrix is the energy of a ground state in which the spin vector in the multidimensional space is normalized (the weak constraint). This does not necessarily imply that the spin variables belonging to each of the spins are normalized (the strong constraint). It has been proven by Niemeyer, however, that the weak constraint implies the strong constraint in the case that the magnetic ions are arranged on a Bravais lattice¹¹). Moreover, Niemeyer has shown that the classical approach of Luttinger and Tisza is equivalent to a variational method in quantum mechanics with a special choice of trial functions.

Another method which avoids the eigenvalue calculation and which is applicable in the case of nonequivalent ions as well consists of calculating first the fields at the ion positions as a function of the spin directions, assuming an initial spin configuration, followed by a rotation of the spins towards the field. In this way the strong constraint is always satisfied. An iterative procedure can be set up which will yield a minimum in the energy for a certain configuration. In general this minimum will be a relative one. It turns out that the minimum found is quite sensitive to the starting conditions and the rate at which the spins are rotated. These calculations suffer from three objections:

a) The translational symmetry of the spin configuration is prescribed. It is assumed that there are n sublattices in each of which the magnetic moments are parallel, with n rather small, to avoid lengthy calculations. For spins situated on the sites of a Bravais lattice, Niemeyer has shown that for $n=8$ the only possible configurations in the classical approach

* We thank drs. H.W.J. Blöte for the use of his computer program.

are the purely ferromagnetic and the purely antiferromagnetic (Néel or layered) configurations, for a hamiltonian containing general dipolar and isotropic exchange interactions. We expect this to be true for systems having strongly anisotropic (Ising-like) interactions in other cases too. In the most general case, however, it is possible that the configuration of lowest energy has a complicated translational symmetry or even no translational symmetry, as shown by experiment (*e.g.* helical structures).

b) The spins are considered as classical vectors. This will effect the absolute values of the energy but is expected to have little influence on the relative positions of the energy levels of the spin configurations. The correction will be most pronounced for $S=1/2$ and isotropic g values.

c) The weak constraint does not necessarily imply the strong constraint for non-Bravais lattices. In some of these cases, if a state is degenerate, it is possible to combine the corresponding eigenvectors to new ones which do satisfy the strong constraint. If a transformation of the coordinates can be found which transforms the spin sites of a Bravais lattice without changing the hamiltonian, Niemeyer's theorem will be valid.

The experimental data on the single ion magnetic properties and the crystal lattice, needed to perform the calculations in this and the previous section are tabulated in table I.1 for the five compounds considered. The dipoles are distributed over a lattice $T = hA + kB + lC$, the position of a dipole in the unit cell (h, k, l) being given by $r = (h + a_i)A + (k + b_i)B + (l + c_i)C$, where i runs from 1 to m , the number of ions in the unit cell. In all cases considered, the ions are magnetically equivalent with effective spin quantum number $S=1/2$. Furthermore, the g tensors have (approximately) axial symmetry. The angles between the g_{\parallel} direction and the crystal axes are ξ_A, ξ_B and ξ_C respectively. The crystal field symmetry is not axial in the case of $\text{DyCl}_3 \cdot 6\text{H}_2\text{O}$ and $\text{ErCl}_3 \cdot 6\text{H}_2\text{O}$, but the difference between g_x and g_y is small and moreover $g_x, g_y \ll g_z$. Electron-spin resonance measurements on concentrated $\text{ErCl}_3 \cdot 6\text{H}_2\text{O}$ ¹²) cast serious doubt on the magnetic data of this compound as they are tabulated in table I.1, which are obtained from e.s.r. measurements on very dilute samples¹³).

1.4 Calculations

The calculations are presented in tables I.2, I.3, I.4 and I.5, using the data of table I.1. All summations extend over the dipoles within the unit cells with $-p \leq h \leq p, -q \leq k \leq q$, and $-r \leq l \leq r$. R denotes the radius of the sphere surrounding these unit cells. Results on the b_2 and b_3 calculations, using the formulas of Wong *et al.*¹⁰), are shown in table I.2. As could be anticipated, the differences between the calculated values for lattices of equal symmetry and comparable lattice constants are largely due to the difference in the g values. The value of b_3 is negative, except for DyES, where it is very small. These negative values can explain the observed downwards deviations from the T^{-2} law for the specific heats on approaching the transition points from high T . The relatively large values of some of the calculated b_3 results and the low (measured) transition points, make it plausible that

Table I.1. Crystallographic and magnetic data.

	space group	A[Å]	B[Å]	C[Å]	α [°]	β [°]	γ [°]	ion in unit cell $i = 1 \dots m$	position			S	ξ_A [°]	ξ_B [°]	ξ_C [°]	g_{\parallel}	g_{\perp}
									a_i	b_i	c_i						
CMN ^{a)}	$R\bar{3}$	11.004	11.004	17.296	90	90	120	1	0	0	0	1/2	90	90	0	0	1.84
								2	1/3	2/3	2/3						
								3	2/3	1/3	1/3						
DyES ^{b)}	$P6/m$	13.906	13.906	7.04	90	90	120	1	1/3	2/3	1/4	1/2	90	90	0	10.8	0
								2	2/3	1/3	3/4						
ErES ^{c)}	$P6/m$	13.91	13.91	7.05	90	90	120	1	1/3	2/3	1/4	1/2	90	90	0	1.47	8.85
								2	2/3	1/3	3/4						
DyCl ₃ ·6H ₂ O ^{d)}	$P2/m$	9.61	6.49	7.87	90	93.65	90	1	1/4	0.1521	1/4	1/2	167	90	63.35	16.52	1.75
								2	3/4	0.8479	3/4						
ErCl ₃ ·6H ₂ O ^{e)}	$P2/m$	9.57	6.47	7.84	90	93.65	90	1	1/4	0.1521	1/4	1/2	257	90	163.35	13.74	0.75
								2	3/4	0.8479	3/4						

^{a)} refs. 14 and 15.^{b)} refs. 16 and 17.^{c)} refs. 16 and 18.^{d)} refs. 19, 20 and 13.^{e)} refs. 19, 20 and 13.

Table 1.2. Values of S_1, \dots, S_{13} , evaluated in a coordinate system where

$$A = A(\sin \zeta_A, 0, \cos \zeta_A),$$

$$B = \{B(\cos \gamma - \cos \zeta_A \cos \zeta_B) \sin \zeta_A, \sqrt{[B^2(\sin \zeta_B)^2 - B_x^2]}, B \cos \zeta_B\},$$

$$C = \{C(\cos \beta - \cos \zeta_A \cos \zeta_C) \sin \zeta_A, \pm \sqrt{[C^2(\sin \zeta_C)^2 - C_x^2]}, C \cos \zeta_C\}.$$

The + or - sign has to be chosen such that a right-handed coordinate system is obtained.

Tabulated values of $S_1, S_2, S_3 \times 10^{-8} \text{ \AA}^{-6}$, those of $S_4, \dots, S_{13} \times 10^{-8} \text{ \AA}^{-9}$.

	CMN	DyES	ErES	DyCl ₃ ·6H ₂ O	ErCl ₃ ·6H ₂ O
p,q,r,m	9,9,5,3	7,7,12,2	7,7,12,2	9,13,11,2	9,13,11,2
$R=80 \text{ \AA}$					
S_1	2216.0	3416.2	3396.7	12947	13236
S_2	839.70	2015.6	2000.7	4024.8	4265.4
S_3	411.22	1778.6	1764.2	2555.4	2462.3
S_4	2.7396	6.7969	6.7280	36.854	38.092
p,q,r,m	3,3,2,3 (4,4,3,3)	4,4,3,2	4,4,3,2	3,3,3,2	3,3,3,2 (4,4,4,2)
S_5	30.284 (30.954)	42.864	42.573	447.75	462.87 (473.19)
S_6	10.526 (10.732)	17.851	17.718	147.15	153.33 (156.58)
S_7	7.8597 (8.0784)	10.444	10.378	118.15	121.64
S_8	0.50607	0.44055	0.43712	8.0424	8.4148
S_9	3.9889	7.6265	7.5651	54.139	56.272 (57.585)
S_{10}	2.9576 (3.0760)	2.8436	2.8292	40.254	43.113
S_{11}	-0.31322	0.052603	0.052256	-0.94645	-1.7205
S_{12}	0.17145	0.048945	0.047409	0.56896	0.75149
S_{13}	1.5625	3.8203	3.7843	18.427	19.656 (20.268)
$b_2[\text{K}^2]$	6.52×10^{-6}	0.0121	0.00666	0.1090	0.0427
$b_3[\text{K}^3]$	-2.21×10^{-8}	0.0009	-0.00121	-0.0686	-0.0182 (-0.0183)
	(-2.19×10^{-8})				

Table 1.3. Susceptibility tensors $C_{10}^{a\beta}$ and $C_{20R}^{a\beta}$ with $R=80 \text{ \AA}$. The weighting function procedure of Peverley⁸) has been used.

Every box contains one component for each of the different substances, in the sequence CMN, DyES, ErES, DyCl₃·6H₂O, ErCl₃·6H₂O. Coordinate system is chosen such that $A=A(1,0,0)$, $B=B(\cos \gamma, \sin \gamma, 0)$, $C=C(\cos \beta, C(\cos \alpha - \cos \beta \cos \gamma) / \sin \gamma, \pm \sqrt{[C^2 - C_x^2 - C_y^2]})$.

$C_{10}^{a\beta}$				$C_{20R}^{a\beta}$			
3.1716 E - 01	0	0	0	- 8.5581 E - 05	- 1.3180 E - 07	0	0
0	0	0	0	0	0	0	0
7.3373 E + 00	0	0	0	- 3.1769 E - 01	3.5098 E - 04	0	0
2.1706 E + 01	0	-9.0920 E + 00	0	- 1.1018 E + 00	0	4.9198 E - 01	0
9.4599 E - 01	0	3.8670 E + 00	0	- 1.5744 E - 02	0	-7.1377 E - 02	0
0	3.1761 E - 01	0	0	- 1.3180 E - 07	- 8.5733 E - 05	0	0
0	0	0	0	0	0	0	0
0	7.3373 E + 00	0	0	3.5098 E - 04	- 3.1728 E - 01	0	0
0	2.9018 E - 01	0	0	0	1.6347 E - 04	0	0
0	5.2695 E - 02	0	0	0	5.3067 E - 06	0	0
0	0	0	0	0	0	0	0
0	0	1.0927 E + 01	0	0	0	1.4167 E + 00	0
0	0	2.0243 E - 01	0	0	0	4.8333 E - 04	0
- 9.0920 E + 00	0	4.1501 E + 00	0	4.9198 E - 01	0	-2.1914 E - 01	0
3.8670 E + 00	0	1.6792 E + 01	0	- 7.1377 E - 02	0	-3.2298 E - 01	0

Table I.4. Calculated values of b_2 and Δ for some special directions, using the data of table I.3.

A, B, C directions of crystal axes

x, y, z directions of main axis of $g^{a\beta}$

h direction of applied field

m direction of measured magnetization

All sums calculated within a sphere of 80 Å, using a weighting function for Δ .

	b_2 [K ²] $H=0$	h	b_2 [K ²] ^{a)} $H=100$ Oe	m	C [$\frac{\text{Kcm}^3}{\text{mole}}$]	Δ [K]	d [K]
CMN	6.52×10^{-6}	$x(=A)$	3.81×10^{-5}	x	0.317	-0.000270	0.000871
DyES	0.0121	$z(=C)$	0.00131	z	10.927	0.1297	0.0308
ErES	0.00666	$z(=C)$ $x(=A)$	0.0000243 0.000882	z x	0.202 7.337	0.00238 -0.0433	0.000569 0.0206
DyCl ₃ ·6H ₂ O	0.1091	z A $y(=B)$	0.00307	z A y	25.566 21.706 0.290	-0.0517 -0.0508 0.0005	0.1733 0.1730 0.0020
ErCl ₃ ·6H ₂ O	0.0427	z A $y(=B)$	0.00213	z A y	17.686 0.946 0.0527	-0.0192 -0.0166 0.0001	0.1212 0.1149 0.0004

a) proportional to H^2 .

Table I.5. Some critical parameters.

	$-E/R$ [K] theor.	corresponding state	transition point [K] exp.	$-E/R$ [K] exp.	ordered state exp.	$-E_c/RT_c$ exp.	$(S_\infty - S_c)/R$ exp.
CMN	0.00189 0.00169	A F M F M	0.0019	0.0022	F.M.	?	0.31
DyES	0.129 0.127	F M A F M	0.115	0.13	F.M.	0.92	0.47
ErES	0.0356 0.0334	A F M A F M	$\lesssim 0.04$?	?	?	?
DyCl ₃ ·6H ₂ O	0.338 0.317	F M A F M	0.289	0.32	F.M.	0.83	0.42
ErCl ₃ ·6H ₂ O	0.245 0.242	F M A F M	0.355	0.272	F.M.	0.323	0.172

higher-order terms contribute considerably to the heat capacity in a rather large temperature range above T_c . Hence a deviation of the experimental specific-heat curve from the one obtained from eq. (1.1.3), with only a limited number of terms, should not be automatically attributed to another type of interaction.

Table 1.3 shows the components of the susceptibility tensors $C_{10}^{a\beta}$ and $C_{20R}^{a\beta}$, evaluated in a coordinate system by choosing the x axis along A , the y axis in the A - B plane and the z axis such that the z component of C is positive. The method of Peverley and Meyer^{5,8)} has been applied using a different weight function

$$W(r) = 1 - \exp [a(r-R)] \quad (1.4.1)$$

where a is an adjustable parameter. This function has the advantage over the one used by Peverley and Meyer that it exactly smoothes the contributions to the sum to zero at the surface of the sphere, $r=R$.

In table 1.4, some special values of C and Δ have been tabulated for the five compounds, derived from table 1.3 by specifying the directions of the applied field and the magnetization measurement. In most experiments these are parallel to each other and to one of the principal axes of the g tensor, which does not necessarily coincide with one of the crystallographic axes. To obtain the contributions arising from the continuum outside the sphere (R), one has to augment Δ by the number headed d multiplied by $\frac{4\pi}{3} - D$, provided that the magnetization is along one of the principal axes of the demagnetization tensor, hence along one of the axes of the sample ellipsoid. This will be the case if the axes of the g tensor coincide with those of the ellipsoid, and if the external field is along one of these axes.

Table 1.5 gives the results of the energy calculations. The largest magnetic unit cell used was obtained by doubling the crystallographic unit cell from table 1.1 in all three directions. A.F.M. and F.M. stand for antiferromagnetic and ferromagnetic ground-state configurations respectively. The ferromagnetic energies given, are for a demagnetized ground state. As pointed out by Griffiths²¹⁾, the existence of a shape independent bulk free energy in zero external field should lead to such a state, provided true thermodynamic equilibrium can be reached. This excludes the possibility of changes in the type of ordering induced by changes in the shape^{3,22)}. For an uniaxially symmetric system formation of needle-shaped domains is expected. The possibility of domain formation in systems ordering by dipolar forces has been pointed out by Kittel²³⁾. It is not clear which magnetostatic mode should be obtained in systems with planar symmetry, such as CMN and ErES. Some experimental data are also included in table 1.5. The transition points follow the same sequence as the energies except for $\text{ErCl}_3 \cdot 6\text{H}_2\text{O}$, where we would have expected a lower transition point. Also the difference between the measured and calculated energy values lies definitely outside the estimated error in the case of $\text{ErCl}_3 \cdot 6\text{H}_2\text{O}$. Moreover, this substance does not exhibit the high value of the short-range ordering entropy which is characteristic for the other compounds.

1.5 Comparison with existing calculations and experimental data

Caloric properties of the five substances will be compared with our calculations in this section. Susceptibility data are known as well, but their analysis is difficult. In particular, reliable data on the Curie-Weiss Δ 's are hard to obtain, because they must be derived from measurements at relatively high temperatures, where the sensitivity of bridge methods becomes low and the magnetic moment may become temperature dependent. The shape dependence and the tensorial character of the susceptibility are additional complications. The low values of the Δ 's found are compatible with the assumption of largely dipolar interactions.

1.5-1 CMN

Extensive measurements and calculations on CMN have been reported^{24,25}). We have repeated the calculations done by Peverley and Meyer⁵) on the susceptibility and by Daniels and Felsteiner²⁶) on the ground state. The value of b_3 has been computed by Wong *et al.*¹⁰), using the crystallographic data of Powell. In a calculation to third order in $1/T$, they introduce isotropic ferromagnetic exchange interactions between nearest neighbours to explain the specific-heat data of Mess *et al.*²⁴). Niemeier¹¹) has proven that the value obtained

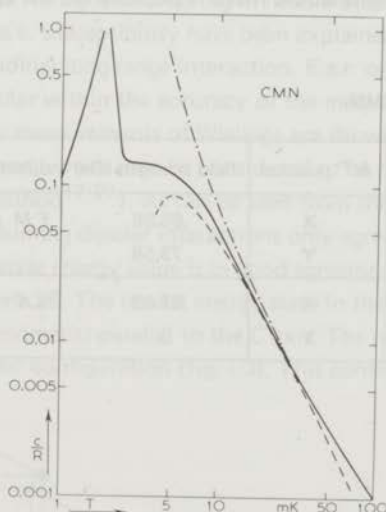


Fig. 1.1. Specific heat of CMN.

Full curve: measurements of ref. 24; dashed curve: $10^8 c/R = 652/T^2 - 2.19/T^3$;

dash-dotted curve: $10^8 c/R = 634/T^2 - 2.08/T^3 + 0.031/T^4$ (ref. 6).

nonetheless favours an antiferromagnetic ground state in the LT approach. Due to a) rather inaccurate specific-heat data, b) the low order of $1/T$ in which the calculations have been performed, and c) the approximations in the LT theory, we do not consider this as a convincing argument for antiferromagnetism in CMN.

The measurements on the specific heat of CMN of ref. 24 are shown in fig. 1.1, together with some calculated curves. Although there is reasonable agreement at intermediate temperatures, the measured specific heat deviates from the calculated asymptotic behaviour at high temperatures. The resulting temperature dependence of the experimental b_2 value is not understood²⁴). A similar comparison has been made by Hudson²⁵), for specific-heat data obtained on powdered samples.

The crystallographic unit cell in table 1.1 is appropriate to the lattice of Ce ions. The true hexagonal unit cell which must be taken if calculations on the divalent ions are performed, is given by Zalkin *et al.*¹⁴). We have used their data to calculate the fields at the divalent ions in the two ordered configurations tabulated in table 1.5, *viz.* the layered antiferromagnetic ground state of ref. 26 and the demagnetized ferromagnetic state. The fields and their directions are shown in table 1.6. It should be emphasized that in the ferromagnetic state the magnetic moments are perpendicular to the C axis. This state arises naturally from our calculations. It has not been considered explicitly in ref. 26. The group theoretical argument quoted by Mess *et al.*²⁴) that ferromagnetic alignment in a trigonal crystal is possible only along the C axis, is probably rendered invalid by the assumption of a demagnetized ferromagnetic state, which makes the resultant magnetic moment zero in all directions. Distorsions would lower the symmetry and this would make it possible for the system to order in macroscopic, needle-shaped domains.

Table 1.6. Fields in CMN

configuration	M^{2+} position	field strength (Oe)	direction
F M in A-A plane	X	65.88	F M alignment
	Y	73.58	
A F M layered ^{a)}	X	67.03	$\pm A$
	Y	0	

^{a)} see ref. 26.

1.5-2 DyES

Measurements on DyES have been published by Cooke *et al.*^{17,27}) and by Wielinga²⁸). These two experiments disagree with respect to the temperature of the transition point (0.13 and 0.115 K respectively) and the shape of the specific-heat curve near T_c . The

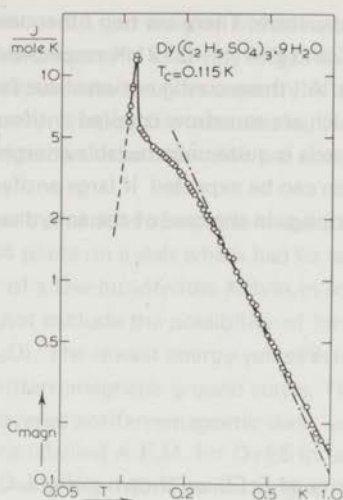


Fig. 1.2. Specific heat of DyES, not corrected for h.f.s. contribution (ref. 27).

Dash-dotted curve: $c/R = 0.0131/T^2 + 0.0009/T^3$.

reported values of b_3 are 0.002 K^3 and -0.001 K^3 respectively. Measurements on the d.c. susceptibility indicate ferromagnetic ordering in needle-shaped domains. The relaxation effects observed in the a.c. susceptibility have been explained by Richards²⁹⁾ on the basis of a dominantly longitudinal long-range interaction. E.s.r. on coupled pairs shows the interaction to be purely dipolar within the accuracy of the measurement³⁰⁾.

In fig. 1.2, heat-capacity measurements of Wielinga are shown which were obtained by the (direct) heat pulse method, which may be considered to be much more accurate than the earlier employed Q - S method^{17,27)}. As can be seen from the figure, the high-temperature behaviour calculated assuming dipolar interactions only agrees with the measured data. The computed ground-state energy value is in good agreement with the experimental one (tabel I.5) taken from ref. 28. The lowest energy state in the LT calculation is the ferromagnetic one with the moments parallel to the C axis. The next higher state pertains to a layered antiferromagnetic configuration (fig. 1.3). This configuration is threefold degenerate,

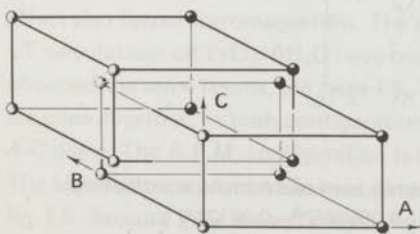


Fig. 1.3. A F M ordering in DyES and ErES.

- moment parallel to C (DyES) or A (ErES).
 - moment parallel to $-C$ (DyES) or $-A$ (ErES).
- There are two other equivalent configurations.

as can be seen from the crystal structure. There are two other nearby antiferromagnetic states having energies $E/R = -0.124$ K and $E/R = -0.121$ K respectively, which correspond to other arrangements of the layers. All these configurations have ferromagnetic chains along the C axis arranged in planes which are somehow coupled antiferromagnetically. Antiferromagnetic alignment along the C axis is quite unfavourable energetically ($E/R = +0.100$ K). Such a ground-state configuration can be expected if large antiferromagnetic (super) exchange interactions are present, e.g. in the case of the anhydrous trichlorides of the rare earths³¹).

1.5.3 ErES

Measurements on the heat capacity of ErES are shown in fig. 1.4. The hyperfine specific heat of the 23% abundant ^{167}Er isotope has been subtracted from the data on samples prepared from natural Er_2O_3 (curve a in fig. 1.4). We have also done measurements on isotopically enriched samples, containing 96.1% ^{170}Er , which has no nuclear moment (curve b in fig. 1.4). The h.f.s. specific heat in the temperature range 0.01-0.2 K has been calculated from the spin hamiltonian, because the high-temperature approximation $c/R = b_N/T^2$ can be used only above 0.2 K, where $b_N = 0.00133$ K². After subtraction of this contribution, the smoothed data on the sample of natural isotopic abundance show an unsharp maximum at 0.04 K. If the nuclear spin-lattice relaxation time becomes long, however, one has to subtract only part of the h.f.s. contribution. Because curve b lies above curve a, we attribute the difference to relaxation effects.

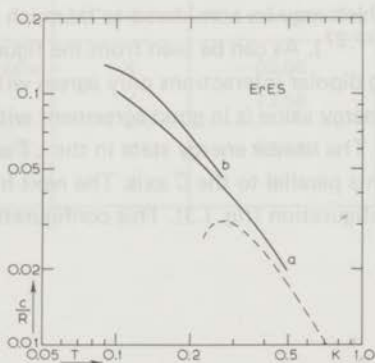


Fig. 1.4. Specific heat of ErES.

Curve a: sample having natural isotopic abundance, corrected for h.f.s. contribution;
 curve b: enriched sample. Dashed curve: $c/R = 0.00666/T^2 - 0.00121/T^3$.

Due to the small samples (about 0.1 g in weight) which we used in our experiments, the contribution of the empty calorimeter is relatively large. This leads to a considerable source of error in the corrected data, because the heat capacity of the empty calorimeter is not known with sufficient accuracy. Despite the inaccuracies, it is clear from the experimental data that the two calculated terms in the expansion are not sufficient to describe the measured data.

Down to 40 mK there are no indications of a phase transition in the susceptibility. The Δ value measured in the *A-A* plane on a slab which had its largest dimensions in this plane is negative and of the order of a few hundredths Kelvin, in accordance with the calculated value (table I.4). This does not exclude the possibility of ferromagnetic ordering (compare $\text{DyCl}_3 \cdot 6\text{H}_2\text{O}$ and $\text{ErCl}_3 \cdot 6\text{H}_2\text{O}$). The lowest energy values calculated with the LT method (table I.5) correspond to antiferromagnetic ground states. The minimum energy is obtained for a threefold degenerate layered antiferromagnetic state, which has the same configurational symmetry as the state labelled A.F.M. for DyES in table I.5, except for the moments being perpendicular to the *C* axis (fig. I.3). The next higher state consists of antiferromagnetic chains along the *C* axis with the moments aligned perpendicular to this axis. Due to the symmetric positions of the ions in the unit cell, the interaction energy between nearest-neighbour chains is zero. Three dimensional long-range order will be induced by the much weaker interactions with the more distant chains. Hence it is not surprising that the transition point of ErES turns out to be at very low temperatures.

In the nearest ferromagnetic state, having $E/R = -0.0216$ K, the moments lie in the *A-A* plane.

I.5.4 — $\text{DyCl}_3 \cdot 6\text{H}_2\text{O}$, $\text{ErCl}_3 \cdot 6\text{H}_2\text{O}$

$\text{DyCl}_3 \cdot 6\text{H}_2\text{O}$ and $\text{ErCl}_3 \cdot 6\text{H}_2\text{O}$ have been extensively studied by us³²). Preliminary data on the Er compound have been published³³). The conjecture of an antiferromagnetic ground state in this letter was based upon a.c. susceptibility measurements which show a downwards deviation of the Curie-Weiss relation extrapolated from susceptibility data between 1 and 3 K, and a sharp fall at T_c . D.c. susceptibility measurements, however, show a constant value of the susceptibility in the limited range below T_c where it can be measured reliably. Specific-heat measurements in an external field and measurements on the magnetothermal effect also favour ferromagnetism. The same arguments apply to $\text{DyCl}_3 \cdot 6\text{H}_2\text{O}$. LT calculations on $\text{ErCl}_3 \cdot 6\text{H}_2\text{O}$ have been performed by Felsteiner³⁴) and we have obtained the same results, see table I.5. The energies of the F.M. and A.F.M. states tabulated are close together. In both configurations, the moments lie along the g_{\parallel} direction in the *A-C* plane. The A.F.M. configuration is layered³²).

The high-temperature specific-heat data of $\text{ErCl}_3 \cdot 6\text{H}_2\text{O}$ and $\text{DyCl}_3 \cdot 6\text{H}_2\text{O}$ are shown in fig. I.5. Because they are sufficiently numerous and precise, we can obtain the coefficients

Table 1.7. High-temperature specific heat of $\text{DyCl}_3 \cdot 6\text{H}_2\text{O}$ ($T > 0.50$ K) and $\text{ErCl}_3 \cdot 6\text{H}_2\text{O}$ ($T > 0.55$ K) fitted to $c/R = \sum_{i=2}^p b_i/T^i$.

$$\delta = \sqrt{\left(\frac{\sum (\Delta(c/R))^2}{(n-p)} \right)}, n = \text{number of fitted points}, M_s = \text{number of } b_i\text{'s where } \delta \text{ stabilizes. } c \text{ in the error-row means constrained } b \text{ value.}$$

		M_s	$\delta \times 10^4$	b_2	b_3	b_4	b_5	b_6	b_7	label
$\text{DyCl}_3 \cdot 6\text{H}_2\text{O}$	all b_i free error	3	8.68	0.1006 0.0013	-0.0448 -0.0017	0.0096 0.0006				1
	b_2 fixed error	5	8.67	0.1090 c	-0.0748 0.0045	0.0474 0.0091	-0.0200 0.0061	0.0038 0.0013		2
	b_2, b_3 fixed error	5	8.73	0.1090 c	-0.0686 c	0.348 0.0008	-0.0118 0.0010	0.0020 0.0003		3
$\text{ErCl}_3 \cdot 6\text{H}_2\text{O}$	all b_i free error	4	10.95	0.0691 0.0070	-0.0564 0.0167	0.0377 0.0129	-0.0085 0.0032			4
	b_2 fixed error	5	10.64	0.0427 c	0.0365 0.0072	-0.0796 0.0164	0.0549 0.0121	-0.0124 0.0029		5
	b_2, b_3 fixed error	6	10.79	0.0427 c	-0.0183 c	0.0979 0.0075	-0.1540 0.0163	0.0938 0.0116	-0.0198 0.0027	6

b_i in the expansion (1.1.3) by computer fitting of the data, provided i is not too high ($i \leq 5$). We have made least squares fits, using a method due to Banachiewicz³⁵, which also gives the probable errors in the dependent variable. Fits have been made with all b_i free or with constrained b_2 or b_2 and b_3 values, taking b_2 and b_3 from table 1.2. 74 points with $T > 0.5$ K and 55 points with $T > 0.55$ K were used in the fit for $\text{DyCl}_3 \cdot 6\text{H}_2\text{O}$ and $\text{ErCl}_3 \cdot 6\text{H}_2\text{O}$ respectively.

As could be anticipated looking at fig. 1.5, a satisfactory fit of the Er data can be obtained using only a $1/T^2$ term in the expansion. Attempts to fit the data to an expansion containing higher powers of $1/T$ result in b_i values which do not alternate in sign and/or do not decrease monotonically in absolute value, irrespective of constraining one or more of the b_i values. In contrast, the Dy data can be fitted reasonably if more terms are used than the one with b_2 . For free b_i values, a good fit can be obtained with three terms in the expansion. Constraining b_2 or b_2 and b_3 does not change the overall behaviour, although the values of the higher coefficients fluctuate considerably. The values of the b_i are shown in table 1.7 for values M_s of the number of terms in the expansion where the variance δ stabilizes. The

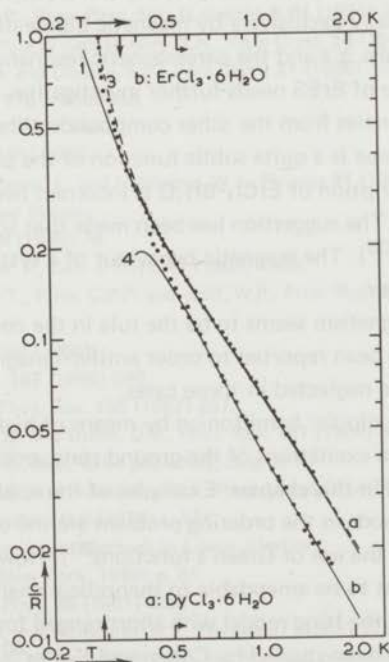


Fig. 1.5. High-temperature specific heat of $\text{DyCl}_3 \cdot 6\text{H}_2\text{O}$ (a) and $\text{ErCl}_3 \cdot 6\text{H}_2\text{O}$ (b).

The transition points and the ranges of the fit to eq. (1.1.3) are shown on the temperature axes. See text.

computed errors probably underestimate the real errors, but with some care, they can be used as a measure of physical significance. The fits labelled 1, 3 and 4 are shown in fig. 1.5, with their continuation to lower temperatures. The extrapolation is particularly good for $\text{DyCl}_3 \cdot 6\text{H}_2\text{O}$, indicating that the specific heat can be described by eq. (1.1.3) with a rather limited number of terms right into the critical region. Hence a continuation by Padé approximant methods may yield reliable information on the expected critical behaviour. Measurements on the critical behaviour and the susceptibility will be published elsewhere³²).

1.6 Conclusions

Some properties of a number of magnetic substances have been calculated and the results have been compared with experimental data, especially with those on the specific heat. From the high-temperature specific-heat data and from the measured values of the total energy of the ordering, we conclude that CMN, DyES, and $\text{DyCl}_3 \cdot 6\text{H}_2\text{O}$ are good examples of substances which order nearly exclusively by magnetic dipole-dipole interactions. The existing data on the Curie-Weiss Δ 's and the paramagnetic resonance and relaxation data confirm this picture. The case of ErES needs further investigation. $\text{ErCl}_3 \cdot 6\text{H}_2\text{O}$, however, deviates in a number of properties from the other compounds. Whether this means that the behaviour of a dipolar substance is a quite subtle function of the parameters in the complete hamiltonian, or that our description of $\text{ErCl}_3 \cdot 6\text{H}_2\text{O}$ is incorrect needs more experimental and theoretical investigation. The suggestion has been made that some of the trichlorides show ferroelectric transitions³⁶). The magnetic behaviour of a system having a strong electric polarization is not clear.

It is remarkable that ferromagnetism seems to be the rule in the compounds studied. Two other dipolar substances have been reported to order antiferromagnetically³⁷). However, crystal field effects can not be neglected in those cases.

To pursue calculations on the dipolar hamiltonian by means of high-temperature expansions or by means of calculations on excitations of the ground state, one needs more refined techniques than those applied in this chapter. Examples of the application of recently developed mathematical methods in the ordering problem are the use of diagrams in the summation of series^{6, 38}) and the use of Green's functions³⁹). However, the critical behaviour seems at present not to be amendable to theoretical analysis with a precision such as obtained in calculations on the Ising model with short-ranged forces for instance.

The ground-state problem has been studied by Cohen and Keffer⁴⁰) using the spin-wave formalism. From their results, pertaining to cubic lattices, they conclude that there are no large quantum mechanical corrections to the value of the ground-state energy, but some configurations may become unstable. Ferromagnetism at $T=0$ should be impossible in simple cubic lattices.

References

- 1) Weiss, P., *J. Phys.* **6** (1907) 667.
- 2) Van Vleck, J.H., *J. Chem. Phys.* **5** (1937) 320.
- 3) Luttinger, J.M. and Tisza, L., *Phys. Rev.* **70** (1946) 954.
- 4) Daniels, J.M., *Proc. Phys. Soc. (London)* **A64** (1953) 673.
- 5) Peverley, J.R. and Meyer, P.H.E., *Phys. Stat. Sol.* **23** (1967) 353.
- 6) Meyer, P.H.E. and O'Keeffe, D.J., *Phys. Rev. B* **1** (1970) 3786.
- 7) Wielinga, R.F., in 'Progress in low Temperature Physics', vol. VI, ed. C.J. Gorter (North-Holland Publ. Co., Amsterdam and London, 1970) Ch. 8.
- 8) Peverley, J.R., *J. Comp. Phys.* **7** (1971) 83.
- 9) Ewald, P.P., *Ann. Phys.* **64** (1921) 253.
- 10) Wong, S., Dembinski, S.T. and Opechowski, W., *Physica* **42** (1969) 565.
- 11) Niemeier, T., *Physica* **57** (1972) 281.
- 12) Bastmeyer, J.D. and Zimmerman, N.J., private communication.
- 13) Schulz, M.B. and Jeffries, C.D., *Phys. Rev.* **159** (1967) 277.
- 14) Zalkin, A., Forrester, J.D. and Templeton, D.H., *J. Chem. Phys.* **39** (1963) 2881.
- 15) Williamson, S.J., Pradaude, H.C., O'Brien, R.F. and Foner, S., *Phys. Rev.* **181** (1969) 642.
- 16) Ketelaar, J.A.A., *Physica* **4** (1937) 619.
- 17) Cooke, A.H., Edmonds, D.T., McKinn, F.R. and Wolf, W.P., *Proc. Roy. Soc. (London)* **74** (1959) 791.
- 18) Bleaney, B. and Scovil, H.E.D., *Proc. Phys. Soc. (London)* **A 64** (1951) 204.
- 19) Marezio, M., Plettinger, H.A. and Zachariasen, W.H., *Acta Cryst.* **14** (1964) 234.
- 20) Graeber, E.J., Conrad, G.H. and Duliere, S.F., *Acta Cryst.* **21** (1966) 1012.
- 21) Griffiths, R.B., *Phys. Rev.* **176** (1968) 655.
- 22) Sauer, J.A., *Phys. Rev.* **57** (1940) 142.
- 23) Kittel, C., *Phys. Rev.* **82** (1951) 965.
- 24) Mess, K.W., Lubbers, J., Niesen, L. and Huiskamp, W.J., *Physica* **41** (1969) 260 and the references contained therein.
- 25) Hudson, R.P., *Cryogenics* **9** (1969) 76.
- 26) Daniels, J.M. and Felsteiner, J., *Can. J. Phys.* **42** (1964) 1469.
- 27) Cooke, A.H., Edmonds, D.T., Finn, C.B.P. and Wolf, W.P., *Proc. Roy. Soc. (London)* **A 306** (1968) 313, 335.
- 28) Wielinga, R.F., thesis, Leiden (1968).
- 29) Richards, P.M., *Phys. Rev.* **187** (1969) 690.
- 30) Dweck, J. and Seidel, G., *Phys. Rev.* **155** (1967) 267.
- 31) Colwell, J.H., Mangum, B.W. and Utton, D.B., *Phys. Rev.* **181** (1969) 843.
- 32) Lagendijk, E. and Huiskamp, W.J., to be published, chapter II.
- 33) Lagendijk, E., Wielinga, R.F. and Huiskamp, W.J., *Phys. Letters* **31A** (1970) 375.
- 34) Felsteiner, J., *J. Phys. (London)* **C 3** (1970) L 174.
- 35) Faddeeva, V.N., In 'Computational Methods in Linear Algebra' (Dover Publications Inc., New York, 1959) p. 81.
- 36) Eisenstein, J.C., *J. Chem. Phys.* **35** (1961) 2097.
- 37) Wielinga, R.F., Lubbers, J. and Huiskamp, W.J., *Physica* **37** (1967) 375.
Note, however, that all data on the susceptibility are from a.c. measurements. The strong rise of χ'' at T_N (fig. 1.4) for $Gd_2(SO_4)_3 \cdot 8H_2O$ and the behaviour of χ' for $GdCl_3 \cdot 6H_2O$ (fig. 1.6) do not rule out ferromagnetic behaviour.
- 38) Marquard, C.D., *Proc. Phys. Soc. (London)* **92** (1967) 650.
- 39) Becker, E. and Plischke, M., *Phys. Rev. B* **1** (1970) 314.
- 40) Cohen, M.H. and Keffer, F., *Phys. Rev.* **99** (1955) 1135.

CHAPTER II

CALORIC AND MAGNETIC PROPERTIES OF TWO COMPOUNDS HAVING PREDOMINANTLY MAGNETIC DIPOLE-DIPOLE INTERACTIONS: DyCl₃·6H₂O AND ErCl₃·6H₂O

Synopsis

Heat-capacity and susceptibility measurements on DyCl₃·6H₂O and ErCl₃·6H₂O show these compounds to order ferromagnetically at $T_c^{\text{Dy}}=0.289$ and $T_c^{\text{Er}}=0.356$, respectively. From the high-temperature specific-heat data, and from the total energy content of the ordering, it is concluded that dipolar interactions strongly predominate in these compounds. Analysis of the critical behaviour shows that the specific heat of DyCl₃·6H₂O is strongly divergent near T_c ($a_{\pm} \approx 0.5$) and the specific heat of ErCl₃·6H₂O is cusp-like ($a_{\pm} < 0$). Measurements on the heat capacity at a constant applied field, and measurements on the magnetothermal effect, indicate the presence of a phase boundary. Measurements on the heat capacity of Y-diluted samples are also presented.

II.1 Introduction

Caloric and magnetic investigations on ionic compounds which are magnetically dilute may yield interesting information on interactions among magnetic moments other than (super) exchange interactions. For example, the thermodynamic behaviour may be dominated by the (unavoidable) magnetic dipole-dipole (MDD) interactions. Various suggestions for other interactions have been made, such as virtual phonon exchange (VPE), but experimental verifications remain scarce and should be based on a variety of measuring techniques, including calorimetry.

Whether or not a lattice of (classical) magnetic dipoles becomes ferromagnetic at low temperatures is a longstanding question¹), which has more recently been raised again for spin $\frac{1}{2}$ magnetic moments in *e.g.* cerium magnesium nitrate and for nuclear moments in CaF₂. If dipolar interactions can cause magnetic ordering, the transition temperatures are expected to be very low, due to the weakness of the forces. Experimentally, temperatures below the liquid helium region became accessible by the method of adiabatic demagnetization in the years around 1940, and accordingly, the dipolar interaction received much interest in those years^{2,3}). More detailed investigations revealed that exchange interactions remain important in substances containing ions of the *3d* group, even if they are magnetically quite dilute, such as the alums or the tutton salts. The exchange interactions among ions of the *4f* group (the rare earths) are expected to be much weaker, because the *4f*

electrons belong to an inner shell. This is born out by experiments on rare-earth compounds such as the double nitrates and the ethyl sulphates. To study the various interactions among magnetic ions, one attempts to vary the ionic species without appreciably altering the surroundings. In this respect rare-earth ethyl sulphates and anhydrous trichlorides have been studied extensively, in particular by e.s.r. measurements⁴). For the trichloride hexahydrates, however, which build a homologous series from Nd to Lu (including Y) such kind of knowledge is lacking.

Calorimetric experiments on the Gd compound⁵) have shown that dipolar interactions predominate in this case. In the present chapter we report on calorimetric experiments on $\text{DyCl}_3 \cdot 6\text{H}_2\text{O}$ and $\text{ErCl}_3 \cdot 6\text{H}_2\text{O}$. We expect the magnetic interactions in these compounds also to be mainly dipolar and, unlike the case of $\text{GdCl}_3 \cdot 6\text{H}_2\text{O}$, crystal field effects may be negligible at temperatures in the region of the ordering temperature.

We have paid special attention to the ordering phenomenon, because experiments on the critical behaviour of compounds in which long-range forces dominate are interesting, in particular since scaling and universality hypotheses may be tested. It is expected that the critical exponents describing the asymptotic behaviour of the thermodynamic and transport properties near the transition point attain classical (*i.e.* molecular field type) values if the ions interact equally with an infinite number of nearest neighbours. Conceptually, this can be translated into an increase of the lattice dimensionality, d . Recently, Wilson and Fisher⁶) have verified the expectation that the critical exponents should have their classical values already if $d=4$. However, measurements can be performed on at most three dimensional systems, hence the effective number of nearest neighbours can only be increased over the coordination number of the lattice by increasing the range of the interaction. Conversely, the number of nearest magnetic neighbours can be decreased effectively by substitution or addition of diamagnetic ions or ion groups either in an ordered or in a disordered (random) way. This may be equivalent to a decrease of the effective dimensionality.

From a theoretical point of view, the short-ranged exchange forces are much more tractable than the long-ranged dipolar forces, which have a complicated angular dependence. Most of the theoretical work on the properties of magnetic solid systems has concentrated on idealized models of exchange interactions, such as the Ising or the Heisenberg model. Recently, reviews have been published which give a complete account of the present theoretical and experimental status, in particular with respect to the critical behaviour⁷). For dipolar lattices, no essentially new results have been obtained since the work of Van Vleck²) on the high-temperature expansions, of Luttinger and Tisza⁸) on the ground-state calculations, and of Holstein and Primakoff⁹) on the inclusion of dipolar interactions into the spin-wave formalism. The calculational techniques, however, have been improved considerably. Summation by the use of diagrams has been introduced by Marquard¹⁰) and by Meyer and O'Keeffe¹¹). Application of Green's functions in the ordered state has been discussed by Becker and Plischke¹²). The summations necessary to calculate the terms to third order in $1/T$ in the high-temperature expansion of the specific heat have been calculated quite accurately by the use of high-speed computers, see *e.g.* Wong *et al.*¹³).

Some of the afore-mentioned techniques have been applied in the previous chapter¹⁴) to calculate the caloric and magnetic properties of a number of substances which have been reported to be dominantly dipolar, including $\text{DyCl}_3 \cdot 6\text{H}_2\text{O}$ and $\text{ErCl}_3 \cdot 6\text{H}_2\text{O}$. We will refer to this chapter as I in the following. Experiments on the high-temperature specific heat of Dy and Er trichloride hexahydrate have been discussed already at some length in I. In this chapter we will investigate the caloric and magnetic properties of these two substances with special emphasis on the critical and ordered regions.

Data have been obtained on the specific heat in zero and non-zero applied field, on the a.c. and d.c. (ballistic) susceptibilities, and on the magnetothermal effect, in the temperature region between 0.05 and 4 K. The assumption of dominantly dipolar coupling between the rare-earth ions appears to be justified by our measurements. Our data are in reasonable agreement with the interaction parameters obtained by other experimentalists. Our measurements indicate ferromagnetic ordering in both compounds at low temperatures.

II.2 Experimental

Temperatures below 1 K have been obtained by the method of adiabatic demagnetization as described before^{15, 16}). The calorimeter consists of a heat sink at about 15 mK, connected via a superconductive heat switch to the thermally linked system of thermometer, Joule heater and sample. The thermometric parameter can be the electric resistivity of a carbon resistor or the magnetic susceptibility of a magnetic salt.

The use and the calibration of carbon resistance thermometers has been described by Edelstein and Mess¹⁷). We have fitted the measured resistance *versus* temperature (R - T) data by polynomials, such as

$$\log R = \sum_{i=1}^m C_i (\log T)^{i-1} \quad (II.2.1)$$

The polynomial used and the number of coefficients in the expansion depend on the accuracy, the number and the range of the R - T data. It is possible¹⁸) to fit the data of a Speer 220 Ω $\frac{1}{2}$ W resistor within experimental scatter by the polynomial (II.2.1) in the temperature range 0.04-2 K with $m \approx 10$. The error in the absolute temperature determination due to errors in the calibration is estimated to be 1%.

Specific-heat measurements have been done with the heat-pulse method and the continuous heating method. The two methods and the errors involved have been discussed thoroughly in ref. 19. In our case, the errors in the specific-heat (c) data using the heat-pulse method arise mainly from extrapolation errors due to:

- a) relaxation effects,
- b) disturbances on the thermometer, such as sudden heat leaks and electromagnetic pulses,
- c) the temperature-dependent heat leak.

The resultant error can be inferred from the scatter in the data points, and is estimated to be

about 2% outside the critical region. Inside the critical region, $|T - T_c| \lesssim 0.1 T_c$, measurements have been performed with a relative temperature step $\Delta T/T_c \approx 2 \times 10^{-3}$. The relative accuracy of the temperature measurement is about 5×10^{-5} , hence the accuracy of the measurement is a few percent in this region too (see, however, below).

The approximation by finite differences introduces a systematic error, $E(\bar{T})$, where \bar{T} is the mean temperature during a heat pulse starting at T and ending at $T + \Delta T$. According to ref. 19:

$$E(\bar{T}) \approx [24 c(\bar{T})]^{-1} (d^2c/dT^2) \bar{T} \Delta T^2 \quad (11.2.2)$$

This error will only be important if there is a strong curvature on the relative scale.

Long relaxation times have been observed near T_c . Therefore we have compiled the data from various runs with different thermometer calibrations to get a sufficient number of data points in the analysis of the critical behaviour. Because the relative accuracy of the temperature determination at temperatures below 1 K is much better than the absolute accuracy (≈ 1 mK), shifts in the temperature scale are necessary in some cases. Errors in the temperature of the order of the relative accuracy are introduced by these shifts. They can give rise to large errors in the specific-heat data if the specific heat is strongly divergent on the relative temperature scale.

To the errors listed already for the heat-pulse method, we should add the effect of the thermal response time in the case of the continuous method. In our experiments the lattice temperature T_L is measured. It has been shown¹⁶⁾ that the response of T_L on switching a heat current \dot{Q} should be a measure of the spin lattice relaxation time τ according to

$$1/\tau = \dot{Q}/c\Delta T_L \quad (11.2.3)$$

Susceptibility data have been obtained by means of a Hartshorn bridge which can operate in the a.c. and the (quasi) d.c. mode. A frequency of 225 Hz and lock-in detection have been used in the a.c. mode. The static susceptibility is measured with a ballistic galvanometer having a deflection time of about 1 s. If the response time of the magnetization becomes of this order, *e.g.* by the effects of domain relaxations, static magnetization measurements are needed to determine the magnetic behaviour.

The specific heat and the transverse susceptibility can be measured in steady magnetic fields up to 1 kOe with a rotatable Helmholtz coil outside the cryostat. A longitudinal field can be applied utilizing a coil which has its axis parallel to the cryostat axis.

11.3 Crystallographic and magnetic data, sample preparation

The crystal structure of $\text{DyCl}_3 \cdot 6\text{H}_2\text{O}$ and $\text{ErCl}_3 \cdot 6\text{H}_2\text{O}$ is isomorphous to the structure of $\text{GdCl}_3 \cdot 6\text{H}_2\text{O}$ ²⁰⁾, which has been shown by Marezio *et al.*²¹⁾ to be monoclinic with space group $C_{2h}^4 (P_2/n)$. Those data of refs 20 and 21 which are relevant for our discussion are

collected in table 1. The two rare-earth ions in the crystallographic unit cell are magnetically equivalent.

Table II.1. Crystallographic data.

	Mol. Wt.	A(Å)	B(Å)	C(Å)	β	$\rho(\text{g/cm}^3)$	ion positions
DyCl ₃ ·6H ₂ O	376.94	9.61	6.49	7.87	93.65°	2.53	$\left\{ \begin{array}{l} \frac{1}{4}, 0.1521, \frac{1}{4} \\ \frac{3}{4}, 0.8479, \frac{3}{4} \end{array} \right.$
ErCl ₃ ·6H ₂ O	381.72	9.57	6.47	7.84	93.65°	2.59	

The crystal structure is shown in fig. II.1. It is visualized most easily as a collection of chains along the monoclinic (*B*) axis. Each ion, *e.g.* 0 in fig. II.1, has two first neighbours at 6.33 Å and 6.30 Å (1 and 2 in fig. II.1) for the Dy and Er compound respectively. Two second neighbours (3 and 4 in fig. II.1) are positioned at 6.49 Å (6.47 Å) and two third neighbours (5 and 6 in fig. II.1) are at 6.70 Å (6.67 Å). Loosely speaking, we can qualify these six ions as nearest neighbours. There are four 'next nearest' neighbours at about 8.4 Å.

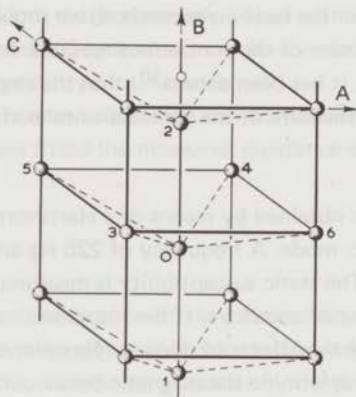


Fig. II.1 Crystal structure of XCl₃·6H₂O (X=Nd. . .Lu, Y). Two monoclinic unit cells are shown, each containing two rare-earth ions. The 'nearest neighbours' of one of the ions (0) are numbered. Equal distances occur in pairs: (1,2), (3,4) and (5,6).

The magnetic properties of the rare-earth ions are determined by the splitting of the ground state of the free ions due to the crystal field at the ionic site. The ground states of Dy³⁺ and Er³⁺ are ⁶H_{15/2} and ⁴I_{15/2} respectively. The ions are surrounded in the hydrated trichlorides by a [Cl₂(OH₂)₆] complex with a twofold axis as the only symmetry element. Hence it is expected that the ground state will split into a number of Kramers doublets, with the *B* axis

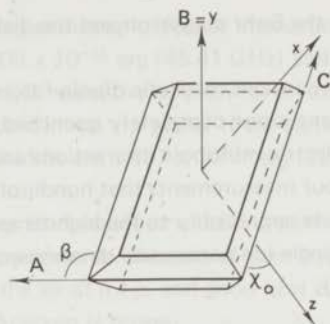


Fig. 11.2. The orientation of the principal axes (x, y, z) of the g tensor compared to the crystallographic axes (A, B, C).

as a magnetic symmetry axis. This is confirmed by optical and paramagnetic resonance measurements^{22,23}), which also have shown that the other magnetic principal axes are not simply related to the crystal axes. It has been conjectured that the magnetic z axis (axis of maximum g) should be an axis of pseudohexagonal symmetry²⁴). The two systems of axes for the ground doublet are pictured in fig. 11.2, which has been taken from ref. 23 (however, the correct identification of the crystallographic axes has been used).

The splitting, expressed in temperature units, between the ground doublet and the next higher doublet is 49 K for $\text{DyCl}_3 \cdot 6\text{H}_2\text{O}$ and 24.5 K for $\text{ErCl}_3 \cdot 6\text{H}_2\text{O}$, according to paramagnetic relaxation measurements on Y-diluted samples²³). Hence below 1 K, only the lowest doublet is populated and we can use the spin hamiltonian formalism to describe the magnetic properties at very low temperatures. The spin hamiltonian which will be adopted in this chapter is:

$$\mathcal{H} = \mathcal{H}_0 + \mathcal{H}_{\text{hfs}} + \mathcal{H}_Z \quad (11.3.1)$$

$$\text{where } \mathcal{H}_0 = \sum_{i < j} S_i^{\alpha} P_{ij}^{\alpha\beta} S_j^{\beta} \quad (11.3.2)$$

$$\mathcal{H}_{\text{hfs}} = \sum_i I_i^{\alpha} A^{\alpha\beta} S_i^{\beta} \quad (11.3.3)$$

$$\mathcal{H}_Z = H^{\alpha} \mu_B \sum_i g_i^{\alpha\beta} S_i^{\beta} \quad (11.3.4)$$

$P_{ij}^{\alpha\beta}$ is the interaction tensor, assumed to be of the form:

$$P_{ij}^{\alpha\beta} = \mu_B^2 \frac{g_i^{\alpha\alpha} g_j^{\beta\beta}}{r_{ij}^3} - 3 \frac{g_i^{\alpha\lambda} g_j^{\beta\nu} r_{ij}^{\lambda} r_{ij}^{\nu}}{r_{ij}^5} + J_{ij}^{\alpha\beta} \quad (11.3.5)$$

The dummy suffix summation convention is applied to Greek suffices. The symbols S^{α} , I^{α} , $A^{\alpha\beta}$, H^{α} , $g^{\alpha\beta}$, μ_B and r_{ij} stand for the effective electron spin ($S = 1/2$ in this case), the nuclear spin, the hyperfine interaction tensor, the external magnetic field, the g tensor or

spectroscopic splitting factor, the Bohr magneton and the distance between the i 'th and j 'th dipole respectively.

The interaction tensor (11.3.5) contains magnetic dipole forces and exchange forces $J_{ij}^{\alpha\beta}$. In general, if the orbital moment is not completely quenched, the interaction will contain other contributions, such as electric multipole interactions and virtual phonon exchange²⁵). We have no indications from our measurements that nondipolar interactions, including the exchange interaction, contribute appreciably to the high-temperature specific heat and the total energy, if we adopt the single ion parameters determined by the optical and resonance measurements^{22,23}).

Table 11.2. Magnetic data.

	X_0	g_x	g_y	$g_{\perp} = \frac{1}{2}(g_x + g_y)$	$g_z = g_{\parallel}$	isotope	abundance	A_z/k	b_N	ref.
DyCl ₃ ·6H ₂ O	-23°	2	1.52	1.76	16.52	161	19%	0.0677	} 0.00232	23
	-23.8°	1.8	1.66	1.73	18.06	163	25%	0.0961		26
		0	0	0	16	161	19%	0.0647	27	
ErCl ₃ ·6H ₂ O	77°	0	1.26	0.58 < g_{\perp} < 0.92 ^{a)}	13.74	167	23%	0.0683	0.00141	23
	76°			0.63	13.26					22

a) The mean value $g_{\perp}=0.75$ was taken in all our calculations.

The measured values of some of the parameters in the spin hamiltonian (11.3.1) are collected in table 11.2. There is strong anisotropy: $g_z \gg g_x \approx g_y$. The g values indicate that the ground doublet has dominant contributions from the $J_z = |\pm 15/2\rangle$ states hence we expect the interactions to be Ising like²⁸). Due to the large distances between the magnetic ions and the localized nature of the $4f$ orbitals, direct exchange will be negligible. Superexchange interactions are very sensitive to the number of intervening ligands, as can be inferred from the large decrease in the superexchange interaction measured within a pair of rare-earth ions in the ethyl sulphates compared to measurements on the same pair in the anhydrous trichlorides, where $|J_{ij}/k|$ amounts to a few kelvin. The decrease, being a factor of about 100 per added ligand, is also observed for ions of the $3d$ group, for instance, if one compares the transition points of anhydrous compounds with similar hydrated compounds, for example Cs₂MnCl₄·2H₂O and β -Cs₂MnCl₄²⁹). Hence we expect superexchange interactions to be of the order of a few hundredths kelvin in the hydrated trichlorides. Assuming the other short-ranged interactions to be of the same order or less, the behaviour of DyCl₃·6H₂O and ErCl₃·6H₂O at low temperatures will be dominated by magnetic dipole-dipole interactions between the effective spins. Its strength can be estimated from the value of the molecular field constant, $4\pi C/3$, which amounts to a few tenths of a kelvin (C is the mean Curie constant). The actual situation can very well be approximated by an axially symmetric g tensor, having $g_{\parallel}=g_z$ and $g_{\perp}=\frac{1}{2}(g_x+g_y)$. The g values of Schulz and Jeffries²³) have been used in all calculations. Results of calculations on the high-temperature specific heat, the Curie-Weiss Δ and the ground-state energy are collected in I. The full widths at half height of the resonance

lines can be calculated assuming anisotropic dipolar interactions³⁰). If the static fields are along the z axis, these are 3.008×10^{-16} erg (45.41 GHz) and 1.889×10^{-16} erg (28.42 GHz) for $\text{DyCl}_3 \cdot 6\text{H}_2\text{O}$ and $\text{ErCl}_3 \cdot 6\text{H}_2\text{O}$ respectively. Even for an axially asymmetric g tensor, the linewidth is (slightly) anisotropic in the x - y plane. If the static field is perpendicular to z and in the B - C plane, the linewidths are 1.497×10^{-16} erg (22.58 GHz) and 0.947×10^{-16} erg (14.30 GHz).

Single crystals which are grown from aqueous solutions starting from 99.9% pure rare-earth oxides have been used in all experiments. Because of their hygroscopicity they are difficult to handle. Protection against the air at n.t.p. and good heat contact at low temperatures can be achieved by ample use of Apiezon N grease.

11.4 Specific heat in zero applied field

Results of heat-capacity measurements on $\text{DyCl}_3 \cdot 6\text{H}_2\text{O}$ and $\text{ErCl}_3 \cdot 6\text{H}_2\text{O}$ obtained in zero external field are shown in fig. 11.3 and 11.4 respectively. The high-temperature behaviour of the specific heat has been discussed in I. The general behaviour in particular with respect to the energy and the entropy involved in the ordering, the critical behaviour, and the behaviour at low temperature will now be discussed in this sequence.

11.4-1 General behaviour, energy and entropy

From the specific heat we can derive the energy and entropy content of the system in the region of the measurement by numerical integration of the data. Because we are primarily interested in the contributions from the electronic spins, we have to subtract the contributions to the heat capacity from other sources. The lattice contribution, $c/R \approx 0.00028 T^3$ according to Pfeffer³¹), has been neglected. The hyperfine specific heat will contribute appreciably only at very low temperatures ($T \lesssim 0.2$ K). We can use the high-temperature approximation:

$$c_{\text{hfs}} T^2/R = A^2/(l+1)/12k^2 \equiv b_N \quad (11.4-1.1)$$

A small change in this correction due to the vanishing of long-range order at $T > T_c$ has been neglected. From our experiments, a value $b_N^{\text{Dy}} = 0.0016 \text{ K}^2$ can be derived in the case of $\text{DyCl}_3 \cdot 6\text{H}_2\text{O}$. This value has to be compared with the calculated value $b_N^{\text{Dy}} = 0.0023 \text{ K}^2$ if one uses the e.p.r. data of ref. 23. The difference can be attributed to long nuclear spin-lattice relaxation times. These effects make a reliable subtraction of the h.f.s. contribution from the measured data difficult. The dashed curve shown in fig. 11.3 and the energy and entropy data have been obtained by subtracting a mean value $b_N^{\text{Dy}} = 0.002 \text{ K}^2$. Because b_N^{Er} could not be obtained from our specific-heat data, we have used the full value from the e.p.r. data, viz. $b_N^{\text{Er}} = 0.0014 \text{ K}^2$.

Data on the energy and entropy at all temperatures can be obtained by suitable extrapolation procedures. At low temperatures, an exponential decay can be expected (11.4-8).

Table II.3. Specific heat (c/R) in mol^{-1} , energy (E/R) in K, entropy (S/R) versus temperature T in K.

a: $\text{DyCl}_3 \cdot 6\text{H}_2\text{O}$							
T	c/R	$-E/R^a$	S/R^a	T	c/R	$-E/R^a$	S/R^a
0	0	0.317 ^{b)}	0	0.3706	0.3627	0.168	0.534
0.1495	0.1092			0.3809	0.3373	0.164	0.544
0.1632	0.1167			0.3996	0.3051	0.158	0.558
0.1713	0.1256			0.4205	0.2774	0.153	0.572
0.1812	0.1447			0.4425	0.2422	0.148	0.585
0.1901	0.1654			0.4603	0.2267	0.143	0.594
0.2007	0.2003	0.313	0.024 ^{b)}	0.4842	0.2095	0.138	0.604
0.2103	0.2388	0.312	0.031	0.5060	0.1934	0.134	0.613
0.2200	0.2946	0.309	0.040	0.5415	0.1723	0.128	0.624
0.2290	0.3564	0.307	0.052	0.5857	0.1509	0.121	0.637
0.2400	0.4677	0.303	0.069	0.6207	0.1391	0.116	0.645
0.2489	0.5876	0.298	0.087	0.6554	0.1269	0.112	0.652
0.2596	0.8018	0.291	0.114	0.6939	0.1162	0.108	0.659
0.2694	1.136	0.282	0.149	0.7433	0.1048	0.102	0.668
0.2802	2.010	0.267	0.206	0.7882	0.0955	0.098	0.671
0.2850	3.455	0.254	0.250	0.8290	0.0890	0.094	0.676
0.2875	6.991	0.241	0.297	0.8725	0.0789	0.091	0.681
0.2881	26.66	0.232	0.327	0.9208	0.0715	0.087	0.685
0.2883	9.425	0.227	0.345	0.9757	0.0655	0.083	0.689
0.2893	3.889	0.221	0.364	1.049	0.0581	0.079	0.693
0.2949	1.478	0.211	0.401	1.131	0.0513	0.074	0.697
0.3005	0.9885	0.205	0.422	1.269	0.0430	0.068	0.702
0.3101	0.7427	0.196	0.449	1.331	0.0394	0.065	0.705
0.3195	0.6196	0.191	0.468	1.457	0.0346	0.060 ^{b)}	0.708
0.3308	0.5180	0.185	0.487	∞	0	0	0.728 ^{b)}
0.3405	0.4676	0.180	0.401				
0.3511	0.4202	0.175	0.514				
0.3622	0.3832	0.171	0.526				
b: $\text{ErCl}_3 \cdot 6\text{H}_2\text{O}$							
0	0	0.274 ^{b)}	0	0.3553	4.212	0.118	0.526
0.1431	0.09300	0.274	0.002 ^{b)}	0.3555	2.590	0.117	0.528
0.1495	0.09803	0.274	0.003	0.3557	1.307	0.116	0.529
0.1622	0.1124	0.273	0.007	0.3559	0.7154	0.116	0.530
0.1693	0.1246	0.273	0.010	0.3569	0.5812	0.115	0.531
0.1824	0.1553	0.271	0.017	0.3600	0.5258	0.114	0.536
0.1912	0.1776	0.270	0.023	0.3705	0.3892	0.109	0.548
0.2006	0.2201	0.269	0.031	0.3800	0.3424	0.106	0.557
0.2130	0.2589	0.266	0.043	0.3977	0.2867	0.101	0.571
0.2208	0.2926	0.264	0.051	0.4233	0.2389	0.094	0.587
0.2303	0.3379	0.262	0.063	0.4538	0.2000	0.088	0.601
0.2392	0.3919	0.259	0.076	0.4896	0.1682	0.081	0.615
0.2523	0.4812	0.254	0.098	0.5326	0.1400	0.075	0.628
0.2601	0.5431	0.250	0.113	0.5829	0.1168	0.069	0.639
0.2731	0.6546	0.242	0.141	0.6418	0.09649	0.063	0.649
0.2838	0.7853	0.234	0.169	0.7090	0.08038	0.057	0.657
0.2901	0.8665	0.229	0.186	0.7487	0.07195	0.054	0.661
0.3022	1.056	0.218	0.224	0.7909	0.06503	0.052	0.665
0.3134	1.244	0.205	0.265	0.8361	0.05771	0.049	0.668
0.3234	1.516	0.192	0.308	0.8866	0.05186	0.046	0.672
0.3296	1.713	0.182	0.338	0.9434	0.04631	0.043	0.675
0.3400	2.180	0.162	0.398	1.004	0.04172	0.041 ^{b)}	0.677
0.3505	3.139	0.135	0.476	∞	0	0	0.697 ^{b)}

^{a)} Corrected for h.f.s. contribution. See text.^{b)} From extrapolations.

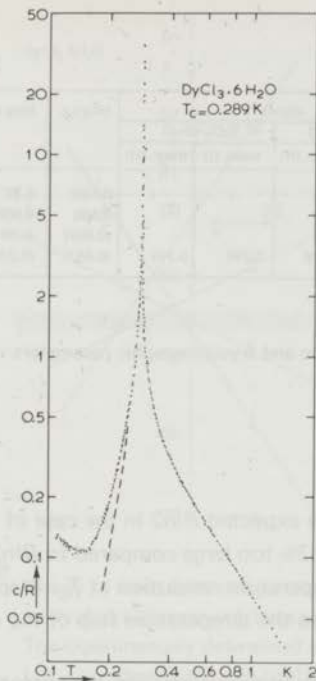


Fig. II.3

Fig. II.3. Specific-heat data of $\text{DyCl}_3 \cdot 6\text{H}_2\text{O}$ versus temperature at zero applied field. Note the very high maximum value: $c/R_{\text{max}} \approx 40$. Dashed curve is obtained after subtraction of the hyperfine specific heat.

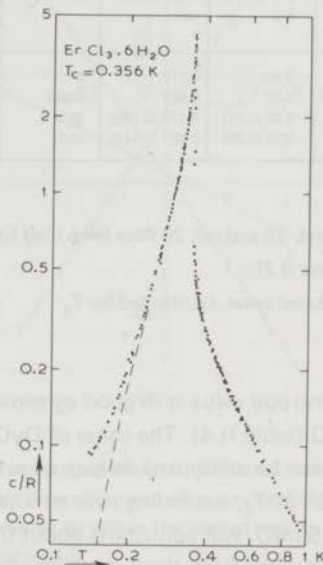


Fig. II.4

Fig. II.4. Specific-heat data of $\text{ErCl}_3 \cdot 6\text{H}_2\text{O}$ versus temperature at zero applied field. Dashed curve is obtained after subtraction of the hyperfine specific heat.

At high temperatures, the series expansions obtained in I can be used for extrapolating the data.

Data on the measured specific heat, and data on the energy and entropy obtained from the corrected specific-heat data with the extrapolation procedures mentioned above are shown as a function of temperature in table II.3. The errors in the $\text{ErCl}_3 \cdot 6\text{H}_2\text{O}$ data amount to about 2%. The errors in the $\text{DyCl}_3 \cdot 6\text{H}_2\text{O}$ energy and entropy data are somewhat larger, mainly because of the strong divergence at T_c . Insufficient temperature resolution close to T_c , may result in sizeable errors on numerical integration due to the finite step method which has been applied (trapezium rule). The total and critical values of the energy and the entropy are collected in table II.4.

Table II.4. Energy and entropy values.

thermodynamic quantity	DyCl ₃ ·6H ₂ O exp.	ErCl ₃ ·6H ₂ O exp.	molec. field	dipolar ^{a)}				Ising s.c.	Ising sq.
				DyCl ₃ ·6H ₂ O		ErCl ₃ ·6H ₂ O			
				theor. (I)	theor. (II)	theor. (I)	theor. (II)		
(S _∞ - S _c)/R	0.40	0.172	0					0.133	0.387
S _c /R	0.32	0.527	0.693					0.560	0.306
-E _c /R	0.32 (1.11)	0.272 (0.765)	(0.5)					(0.665)	(0.881)
(E _c - E ₀)/R	0.08 (0.29)	0.157 (0.442)	(0.5)	0.338	0.316	0.246	0.244	(0.447)	(0.275)

^{a)} Values of ref. 23 and ref. 20 have been used for the magnetic and crystallographic parameters (tables II.1 and II.2).

() means reduced value, *i.e.* divided by T_c .

The total entropy value is in good agreement with the expected $R \ln 2$ in the case of ErCl₃·6H₂O (table II.4). The value of DyCl₃·6H₂O is 3% too large compared to $R \ln 2$. This difference can be attributed to lack of sufficient temperature resolution at T_c . A specific-heat value of $50R$ at T_c , extending over an interval equal to the temperature step of the measurement (≈ 0.5 mK), will contribute about 0.05 to S/R .

The contributions from short- and long-range ordering to the energy and the entropy are quite different in the case of DyCl₃·6H₂O and ErCl₃·6H₂O. The large value of the short-range ordering entropy in DyCl₃·6H₂O is a common feature of some other dipolar compounds, see I.

II.4.2 Energy, compared to calculations

Assuming exclusively dipolar interactions, the ground-state energy and the ground-state magnetic configuration can be calculated according to the method of Luttinger and Tisza⁸⁾, see I. Due to the Ising-like interactions one expects this method to yield quantitatively good results. The calculated values of the total energies in the demagnetized ferromagnetic (FM) ground state (I) and the antiferromagnetic (AFM) first excited state (II) using data from tables II.1 and II.2 are included in table II.4. The same ground state (I) was obtained, when applying the iterative method described in I. Calculated data on the molecular field model and the 3-d Ising model have been included too, since these models may be appropriate approximations. The experimental data on the Er compound are in reasonable agreement with 3-d Ising model predictions. The data on the Dy compound, however, show a large contribution to the energy and the entropy from the region above T_c . An increase of the short-range ordering contribution to the energy and the entropy is observed in Ising model calculations if one lowers the dimension. Hence, for comparison, 2-d Ising model values have been included.

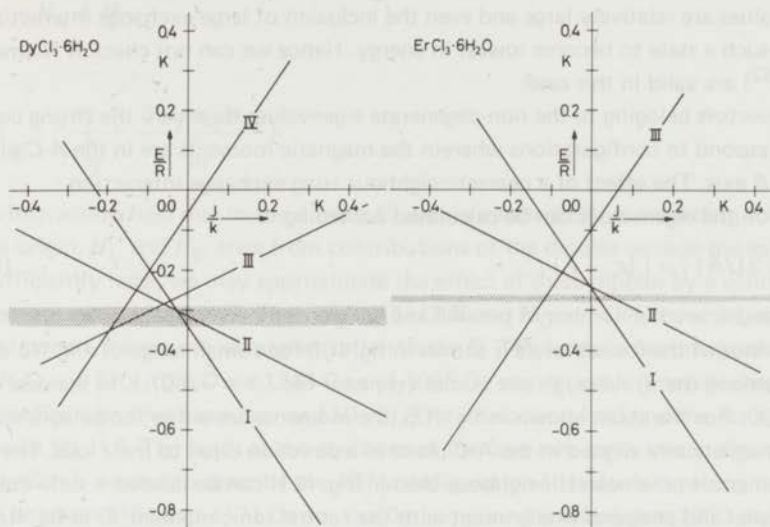


Fig. 11.5. Energy of some spin configurations *versus* the exchange parameter calculated according to the method of Luttinger and Tisza assuming dipolar interaction and Ising n.n. exchange interaction. The experimentally determined values of the energy lie within the shaded regions. The labels I, II denote the spin configuration, see table II.5.

As can be seen from table II.4 and fig. 11.5, the calculated (dipolar) and measured values of the energy agree quite well. However, there are too many uncertainties in the calculated and measured data to decide whether the FM configuration (I) or the AFM configuration (II) is favoured. A possible source of error is the use of erroneous g values in the calculation. E.s.r. measurements on concentrated samples⁵¹⁾ show g_z to be appreciably smaller than reported in the literature^{22,23)}. Moreover, a complicated resonance pattern is observed in the case of $\text{ErCl}_3 \cdot 6\text{H}_2\text{O}$. A different g_z value shifts the calculated energy values but does not alter the sequence of the eigenstates in first approximation. Another source of error is the neglect of exchange interactions. Inclusion of exchange interactions does not only shift the energy values but also causes some states to decrease in energy compared to others. To study this effect, we have to examine the ground-state calculation more extensively. The solution of the Luttinger and Tisza eigenvalue problem using the completely doubled crystallographic unit cell as a magnetic unit cell yields 48 energy values and spin configurations. Due to the low crystal symmetry only twofold degeneracies occur. The configurations are the same in $\text{DyCl}_3 \cdot 6\text{H}_2\text{O}$ and $\text{ErCl}_3 \cdot 6\text{H}_2\text{O}$, but the corresponding energy values are in a different sequence if arranged according to magnitude. There are twelve twofold degenerate eigenvalues. We have not tried to combine the two eigenvectors belonging to such an eigenvalue to new vectors which satisfy the so-called 'strong constraint', because the correspond-

ing eigenvalues are relatively large and even the inclusion of large exchange interaction does not cause such a state to become lowest in energy. Hence we can not check if Niemeier's theorems³²⁾ are valid in this case.

The eigenvectors belonging to the non-degenerate eigenvalues do satisfy the strong constraint. They correspond to configurations wherein the magnetic moments are in the *A-C* plane or along the *B* axis. The effect of a nearest-neighbour Ising exchange interaction $-2J S_i^z S_j^z$ on the eigenvalues can be calculated according to:

$$|\partial(E/R) / \partial(J/k)| = |z_+ - z_-|, \quad (11.4-1.2)$$

where z_+ and z_- are the number of parallel and antiparallel nearest neighbours respectively.

The behaviour of the lowest levels is shown in fig. 11.5 for a small range of J/k . No degenerate cases are among them, although one comes very near for $J/k \approx -0.07$ K in the case of $\text{ErCl}_3 \cdot 6\text{H}_2\text{O}$. For the states shown in fig. 11.5, the moments are either ferromagnetically or antiferromagnetically aligned in the *A-C* plane in a direction close to the *z* axis. The directions of the moments in the nearest-neighbour cluster (fig. 11.1) can be labeled + or - corresponding to parallel and antiparallel alignment with the central ionic moment (0 in fig. 11.1) respectively, see table 11.5.

Table 11.5. Spinconfiguration of nearest neighbours 1 6, see figs. 11.1 and 11.5.

	I		II		III		IV
	Dy	Er	Dy	Er	Dy	Er	Dy
E/R ($J/k=0$)	-0.338	-0.246	-0.316	-0.244	-0.253	-0.098	-0.053
1	+	+	-	-	-	-	-
2	+	+	-	-	-	-	-
3	+	+	+	+	-	-	-
4	+	+	+	+	-	-	-
5	+	+	+	+	+	-	-
6	+	+	+	+	+	-	-

It is clear from fig. 11.5 that in this approximation the experimental values can be explained only if the value of J/k is slightly positive or relatively strongly negative. Results of calculations on the high-temperature specific heat adopting this negative J value lie definitely outside the experimental error.

11.4-3 Dipolar fields

The dipolar fields at the rare-earth sites in the configurations (I) and (II) have been calculated by a lattice summation. The resultant field H_R is given by

$$H_R = H_I + H_L + H_D$$

where

$$H_I = \sum_{r_{oj} < R} \left(-\frac{\mu_j}{r_{oj}^3} + \frac{3(\mu_j \cdot r_{oj})r_{oj}}{r_{oj}^5} \right).$$

H_I is the interaction field due to the dipoles (j) within a sphere (R) surrounding the dipole (0) in the origin. H_L and H_D arise from contributions of the dipoles outside the sphere. If R is sufficiently large, we may approximate the effect of these dipoles by a volume distribution of magnetization M . Then $H_L = (4\pi/3)M$ and $H_D = -DM$, assuming an ellipsoidal sample shape with demagnetization factor D . The fields in ferromagnetic $DyCl_3 \cdot 6H_2O$ and $ErCl_3 \cdot 6H_2O$ are 1249 Oe and 1065 Oe respectively. A needle-shaped domain configuration has been assumed ($D=0$). The interaction field and the resultant field are shown in fig. 11.6. The fields at the positions of the four rare-earth ions in the magnetic unit cell which is needed to describe the AFM configuration (II) (doubling along the B axis only) are between 1151 and 1171 Oe for the Dy compound and between 1050 and 1065 Oe for the Er compound. They are aligned approximately along the magnetic z axis (fig. 11.6).

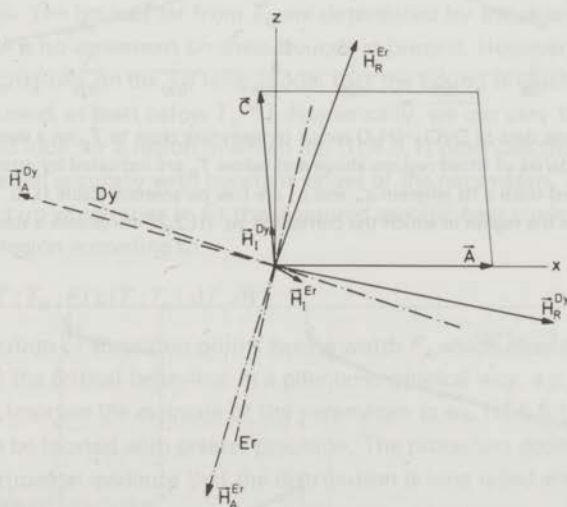


Fig. 11.6. Dipolar fields in ordered $DyCl_3 \cdot 6H_2O$ and $ErCl_3 \cdot 6H_2O$. Full vectors: FM configuration, \vec{H}_R is the resultant field, \vec{H}_I is the interaction field. The Lorentz field, $\vec{H}_L = \vec{H}_R - \vec{H}_I$ is not indicated. Dashed vectors: AFM configuration, only one direction shown. Dash-dotted lines: magnetic z axes. The crystallographic axes and the vectors are (separately) to scale.

11.4.4 Critical behaviour

The critical behaviour is shown in more detail in figs. 11.7 and 11.8. We will first discuss the general methods which have been developed to analyse divergences in the specific heat. Thereafter we will give the results of the analysis for $\text{DyCl}_3 \cdot 6\text{H}_2\text{O}$ and $\text{ErCl}_3 \cdot 6\text{H}_2\text{O}$ separately. The discussion of the results in terms of critical exponent theory will be postponed until after the results on the heat-capacity measurements in applied field and the susceptibility measurements have been given (11.9).

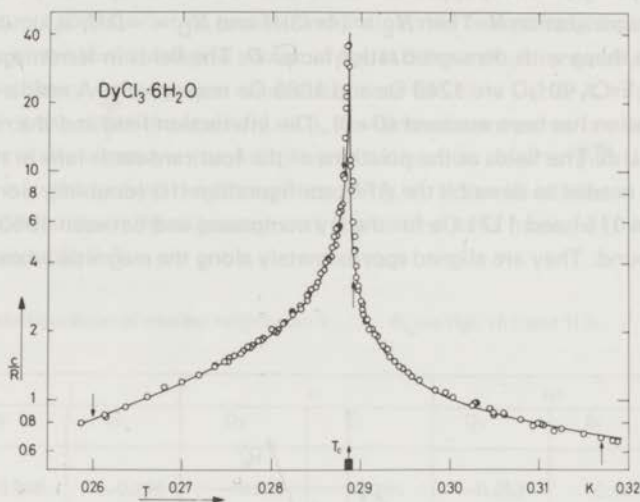


Fig. 11.7. Specific-heat data of $\text{DyCl}_3 \cdot 6\text{H}_2\text{O}$ versus temperature close to T_c on a semilogarithmic scale. The boundaries of fitted regions above and below T_c are indicated by arrows. The full curve is calculated from a fit wherein a_+ and a_- are free parameters (table 11.6). The black spot at T_c denotes the region in which the correction eq. (11.2.2) introduces a sizeable error.

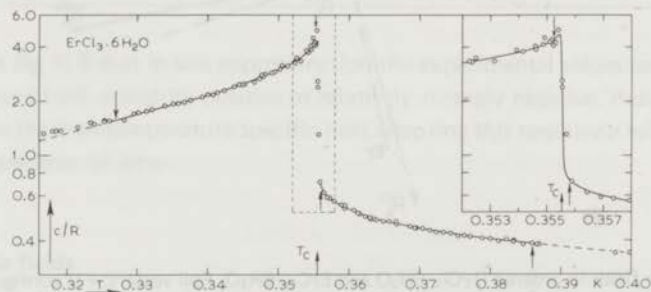


Fig. 11.8. Specific-heat data of $\text{ErCl}_3 \cdot 6\text{H}_2\text{O}$ versus temperature close to T_c on a semilogarithmic scale. Compare fig. 11.7. The inset shows the calculated rounded specific-heat curve (table 11.6).

11.4-5 Analysis of specific-heat curves near T_c

The analysis of data on the specific heat near a transition point has been described before³³). It is good practice to start with a comparison of the general shape of the curve with appropriate model calculations. Presumably, a good approximation in our case is the longitudinal dipolar interaction on a monoclinic lattice. No detailed calculations of the thermodynamic properties of such a system near or below T_c exist at present. Concentrating on the range of the interaction we may expect molecular field type behaviour, while concentrating on the anisotropy of the interaction, the three dimensional Ising model may be appropriate. The shape of the specific-heat curve of $\text{ErCl}_3 \cdot 6\text{H}_2\text{O}$ is somewhat reminiscent of the 3-d n.n. simple cubic Ising model with $S=1/2$. The shape of the $\text{DyCl}_3 \cdot 6\text{H}_2\text{O}$ curve, however, is widely different from that of either model, as can also be inferred from the critical values of the entropy and the energy (table 11.4).

Next, one can apply a critical exponent analysis on the data near T_c . This means that one tries to fit the measured specific-heat data in a certain region by a simple power law:

$$c/R = Q_{\pm} + P_{\pm} (1 - \epsilon_{\pm}^{-a_{\pm}}) / a_{\pm} \quad (11.4-5.1)$$

where $\epsilon_{\pm} = 1 - (T_c/T)^{\pm 1}$. This can be done graphically, if the second term is dominant, or by least-squares methods on a computer.

The temperature region in which eq. (11.4-5.1) is a good approximation is called the critical region. Experimentally, it is bounded close to T_c by the rounding effects observed in many detailed experiments. The bounds far from T_c are determined by the extent of the validity of the theory. There is no agreement on these bounds at present. However, recently it has been shown by calculations on the 3-d Ising model that the bound is much closer to T_c than previously assumed, at least below T_c ³⁴). Numerically, we can vary the bounds within reasonable limits and look for a region in which eq. (11.4-5.1) describes the specific-heat data within the experimental accuracy with constant values of the parameters. An iterative procedure can be set up which tries to fit the measured specific-heat curve also in the rounded transition region according to:

$$c_{\text{sample}}/R = \int_0^{\infty} D(T; T_c, F) c(T; T_c) dT_c/R \quad (11.4-5.2)$$

where D is a distribution of transition points having width F , which describes the influence of imperfections on the critical behaviour in a phenomenological way, e.g. a gaussian¹⁵). This procedure will improve the estimate of the parameters in eq. (11.4-5.1), because the transition point can be located with greater precision. The procedure depends on the choice of D . There is experimental evidence that the distribution is long tailed and/or asymmetric in specific cases^{35, 36}).

11.4-6 $\text{DyCl}_3 \cdot 6\text{H}_2\text{O}$

The specific-heat anomaly in $\text{DyCl}_3 \cdot 6\text{H}_2\text{O}$ reaches a very high value and on our scale, it appears to be unbounded. Hence there is a distinct possibility of a first-order phase transition.

To investigate this further, we have used the continuous heating method. Two heating curves are shown in fig. 11.9. There is no horizontal part in the curves, which should have indicated the presence of a latent heat. The transition point is identified with the inflection point of the heating curve. This point is not uniquely determined, due to insufficient temperature resolution or to intrinsic effects such as relaxations or rounding. The thermal response times given by the difference between the transition points obtained in the same experiment from heat-pulse and continuous-heating measurements or from the temperature fall if the heat current is switched off, are of the order of 10^7 s, according to formula (11.2.3). From the dashed line in fig. 11.9, we estimate the maximum observed heat capacity to be $55R$. The observed width of the maximum is about 0.2 mK.

The strong curvature of the specific heat near T_c will hamper an accurate analysis of heat-pulse data in view of the unavoidable heat leak, because the temperature drifts observed on the recorder before and after the heat pulse will be curved, even in the absence of relaxation. The region where the correction (11.2.2) due to the finite temperature step becomes of the order of $1R$ is indicated by the black dot around T_c in fig. 11.7.

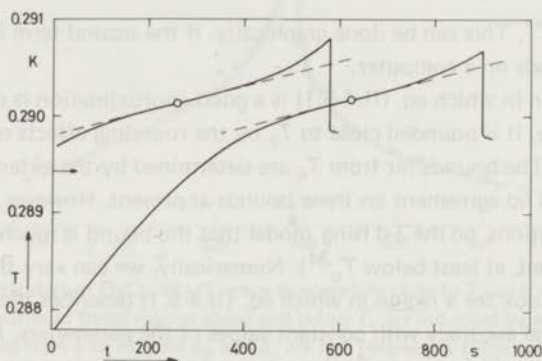


Fig. 11.9. Temperature *versus* time during two continuous heating experiments on $\text{DyCl}_3 \cdot 6\text{H}_2\text{O}$. The circles indicate the estimated transition point. The transition point obtained from heat-pulse measurements is shown by an arrow. Note the sudden change of temperature if the heat current is switched off.

A logarithmic plot of the specific-heat data *versus* ϵ_{\pm} in the range $10^{-4} < \epsilon_{\pm} \lesssim 10^{-1}$ is shown in fig. 11.10. Because the divergence is so strong, the second term in eq. (11.4-5.1) predominates and graphical analysis will probably yield good results. The behaviour can be fitted reasonably well to a pure power law having $a_{\pm} \approx 0.5$, if we choose $T_{c+} = 0.2886$ and $T_{c-} = 0.2884$. Large changes in ϵ_{\pm} near T_c occur if we vary T_c within these bounds, as is indicated by the differences between the open and closed symbols in fig. 11.10. These changes give rise to curvatures in the log plots which invalidate this simple analysis. In our opinion, if there appear to be two transition points in our data, this has to be ascribed to the

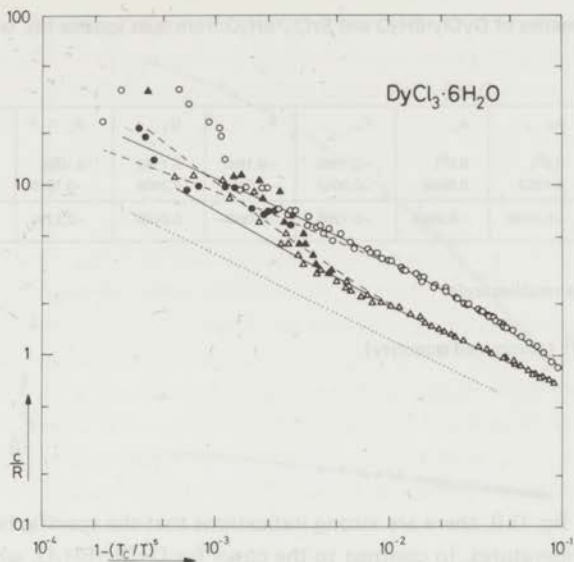


Fig. 11.10. Specific-heat data of $\text{DyCl}_3 \cdot 6\text{H}_2\text{O}$ versus $\epsilon_{\pm} = 1 - (T_c/T)^{\pm 1}$ on a logarithmic scale. Circles: $T < T_c$; triangles: $T > T_c$. Open symbols: $T_c = 0.2886$; the full curves are calculated from a fit on the data having $2 \times 10^{-3} \leq \epsilon_{\pm} \leq 10^{-1}$, see table II.6. Closed symbols: $T_c = 0.2884$, the dashed curves are calculated from a fit on the data having the same ϵ range. A pure power law having $\alpha = 0.5$ is also shown (dotted line).

errors made in the compilation of data of different runs and not to thermal hysteresis, as could occur if the transition changes to first order. Such a change can be induced by the compressibility⁷⁰).

The iterative procedure described in II.4-5 does not converge in the case of $\text{DyCl}_3 \cdot 6\text{H}_2\text{O}$, mainly because the choice of T_c has a strong influence on the analysis, and because no reliable upper bound on c/R can be given. However, fits can be made which describe the heat-capacity curve of $\text{DyCl}_3 \cdot 6\text{H}_2\text{O}$ satisfactorily if we exclude the region close to T_c . The results of such fits are shown in table II.6. The calculated curve, using $T_{c+} = T_{c-} = 0.2886$ and unconstrained a_{\pm} is shown in fig. 11.9 as the full curve. The bounds used in the fit are also indicated in the figure. Varying T_c yields a_{\pm} values which vary between 0.2 and 1, without improving the fit appreciably on either side of T_c .

Concludingly, the strong divergence of the specific heat of $\text{DyCl}_3 \cdot 6\text{H}_2\text{O}$ can be described satisfactorily by eq. (II.4-5.1) in the region $10^{-3} < \epsilon_{\pm} \leq 10^{-1}$ with high values of a_{\pm} .

Although it is not proven, the values $a_{\pm} = 0.5$ seem likely.

Table II.6. Critical parameters of $\text{DyCl}_3 \cdot 6\text{H}_2\text{O}$ and $\text{ErCl}_3 \cdot 6\text{H}_2\text{O}$ from least squares fits, with the constraint $T_{\alpha^+} = T_c = T_{\alpha^-}$.

	$T_c^a)$	a_+	a_-	P_+	P_-	Q_+	Q_-	$\delta_+ (\%)^c)$	$\delta_- (\%)^c)$
$\text{DyCl}_3 \cdot 6\text{H}_2\text{O}$	0.2885	0.5 ^{b)}	0.5 ^{b)}	-0.1058	-0.1847	0.1762	0.1088	46.4	14.06
	0.2886	0.4253	0.5968	-0.0652	-0.2631	0.3608	-0.1910	10.9	8.9
$\text{ErCl}_3 \cdot 6\text{H}_2\text{O}$	0.35553	-0.0688	-0.2648	-0.1205	-2.058	0.0406	-2.212	0.8	2.6

a) T_c is determined on a relative scale.

b) constrained value.

c) $\delta = \Sigma[\Delta(c/R)/(c/R)]^2$ (minimized quantity).

II.4-7 $\text{ErCl}_3 \cdot 6\text{H}_2\text{O}$

As can be seen from fig. II.8, there are strong indications that the specific heat of $\text{ErCl}_3 \cdot 6\text{H}_2\text{O}$ is bounded at all temperatures. In contrast to the curve for $\text{DyCl}_3 \cdot 6\text{H}_2\text{O}$, which remains of a symmetric λ shape on an enlarged temperature scale, the curve for $\text{ErCl}_3 \cdot 6\text{H}_2\text{O}$ shows a strongly asymmetric cusp-like behaviour. Log plots and semi-log plots of c/R vs ϵ_{\pm} are shown in figs. II.11 and II.12. The data points having $T > T_c$ are on a straight line for $10^{-3} < \epsilon_{\pm} < 10^{-1}$ in the semi-log plot, indicating (nearly) logarithmic behaviour.

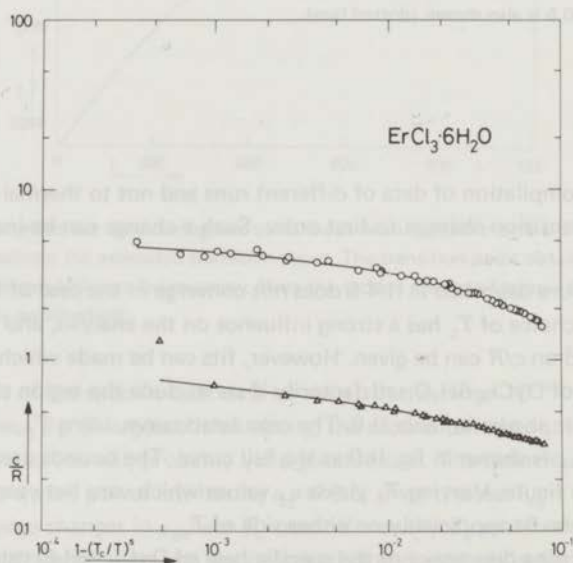


Fig. II.11. Specific-heat data of $\text{ErCl}_3 \cdot 6\text{H}_2\text{O}$ versus $\epsilon_{\pm} = 1 - (T_c/T)^{\pm 1}$ on a logarithmic scale. $\circ: T < T_c; \triangle: T > T_c$. The curves are calculated using the data of table II.6.

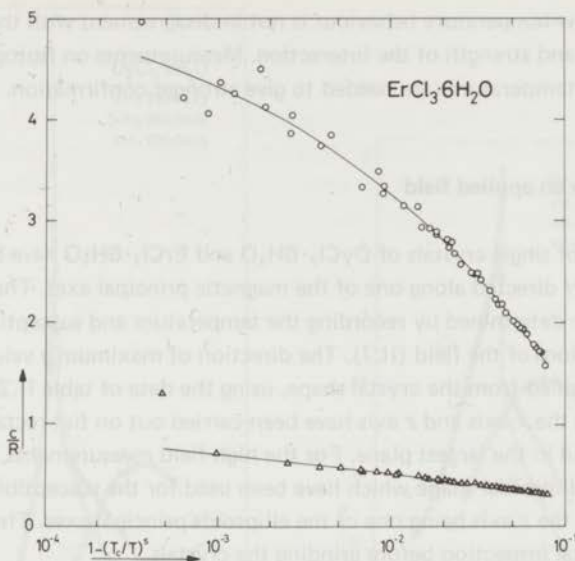


Fig. 11.12. Compare fig. 11.11. A semilogarithmic scale has been used.

If the specific heat remains finite, the first term in eq. (11.4-5.1) is the dominant part, hence $a_{\pm}=0$. In these cases, the (negative) values of a_{\pm} determined from eq. (11.4-5.1), for example from least-squares fits on the data, are called the singular parts of the critical exponents⁷⁾. The iterative procedure is found to converge, yielding values of the parameters which are tabulated in table II.6. A narrow gaussian distribution of transition points ($\Delta T_c/T_c=10^{-4}$) has been assumed and the finite-step method of Wielinga¹⁵⁾ has been used to calculate the rounded curve, which is given by the full curve in fig. 11.8.

11.4-8 Low-temperature behaviour

We expect the electronic heat capacity in both compounds to fall exponentially at very low temperatures, due to the development of an energy gap in these near Ising systems, *viz.*

$$c/R = (\Delta/T)^2 \exp(-\Delta/T) \quad (11.4-8.1)$$

where $\Delta = \mu_B g |H_e|/k$ is the energy gap.

Assuming the effective field H_e to be the field calculated in the ferromagnetic configuration (11.4-1), and $g = g_{\parallel}$, we get $\Delta_{\text{O}}^{\text{Dy}}/k = 1.38$ K and $\Delta_{\text{O}}^{\text{Er}}/k = 0.98$ K for the energy gaps at $T=0$. The specific heat calculated from eq. (11.4-8.1) is in reasonable agreement below 0.2 K with the corrected data of $\text{ErCl}_3 \cdot 6\text{H}_2\text{O}$. In the case of $\text{DyCl}_3 \cdot 6\text{H}_2\text{O}$, the data do not extend to sufficiently low temperatures, but eq. (11.4-8.1) seems a reasonable extrapolation. We

conclude that the low-temperature behaviour is not in disagreement with the assumed spin dimensionality and strength of the interaction. Measurements on isotopically enriched samples at very low temperatures are needed to give stronger confirmation.

11.5 Specific heat in an applied field

The heat capacities of single crystals of $\text{DyCl}_3 \cdot 6\text{H}_2\text{O}$ and $\text{ErCl}_3 \cdot 6\text{H}_2\text{O}$ have been measured in an external field H directed along one of the magnetic principal axes. The positions of these axes have been determined by recording the temperature and susceptibility variations upon adiabatic rotations of the field (11.7). The direction of maximum g value agreed with the direction determined from the crystal shape, using the data of table 11.2. The low-field measurements along the x axis and z axis have been carried out on flat rectangularly shaped crystals with the field in the largest plane. For the high-field measurements, we made samples of an approximate ellipsoidal shape which have been used for the susceptibility measurements as well (11.7), the z axis being one of the ellipsoids principal axes. The z axis was determined by optical inspection before grinding the crystals.

From the results, shown in figs. 11.13 and 11.14, a very slight shift in the paramagnetic region is observed when the field is along the x or y axis, as could be expected from the small corresponding g values. There is no change in the general and the critical behaviour within the accuracy of the measurements in a field of 350 Oe. However, if the field is directed along the z axis, large effects are observed. At 350 Oe, there is only a shift in the paramagnetic region, and some rounding in the critical region, but in a field of 1 kOe, the curve has completely altered its shape. The shifts in the paramagnetic region can be calculated using the methods outlined in I by adding the field-dependent terms to the high-temperature expansion. The contributions to the $1/T^2$ term due to the external field are shown in the figure.

It has been argued³⁷⁾ that the phase diagram of a ferromagnet will be a line from $T=T_c$ to $T=0$ on the T axis in the H - T plane. Measurements on $\text{CuK}_2\text{Cl}_4 \cdot 2\text{H}_2\text{O}$ ³⁸⁾ and EuS ³⁹⁾ in fields well below the molecular field at $T=0$, however, show a behaviour of the specific heat near T_c which closely resembles the (singular) behaviour at $H=0$, except for a shift of the specific-heat maximum to lower temperatures and an increase in the broadening of the peak. At large fields, the maximum shifts again to higher temperatures and the curve flattens over a relatively large temperature interval. In fields very large compared to the interaction between the spins, the specific-heat curve becomes the well known Schottky anomaly. To explain these effects, Arrott⁴⁰⁾ has remarked that a ferromagnet will show a phase transition in a non-zero external field, as long as this field is cancelled by the demagnetizing field. Wojtowicz and Rayl⁴¹⁾ have calculated the resulting phase boundary for a very special geometry (toroidal sample with a field applied perpendicular to the toroidal plane) in the molecular field approximation. This calculation has been extended by Durczewski⁴²⁾. Griffiths⁴³⁾ has given general arguments for the existence of the phase boundary and the

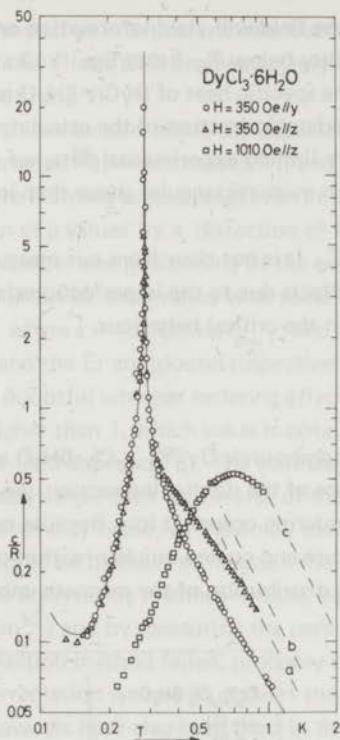


Fig. II.13

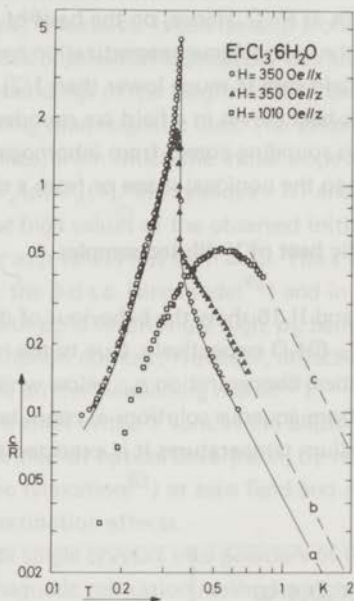


Fig. II.14

Fig. II.13. Specific-heat data of $\text{DyCl}_3 \cdot 6\text{H}_2\text{O}$ versus temperature in an applied magnetic field. Full curve: $H=0$. The dashed lines show the expected T^{-2} behaviour at high temperatures: a: $H=0$, b: $H=350 \text{ Oe//z}$; c: $H=1010 \text{ Oe//z}$.

Fig. II.14. Specific-heat data of $\text{ErCl}_3 \cdot 6\text{H}_2\text{O}$ versus temperature in an applied magnetic field. Full curve: $H=0$. Dashed lines: compare fig. II.13.

shape of the specific-heat curve. It can be shown⁴⁴⁾ that in the absence of hysteresis and with the field along a main axis of the ellipsoidal sample, which is also assumed to be an easy direction, the internal field, $H_1 = H - DM$, will be zero for $H < DM_0$ (M_0 is the spontaneous magnetization). Then, according to Griffiths, the specific heat in a fixed field H will not be different from its zero field value for temperatures below T_1 , where T_1 can be obtained from $M_0(T_1) = H/D$. At T_1 there will be a singularity in the specific heat, which shape depends on the behaviour of the magnetization curve for H going to zero. For anisotropic ferromagnetic systems we expect the initial susceptibility $\chi_0(T)$ to exist below T_C ⁴⁵⁾ and the heat capacity will show a discontinuity at T_1 . Otherwise the heat capacity will be continuous. If these theories are applicable to $\text{DyCl}_3 \cdot 6\text{H}_2\text{O}$ and $\text{ErCl}_3 \cdot 6\text{H}_2\text{O}$,

measurements on the specific heat as a function of the field will yield information on the spontaneous magnetization and the initial susceptibility below T_C . From figs. II.13 and II.14 we infer that the temperature of the maximum of the specific heat of $\text{DyCl}_3 \cdot 6\text{H}_2\text{O}$ and $\text{ErCl}_3 \cdot 6\text{H}_2\text{O}$ does not shift in fields which are a considerable fraction of the calculated dipolar fields at $H=0$. Hence, on the basis of our very limited experimental data, we conclude that the spontaneous magnetization has a much more rectangular shape than in the molecular field case (β much lower than $1/2$).

The specific-heat curves in a field are rounded near T_C . It is not clear from our measurements whether this rounding comes from inhomogeneity effects due to the imperfections in the sample and to the nonideal shape or from a change in the critical behaviour.

II.6 Specific heat of Y-diluted samples

Figs. II.15 and II.16 show the behaviour of diluted compounds $\text{Dy}_p\text{Y}_{1-p}\text{Cl}_3 \cdot 6\text{H}_2\text{O}$ and $\text{Er}_p\text{Y}_{1-p}\text{Cl}_3 \cdot 6\text{H}_2\text{O}$ respectively. Due to the long range of the dipolar interaction, we expect that the critical concentration p_C , below which no ordering occurs, is low. Because crystals are grown from aqueous solutions at room temperature and cooled quickly (within one hour) to liquid-helium temperatures it is expected that the distribution of the magnetic moments

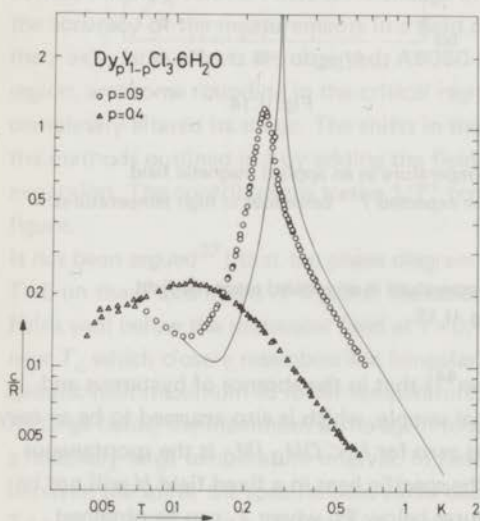


Fig. II.15

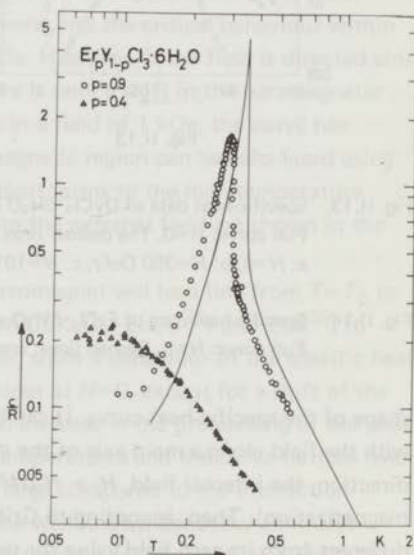


Fig. II.16

Fig. II.15. Specific-heat data of $\text{Dy}_p\text{Y}_{1-p}\text{Cl}_3 \cdot 6\text{H}_2\text{O}$ per mole versus temperature. Full curve: $p=1$.

Fig. II.16. Specific-heat data of $\text{Er}_p\text{Y}_{1-p}\text{Cl}_3 \cdot 6\text{H}_2\text{O}$ per mole versus temperature. Full curve: $p=1$.

correspond to an intermediate case between annealed and quenched. We expect substitutional grow of the Y ions (site problem). Only a slight change of the unit cell parameters is expected on substituting Y.

Not much can be said about the expected critical behaviour which can exhibit unperturbed⁴⁶), renormalized⁴⁷), and complex⁴⁸) features. It can be seen from the figures that there is strong broadening, even at high values of p , which is probably due to a distribution of g values by a distortion of the surroundings of the magnetic ions, dependent on the number and positioning of the neighbouring (dia)magnetic ions. The values of $T_c(p)$ for $p=0.9$ can be determined with some confidence, from which the initial slope s can be derived, where $s = (dt_c(p)/dp)_{p=1}$, and $t_c(p) = T_c(p)/T_c(1)$. This yields $s=1.7$ and $s=1.5$ for the Dy and the Er compound respectively. These high values of the observed initial slopes make it doubtful whether ordering effects occur at p values less than 0.35. The s values are much higher than 1, which value is obtained for the 3-d s.c. Ising model⁴⁹) and in the effective-field approach⁵⁰). The estimated value of p_c is surprisingly high, p_c being appreciably larger than the inverse of the coordination number. However, inflections in the $t_c(p)$ curves may occur, as shown by calculations on the Heisenberg model⁴⁹).

It appears to be difficult to measure the concentration of the Y ions in the diluted crystals. We made analyses by chemical means, by the method of optical absorption, by neutron activation⁵²) and by measuring the paramagnetic relaxation⁵³) at zero field and at 5.3 kHz. The activation method failed, probably due to extinction effects.

Before irradiation we had to convert the chloride single crystals into powders of the oxide. These powders have also been used in the paramagnetic relaxation method which gives reasonably accurate results at liquid-helium temperature ($\pm 2\%$). In the optical absorption measurement we can use the original crystals, but this method proved to be quite inaccurate (10%). The concentrations $p = 0.90 \pm 0.02$ and $p = 0.41 \pm 0.02$ obtained for the two samples of Dy-YCl₃·6H₂O correspond to crystals which have been grown from aqueous solutions containing 85% and 30% Dy respectively. The preferent growth of the Dy ion is in accordance with activation analyses on samples with very low magnetic ion concentrations⁵⁴). The same p values have been adopted for the Er-Y compounds, which were grown in the same way.

II.7 Susceptibility

Measurements of the zero-field a.c. (225 Hz) and d.c. (ballistic) susceptibilities of DyCl₃·6H₂O and ErCl₃·6H₂O along the magnetic z axis are shown in figs. II.17 and II.18 respectively. There is no difference between the a.c. and d.c. data above T_c , although a rise in χ'' is observed in this region, which indicates that relaxation effects become important near T_c . The data have been fitted at temperatures above 1 K by a Curie-Weiss relation:

$$\chi = C/(T-\Delta) \quad (II.7.1)$$

where C is the Curie constant and Δ the Curie-Weiss constant. Both depend on direction. They can be calculated from the general theory outlined in I. The measured and calculated

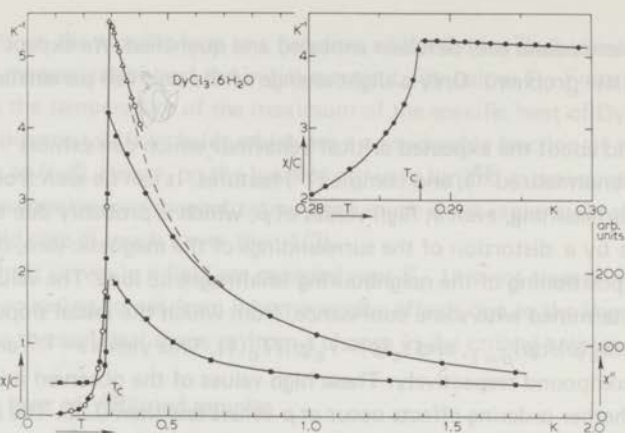


Fig. 11.17. Susceptibility data of $\text{DyCl}_3 \cdot 6\text{H}_2\text{O}$ versus temperature. Circles: χ' (225 Hz) data. Triangles: χ_0 (ballistic) data. Squares: χ'' (225 Hz) data. Open symbols: χ^{zz} , black symbols: χ^{AA} . Dashed curve: Curie-Weiss relation, $\Delta=0.140$ K, obtained from a fit on the high-temperature χ^{AA} data. Inset: high resolution χ^{AA} (225 Hz) data.

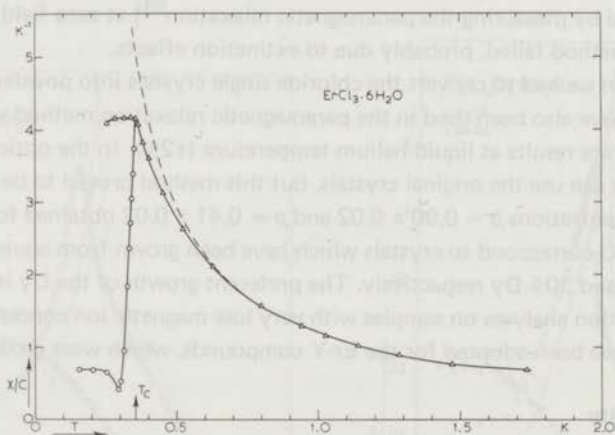


Fig. 11.18. Susceptibility data of $\text{ErCl}_3 \cdot 6\text{H}_2\text{O}$ versus temperature. For symbols, compare fig. 11.17. Dashed curve: Curie-Weiss relation, $\Delta=0.160$ K, obtained from a fit on the χ^{zz} (225 Hz) data.

values are shown in table II.7. There is a large shape contribution to the measured values, which can be calculated from the estimated demagnetization factor D . These have been determined from the shape, which was approximately ellipsoidal, by measuring the ellipsoid axes and also from the phase boundary measurements described in II.8. The two values do not agree very well, especially in the case of $\text{DyCl}_3 \cdot 6\text{H}_2\text{O}$. We ascribe the difference to the error made in the approximation of the sample shape by an ellipsoid. The value of D from

the phase boundary measurements has been used in table II.7. The calculated and measured values of Δ are not in good agreement. In our opinion, the discrepancy may be attributed to the use of relation (II.7.1) in a temperature region in which the calculated value of Δ , obtained by a truncation of the susceptibility series after the $1/T^2$ term, is no good approximation. The importance of higher order terms in the expansion of the thermodynamic properties is also clear from the high-temperature specific-heat measurements, especially in the case of $\text{DyCl}_3 \cdot 6\text{H}_2\text{O}$ (see I).

Table II.7. Susceptibility data.

	direction	Δ		C calc.	$\chi(T_c)D$
		meas.	calc. ^{a)}		
$\text{DyCl}_3 \cdot 6\text{H}_2\text{O}$	z	0.21 ± 0.03	0.41	25.566	1.42
$\text{ErCl}_3 \cdot 6\text{H}_2\text{O}$	z	0.16 ± 0.03	0.22	17.686	1.09

^{a)} See I, Δ corrected for shape effects.

Below T_c there is a steep fall in the a.c. (225 Hz) susceptibility χ' , which occurs in the imaginary part χ'' as well. The discontinuity in $d\chi'/dT$ is clearly demonstrated in the inset in fig. II.16. Within the accuracy of the measurement, the temperature at which it occurs coincides with the temperature of the specific-heat maximum. The decrease has been interpreted as an indication of antiferromagnetic ordering earlier⁵⁵). The d.c. (ballistic) susceptibility, however, shows a quite different behaviour below T_c . It remains constant down to 0.25 K in the case of $\text{ErCl}_3 \cdot 6\text{H}_2\text{O}$ when measured either along the z axis or along the A axis, which is a clear indication of ferromagnetism. The value of $\chi(T_c)D$ which should be 1 for a ferromagnetic system ordered in freely movable domains is given in table II.7. The calculated value of C has been used to convert the measured $\chi(T_N)/C$ value. The result depends on the Δ fit criticised before. In view of the crude approximations, the agreement for $\text{ErCl}_3 \cdot 6\text{H}_2\text{O}$ is good. Below 0.25 K no reliable ballistic measurements could be performed, which indicates the onset of long relaxation times below T_c probably due to the formation of needle-shaped domains in the strongly anisotropic system. Ballistic measurements did not give reliable results on $\text{DyCl}_3 \cdot 6\text{H}_2\text{O}$ below T_c , possibly related to the even larger anisotropy in this compound.

We conclude that long-range order sets in quite abruptly, giving rise to domain formation at or close to T_c . This is in accordance with the a.c. susceptibility behaviour.

We have recorded the temperature and the a.c. susceptibility along the B axis when a field of 300 Oe is rotated adiabatically in the A - C plane. Above T_c , the temperature T and the susceptibility χ' vary periodically. The positions of the maxima and the minima are in agreement with the estimated directions of the x and z axis, using data of tables II.1 and II.2.

These measurements enable us to determine the directions of the magnetic axes to within one degree. Below T_c , rotational diagrams of χ'' show the same periodicity as observed in rotational diagrams of χ' and T above T_c . Hence the principal axes of the g tensor are the magnetic anisotropy axes below T_c , as could be expected. No periodic variations of the temperature are observed below T_c , which suggests that the susceptibility variations are due to the effects of switching the domains and not to a change of the single domain magnetization.

We expect the relaxation times to become long also within the domains, because the presence of a large effective field at the ion site makes spin-spin processes improbable. This is confirmed by the fact that no reliable ballistic measurements could be carried out with our apparatus in the paramagnetic region in external fields above 100 Oe.

The slow rise of the susceptibility in the paramagnetic region which is even slower than the one predicted from eq. (II.7.1), if we use the constants determined from least-squares fits in the liquid-helium region, suggests classical behaviour near T_c for both compounds, *viz.* $\gamma_* = 1$. This is confirmed by a critical exponent analysis on the data shown in the inset of fig. II.17, which yields $\gamma_*^{Dy} = 1.1 \pm 0.1$. The determination of this number depends on the analysis of the high-temperature susceptibility data and the determination of the demagnetization factor, the results of which are in doubt in particular for $DyCl_3 \cdot 6H_2O$, see table II.7. In our opinion, however, the main conclusion of a classical divergence in the susceptibility above T_c is correct. This does not imply that eq. (II.7.1) should describe the susceptibility correctly in the whole paramagnetic region.

II.8 Magnetothermal effect

The variation of the temperature upon slow adiabatic variation of the magnitude of an external field H directed along the z axis of approximately ellipsoidal samples of $DyCl_3 \cdot 6H_2O$ and $ErCl_3 \cdot 6H_2O$ have been recorded by a carbon resistor thermometer. The results are shown in fig. II.19.

The temperature variation ΔT for an uniformly magnetized system on a field variation ΔH is given by⁵⁶):

$$\Delta T = -\frac{T}{c_H} \left(\frac{\partial M}{\partial T} \right)_H \Delta H \quad (II.8.1)$$

For a ferromagnetic system this equation presumably applies when there is a change in the one-domain magnetization, hence if there is a change in the internal field H_i . As argued before (II.5), if $H \leq DM_0$ then $H_i = H - DM = 0$, for a system in which the domain configuration is in true thermodynamic equilibrium. Accordingly, we expect the temperature variations to be small until the value $H = DM_0$ is reached, unless irreversible effects such as eddy current heating are important. Thereafter, according to eq. (II.8.1), the temperature starts to rise,

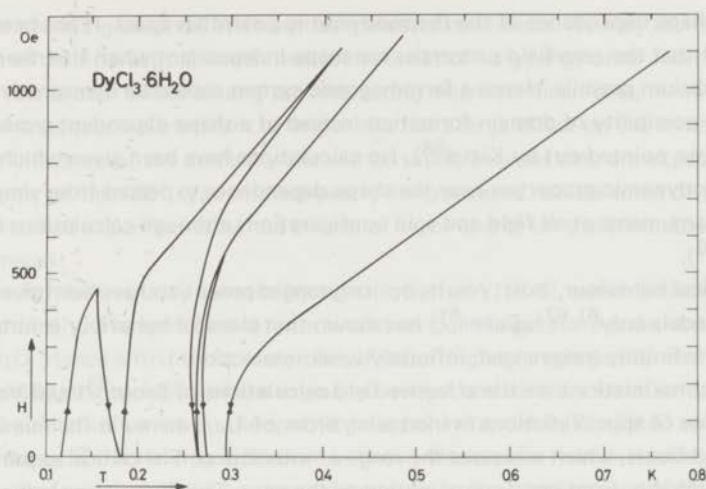


Fig. 11.19. Isentropes of $\text{DyCl}_3 \cdot 6\text{H}_2\text{O}$ in the H - T plane. The field has been varied along the z axis, using an ellipsoidal sample. At low temperatures, irreversible effects are observed. The isentropes of $\text{ErCl}_3 \cdot 6\text{H}_2\text{O}$ show analogous behaviour.

approximately proportionally to the field. This rise may continue until the magnetization reaches its saturated value at $T=0$. The slope dH/dT shows how much long-range order the domains have, hence we expect this slope to increase on decreasing T . These effects are observed in the $T(H)$ curves, fig. 11.19. The rounded kink in the curves is attributed to crossing the phase boundary DM_0 . The rounding occurs due to inhomogeneities of the sample and non-ideality of the shape.

A slight reversible cooling is observed at low fields near T_c . Appreciable cooling is expected if the field is varied adiabatically in a system with predominant antiferromagnetic interactions. In that case, the $T(H)$ curves may show pronounced temperature minima, which correspond to breaking the antiferromagnetic short- or long-range ordering. This occurs at fields which are of the order of the molecular field at $T=0$. These are about 1 kOe in both systems in the antiferromagnetic configuration (II), which is much higher than the field values at which the kink occurs in our measurements. Therefore we consider the small cooling effects at low fields as insignificant.

In conclusion, we ascribe the observed magnetothermal effects to ferromagnetic ordering below T_c .

11.9 Discussion of the critical behaviour

First it should be remarked that the applicability of thermodynamics to dipolar lattices has not yet been settled completely. Due to the long range of the dipolar interaction, the

possibility of shape dependence of the thermodynamic potentials arises. It has been proven by Griffiths⁵⁷) that the zero-field properties are shape independent when true thermodynamic equilibrium prevails. Hence a ferromagnetic system should be demagnetized in zero field. The possibility of domain formation instead of a shape-dependent ground-state ordering has been pointed out by Kittel⁵⁸). No calculations have been given which show that the thermodynamic properties have the shape dependence expected from simple magnetostatic arguments at all field and spin configurations although calculations for specific cases exist^{59,60}).

About the critical behaviour, exact results on long-ranged potentials have been given for one-dimensional models only^{61,62}). Baker⁶¹) has shown that classical behaviour is obtained in the limit of an infinitely long-ranged, infinitely weak interaction.

Closed-form approximations are the effective-field calculations of Brout⁶³) and Vaks *et al.*⁶⁴). These are a series of approximations in increasing order of $1/z$, where z is the number of interacting neighbours, which measures the range of interaction. The critical exponents fluctuate considerably from one approximation to the next. This fluctuating behaviour is not substantiated by series-expansion methods⁶⁵). In the general theory of critical exponents of Griffiths⁶⁶), it is conjectured that the exponents change their values discontinuously at specific values of the range parameter.

Another closed-form approximation which has been applied to long-range forces is the spherical model^{63,67}). This approximation is physically unrealistic but it yields surprisingly good results in some cases.

The dipolar interaction in a three-dimensional system does not belong to the class of long-ranged pair potentials for which classical behaviour is expected, although it has been conjectured that it 'induces' a classical value of β near the transition point⁷). Generally, however, classical behaviour is expected *outside* a region around T_c , which shrinks with increasing range of interaction. Inside this region unchanged short-range values of the critical exponents should be found.

Apart from the effects of the ranges of the interactions present in the system, other parameters which may influence the critical behaviour have to be taken into account, such as:

- a) spin dimensionality and sign of the interaction,
- b) hidden variables⁴⁷),
- c) random imperfections^{46,48}).

As to a), the pair interaction in $\text{DyCl}_3 \cdot 6\text{H}_2\text{O}$ and $\text{ErCl}_3 \cdot 6\text{H}_2\text{O}$ is Ising-like, but the sign and the strength of the interaction depend on the angle between the z axis and the line which connects the members of the pair. In the n.n. Ising model no change in the critical behaviour in zero field is expected if the sign or the strength of the n.n. interaction depends upon the direction of the pair bond in the crystal. The influences of b) have been discussed by Fisher⁴⁷) and Gunther *et al.*⁶⁸). They should lead to renormalized or normal behaviour or to a change of the transition to first order, depending on the constraint on the hidden variable. In particular, compressibility effects can make the transition first order^{68,69,70}). The influences of c) are lumped in a rounding of the transition in most cases.

There is no rounding observed with our temperature resolution. We may ascribe this to the long range of the interaction, which makes the onset of long-range order insensitive to broken or disturbed bonds among the interacting magnetic ions. Note, however, that the addition of an appreciable amount of impurities has a large effect on the critical behaviour (11.6). The influence of the domain walls will be small, because they are expected to be very thin, and only of the 180° type in these nearly Ising systems. Unless some of the variables can be controlled experimentally, the effects of a), b) and c) on the critical behaviour cannot be disentangled.

We have varied the impurity content by substitution of Y (11.6), which broadens the heat-capacity anomaly. The specific heat is bounded on our temperature scale, also in the case of $\text{DyCl}_3 \cdot 6\text{H}_2\text{O}$. Hence a first-order transition, if occurring at zero impurity content, is destroyed. Experimentally, the variation of the impurity content and also the variation of the external field, has a similar influence on the specific-heat behaviour of $\text{DyCl}_3 \cdot 6\text{H}_2\text{O}$ and $\text{ErCl}_3 \cdot 6\text{H}_2\text{O}$. Hence we doubt if the striking difference between the specific-heat anomalies can be explained by the inclusion of the corresponding terms in the hamiltonians of the systems. The observed critical exponents are collected in table 11.8, together with some model calculations. MFA stands for molecular field or zeroth self consistent field approximation and RPA stands for random phase or first consistent field approximation^{63,64}). Although the RPA values are in agreement with the values of a_\pm and γ_\pm of $\text{DyCl}_3 \cdot 6\text{H}_2\text{O}$, the validity of this theory, which leads to an Ornstein-Zernike type of correlation function, is in doubt, especially near T_c .

Table 11.8. Critical exponents of $\text{DyCl}_3 \cdot 6\text{H}_2\text{O}$ and $\text{ErCl}_3 \cdot 6\text{H}_2\text{O}$ compared with various models.

	$\text{DyCl}_3 \cdot 6\text{H}_2\text{O}$	$\text{ErCl}_3 \cdot 6\text{H}_2\text{O}$	MFA ^{a)}	RPA ^{a)}	n.n. Ising $d=3^b)$	n.n. Ising $d=2^b)$	renormalized Ising $d=3^b)$
a_+	0.43 ± 0.06	-0.07 ± 0.05	0 (cusp, $a_+ = 0$)	1/2	1/8	0(log)	-1/7
a_-	0.60 ± 0.09	-0.26 ± 0.06	0 (cusp, $a_- = 0$)	1/2	1/16	0(log)	-1/5
$\beta^c)$	0.15 ± 0.10		1/2	1/4	5/16	1/8	1/3
γ_+	1.1 ± 0.1		1	1	5/4	7/4	10/7
γ_-			1	1	21/6	7/4	7/5

a) ref. 63.

b) ref. 47. Rationalized numbers for the 3-d Ising model are approximately only.

c) The value of β in RPA and for $\text{DyCl}_3 \cdot 6\text{H}_2\text{O}$ is obtained by the use of the scaling relations $2\beta = 2 - (a_- + \gamma_-)$ and $\gamma_- = \gamma_+$.

Applying the scaling relations⁷⁾ yields the value of β (table 11.8). However, it is doubtful whether scaling relations can be applied to systems in which long-range forces dominate the critical behaviour.

Investigations on critical exponents in nearly pure dipolar substances have been reported for $\text{Gd}_2(\text{SO}_4)_3 \cdot 8\text{H}_2\text{O}$ and $\text{GdCl}_3 \cdot 6\text{H}_2\text{O}$ ^{5,15}). Sharp transitions with high values of a have been found in these systems (e.g. $a_- = 0.6$ for the sulphate), which resembles the case of $\text{DyCl}_3 \cdot 6\text{H}_2\text{O}$. Detailed investigations of the critical behaviour have been done for DAG⁷¹⁾ and GdCl_3 ⁷²⁾, which have large admixtures of exchange interactions. These systems have

low or negative values of α , like $\text{ErCl}_3 \cdot 6\text{H}_2\text{O}$.

In view of the foregoing, it is clear that more experimental and theoretical information is needed before definite conclusions on the critical behaviour of dipole-coupled systems can be given.

11.10 Conclusions

The specific heats of $\text{DyCl}_3 \cdot 6\text{H}_2\text{O}$ and $\text{ErCl}_3 \cdot 6\text{H}_2\text{O}$ in zero external field show sharp anomalies at 0.289 and 0.356 K respectively. The singularity of $\text{ErCl}_3 \cdot 6\text{H}_2\text{O}$ is cusp-like, but the singularity of $\text{DyCl}_3 \cdot 6\text{H}_2\text{O}$ is a strongly divergent symmetrically shaped λ anomaly, and the possibility of a first-order transition with a very small latent heat is not excluded by our measurements. The value of the specific heat of $\text{DyCl}_3 \cdot 6\text{H}_2\text{O}$ becomes so large ($\sim 50 \text{ R}$), that finite size effects should be observable if the transition is second order. This point needs a more careful experimental study.

Measurements of the specific heat in an external field, susceptibility measurements, and magnetothermal measurements indicate the onset of ferromagnetism at the transition point. From these measurements we conclude that both compounds have a strong uniaxial anisotropy, which leads to an ordering in needle-shaped domains. The existence of a shape induced phase boundary is inferred from the measurements. We expect the spontaneous magnetization curve to be rectangularly shaped.

The interactions responsible for the ordering effects are mainly dipolar, which is concluded from the measured energy and high-temperature specific heat, using the magnetic parameters obtained by other investigators. This is in accordance with the expectations obtained from general considerations on the interactions.

We conclude from our measurements that $\text{DyCl}_3 \cdot 6\text{H}_2\text{O}$ and $\text{ErCl}_3 \cdot 6\text{H}_2\text{O}$ are anisotropic dipolar ferromagnets, comparable to DyES^{73} and $\text{Tb}(\text{OH})_3^{74}$. More measurements are needed to exclude completely the possibility of a more complicated magnetic behaviour such as metamagnetism with a very low transition field. The shape-dependent properties, in particular the susceptibility and the magnetization need fuller experimental and theoretical investigation. E.s.r. on coupled pairs probably could give more precise information on the nature of the interactions.

References

- 1) Keffer, F., in 'Handbuch d. Phys.', ed. S. Flügge (Springer Verlag, Berlin) vol. XVIII/2, p. 93.
- 2) Van Vleck, J.H., J. Chem. Phys. **5** (1937) 320.
- 3) Hebb, M.H. and Purcell, E.M., J. Chem. Phys. **5** (1937) 338.
- 4) Baker, J.M., Rep. Progr. Phys. **34** (1971) 109.
- 5) Wielinga, R.F., Lubbers, J. and Huiskamp, W.J., Physica **37** (1967) 375 (commun. Kamerlingh Onnes Lab. Leiden No. 3616).
- 6) Wilson, K.G. and Fisher, M.E., Phys. Rev. Letters **28** (1972) 241.
- 7) Kadanoff, L.P. *et al.*, Rev. Mod. Phys. **39** (1967) 395; Fisher, M.E., Rep. Progr. Phys. **30** (1967) 615; Heller, P., *ibidem* p. 731; Wielinga, R.F., in 'Progr. low Temp. Phys.', ed. C.J. Gorter (North-Holland Publ. Co., Amsterdam) vol. VI, ch. 10.
- 8) Luttinger, J.M. and Tisza, L., Phys. Rev. **70** (1946) 954.
- 9) Holstein, T. and Primakoff, H., Phys. Rev. **58** (1940) 1098.
- 10) Marquard, C.D., Proc. Phys. Soc. (London) **92** (1967) 650.
- 11) Meyer, P.H.E. and O'Keeffe, D.J., Phys. Rev. B **1** (1970) 3786.
- 12) Becker, E. and Plischke, M., Phys. Rev. B **1** (1970) 314.
- 13) Wong, S., Dembinski, S.T. and Opechowski, W., Physica **42** (1969) 565.
- 14) Lagendijk, E., Blöte, H.W.J. and Huiskamp, W.J., Physica, to be published, chapter I.
- 15) Wielinga, R.F., thesis, Leiden (1968).
- 16) Mess, K.W., thesis, Leiden (1969).
- 17) Edelstein, A.S. and Mess, K.W., Physica **31** (1965) 1707 (commun. Kamerlingh Onnes Lab., Leiden No. 344c).
- 18) See appendix.
- 19) Cochran, J.F., Shipmann, C.A. and Neighbor, J.E., Rev. Sci. Instrum. **37** (1966) 499.
- 20) Graeber, E.J., Conrad, G.H. and Duliere, S.F., Acta Cryst. **21** (1966) 1012.
Slightly different values ($\approx 0.2\%$) of the unit cell parameters have been reported by Ivanov, V.I., Kristallografiya **13** (1968) 905 (transl. Sov. Phys. Cryst. **13** (1969) 786).
- 21) Marezio, M., Plettinger, H.A. and Zachariasen, W.H., Acta Cryst. **14** (1961) 234.
- 22) Hellwege, K.H., Hüfner, S. and Kahle, H.G., Z. Physik **160** (1960) 162.
- 23) Schulz, M.B. and Jeffries, C.D., Phys. Rev. **159** (1967) 277.
This paper contains many references to the earlier literature.
- 24) Dieke, G.H. and Crosswhite, H.M., J. Opt. Soc. Am. **46** (1956) 885.
- 25) Baker, J.M., Rep. Progr. Phys. **34** (1971) 109.
- 26) Gramberg, G., Z. Physik **159** (1969) 125.
- 27) Wickman, H.H. and Nowick, I., J. Phys. Chem. Sol. **28** (1967) 2099.
- 28) Levy, P.M., Phys. Rev. **177** (1969) 509.
- 29) Blöte, H.W.J. and Huiskamp, W.J. Physica **53** (1971) 445 (commun. Kamerlingh Onnes Lab., Leiden No. 386a).
- 30) Abragam, A. and Bleaney, B., 'Electron Paramagnetic Resonance of Transitions' (Clarendon Press, Oxford, 1970). We thank drs. N. de Boo for writing the computer program and performing the calculations.
- 31) Pfeffer, W., Z. Physik **162** (1961) 413; **164** (1961) 295.
- 32) Niemeyer, T., Physica **57** (1972) 281.
- 33) See *e.g.* Wielinga, R.F., Comm. Solid State Phys. **3** (1970) 59.
- 34) Gaunt, D.S. and Domb, C., J. Phys. (London) C **1** (1968) 1038.
- 35) Dunlop, B.D. and Dash, J.G., Phys. Rev. **155** (1967) 460. These are measurements on metallic systems.
- 36) Domain formation has been mentioned as a source of asymmetric rounding, see refs. 7 and 33.
- 37) See *e.g.* Fisher, M.E., in 'Lectures in Theoretical Physics' (University of Colorado Press, Boulder, 1964) p. 17, fig. 3.4.

- 38) Miedema, A.R., Van Kempen, H. and Huiskamp, W.J., *Physica* **29** (1963) 1266 (commun. Kamerlingh Onnes Lab., Leiden No. 366a) and Lagendijk, E., unpublished.
- 39) Van der Hoeven, B.J.C., Teaney, D.T. and Maruzzi, V.L., *Phys. Rev. Letters* **20** (1968) 719; **20** (1968) 722.
- 40) Arrott, A., *Phys. Rev. Letters* **20** (1968) 1029.
- 41) Wojtowicz, P.J. and Rayl, M., *Phys. Rev. Letters* **20** (1968) 1489.
- 42) Durczewski, K., *Phys. Letters* **31A** (1970) 56.
- 43) Griffiths, R.B., *J. Appl. Phys.* **40** (1969) 1542.
- 44) Kneller, E., 'Ferromagnetismus', (Springer Verlag, 1962) p. 472 ff.
- 45) Fisher, M.E., *J. Appl. Phys.* **38** (1967) 981.
- 46) Watson, P.G., *J. Phys. (London)* **C 3** (1970) L25.
- 47) Fisher, M.E., *Phys. Rev.* **176** (1968) 257.
- 48) McCoy, B.M., *Phys. Rev. Letters* **23** (1969) 383.
- 49) Heap, B.R., *Proc. Phys. Soc. (London)* **82** (1963) 252.
- 50) Sato, H., Arrott, A. and Kikuchi, R., *J. Phys. Chem. Sol.* **10** (1959) 19.
- 51) Bastmeyer, J.D. and Zimmerman, N.J., private communication.
- 52) We thank Dr. E.R. Reddingius and Drs. J.J. Bosman of the Reactor Centrum Nederland for performing the activation. Drs. H.B. Brom and Dr. L. Niesen assisted in the analysis of the results.
- 53) We thank Mr. A. Van der Bilt, Drs. J.A. Roest and Dr. A.J. van Duyneveldt for performing these measurements.
- 54) Brom, H.B., private communication.
- 55) Lagendijk, E., Wielinga, R.F. and Huiskamp, W.J., *Phys. Letters* **31A** (1970) 375.
- 56) Morrish, A.H., 'The Physical Principles of Magnetism', (John Wiley & Sons, Inc., New York, 1965) p. 273.
- 57) Griffiths, R.B., *Phys. Rev.* **176** (1968) 655.
- 58) Kittel, C., *Phys. Rev.* **82** (1951) 965.
- 59) Levy, P.M., *Phys. Rev.* **170** (1968) 595.
- 60) Horner, H., *Phys. Rev.* **172** (1968) 535.
- 61) Baker, G.A., *Phys. Rev.* **126** (1962) 2071.
- 62) Dyson, F.J., *Commun. Math. Phys.* **12** (1969) 91.
- 63) Brout, R., 'Phase transitions' (W.A. Benjamin, Inc., New York, 1965).
See also Brout, R., *Physica* **50** (1970) 149.
- 64) Vaks, V.G., Larkin, A.T. and Pikin, S.A., *Zh. Eksperim. i Teor. Fiz.* **51** (1966) 361,
(transl. *Sov. Phys. JETP* **24** (1967) 240).
- 65) Dalton, N.W. and Wood, D.W., *J. Math. Phys.* **10** (1969) 1271.
- 66) Griffiths, R.B., *Phys. Rev. Letters* **24** (1970) 1479.
- 67) Joyce, G.S., *Phys. Rev.* **146** (1966) 349.
- 68) Gunther, L., Bergman, D.J. and Imry, Y., *Phys. Rev. Letters* **27** (1971) 558.
- 69) Baker, G.A. and Essam, J.W., *J. Phys. (Paris)* **32** (1971) C1-1015.
- 70) Domb, C., *Proc. Phys. Soc. (London)* **88** (1966) 260.
- 71) Keen, B.E., Landau, D.P. and Wolf, W.P., *J. Appl. Phys.* **38** (1967) 967.
- 72) Landau, D.P., *J. Phys. (Paris)* **32** (1971) C1-1012.
- 73) Cooke, A.H., Edmonds, D.T., Finn, C.B.P. and Wolf, W.P., *Proc. Roy. Soc. (London)* **306** (1968) 313, 335.
- 74) Meissner, H.E. and Wolf, W.P., *J. Appl. Phys.* **40** (1969) 1038. Abstract only.

CHAPTER III

CALORIMETRIC STUDY OF A RANDOM ISING SPIN SYSTEM: $\text{Co}_p\text{Zn}_{1-p}\text{Cs}_3\text{Cl}_5$

Synopsis

Specific-heat and susceptibility measurements are presented on the magnetically diluted system $\text{Co}_p\text{Zn}_{1-p}\text{Cs}_3\text{Cl}_5$. The results are in good agreement with theoretical predictions on the random spin model for Ising interactions in three dimensions. High-resolution specific-heat measurements show that the singularity remains relatively sharp down to low concentrations of the magnetic ions.

III.1 Introduction

The study of diluted magnetic compounds as a function of the concentration p of the magnetic ions may yield interesting information on the interactions which lead to magnetic ordering. Theoretically, it has been shown that the behaviour of a diluted compound depends on the range of the interaction and the number of interacting spin components. The behaviour may also depend on the dimension of the spatial ordering. Most theories concentrate on idealized models of diluted magnetic systems, for example the random spin model¹). In this model it is assumed that there are interactions among nearest neighbours only and that the sole effect of introducing a non-magnetic ion (or a vacancy) is the breaking of the corresponding interaction bonds. Moreover, the hamiltonian describing the interaction among nearest neighbours is assumed to have a simple form, *i.e.* either Ising, $\mathcal{H}_{ij}^I = -2J S_i^z S_j^z$, or Heisenberg, $\mathcal{H}_{ij}^H = -2J S_i \cdot S_j$ (spin quantum number $S = 1/2$ is assumed in most cases). The distribution of the non-magnetic ions is assumed to be random and independent of the temperature and the magnetic field (quenched system). In the opposite case of an annealed system, thermodynamic equilibrium prevails at all temperature and field values.

Experimentally, not many systems are known for which the random spin model is a good approximation. Difficulties arise because:

- a) In some cases dilution offers a chemical problem. For instance, experiments similar to those described in this chapter were attempted on the Heisenberg spin system $\text{Cu}(\text{NH}_4)_2\text{Br}_4 \cdot 2\text{H}_2\text{O}$. However, we did not succeed in substituting Zn, Hg, Cd or Mg ions.
- b) The interaction may have a long range and/or may not correspond to a simple model hamiltonian. This case is encountered in many alloys, of which magnetic ordering as a function of concentration of magnetic constituents has been extensively studied.

c) The single ion properties may change due to a change in the surroundings. For example, the sign of the crystal field changes if Ce ethyl sulphate is diluted by the substitution of La. Furthermore, due to a change of the lattice constant, the pair interactions may change. In particular, exchange forces are a very sensitive function of the distance. This is verified by experiments on Eu compounds, *e.g.* EuO^6).

d) The heat treatment may be very important, especially in metallic systems. Clustering effects which cause a deviation from randomness are sometimes observed, depending on sample preparation.

In this chapter experiments on the system $\text{Co}_p\text{Zn}_{1-p}\text{Cs}_3\text{Cl}_5$ are presented, and the results are shown to be in good agreement with calculations on random spin systems^{7,8,9,10}). We expect $\text{Co}_p\text{Zn}_{1-p}\text{Cs}_3\text{Cl}_5$ mixed compounds to be good examples of random spin systems, because:

a) CoCs_3Cl_5 and ZnCs_3Cl_5 can be mixed in all proportions.

b) The undiluted compound CoCs_3Cl_5 is a nice example of the three-dimensional (3-d) Ising antiferromagnet (AFM) with spin quantum number $S=1/2$ and predominantly nearest neighbour (n.n.) interactions^{2,3}).

c) There is only a very small change of the lattice constant and of the Co-Co n.n. exchange interactions on dilution^{2,4,5}).

d) The samples have been prepared from the melt. Hence a randomly frozen-in configuration of magnetic moments is expected if the samples are cooled quickly to room temperature and below (quenched system).

With regard to b), it has been shown that the combined effect of the n.n. exchange interaction and the dipolar interaction is represented in a very good approximation by the simple cubic (s.c.) 3-d Ising model having predominantly n.n. interactions along the *C* axis and in the *A-B* plane, which are equal in magnitude but opposite in sign^{2,5}). Hence the configuration of lowest energy will be a layered antiferromagnetic one. This configuration is favoured not only by the n.n. forces, but also results as the ground state from a Luttinger and Tisza¹¹) calculation, assuming exclusively (long-ranged) dipolar interactions. The corresponding energy is $E^{\text{dip}}/R = -0.0633$ K. The dipolar interactions between nearest neighbours amount to $E_{\text{n.n.}}^{\text{dip}}/R = -0.103$ K. Adding to E^{dip}/R the energy from the n.n. exchange interactions in the layered (AFM) configuration, using the exchange constants of ref. 5, yields $E/R = -0.315$ K, which should be compared with the experimental value, $E/R = -0.331$ K, obtained from specific-heat measurements on the concentrated compound²).

Neutron diffraction measurements, however, indicate that the ordered state has the Néel configuration, which can be explained if one assumes a relatively large ferromagnetic fourth neighbour interaction¹²).

We have measured the specific heat and the susceptibility of a series of these compounds with $p = 1, 0.9, 0.8, 0.7, 0.5, 0.4$ and 0.35 . High-resolution specific-heat measurements near the transition points have been performed. The specific-heat peaks remain sharp even at low p values. From the shape of the curves we infer a change to cusp-like behaviour.

III.2 Preparation*

The mixed compositions were prepared from CoCs_3Cl_5 and ZnCs_3Cl_5 by melting in a platinum crucible contained in an evacuated silica ampoule at 700°C . X-ray powder patterns showed the samples to have the CoCs_3Cl_5 structure; no second phase could be detected. ZnCs_3Cl_5 and CoCs_3Cl_5 have the same crystal structure with nearly identical lattice parameters⁴, $A=9.25 \text{ \AA}$, $C=14.50 \text{ \AA}$ and $A=9.22 \text{ \AA}$, $C=14.55 \text{ \AA}$ respectively. Therefore the occurrence of completely mixed crystals could not be deduced unambiguously from the X-ray data, the width of the reflection lines being comparable to the separation of the lines for $p=0$ and $p=1$.

The component CoCs_3Cl_5 (Co content $10.6 \pm 0.5\%$, theor. 9.3) was obtained from an aqueous solution containing excess of CsCl. ZnCs_3Cl_5 (Zn content $10.6 \pm 0.3\%$, theor. 10.2) was prepared by heating CsCl with carefully dried ZnCs_2Cl_4 which was obtained from an aqueous solution of CsCl and ZnCl_2 .

III.3 Experimental

The apparatus for measuring heat capacities and susceptibilities in the temperature region $0.05 < T < 2 \text{ K}$ has been described before^{2,3}. We have used Speer 220Ω 1/2 W carbon resistors as thermometers. These are calibrated against a magnetic susceptibility thermometer (e.g. a slab of cerium magnesium nitrate), by extrapolating the Curie-Weiss relation, which is determined in the liquid ^4He region. Resistances are measured by a Wheatstone bridge and susceptibilities are measured with the aid of a Hartshorn bridge. Both bridges use lock-in detection at 675 and 260 Hz respectively. D.c. susceptibilities can also be measured, using a ballistic galvanometer.

A polynomial expansion has been fitted to the resistance *versus* temperature (R - T) data¹³ e.g.

$$\log(R) = \sum_{i=1}^{10} c_i [\log(T)]^{i-1}.$$

Heat-capacity data have been obtained applying the usual heat-pulse method. All measurements have been performed on powdered samples. Apiezon N grease has been used for thermal contact. At low temperatures long relaxation times were observed, especially in the samples with low p values.

* The samples have been prepared by Dr. P.F. Bongers from the Philips Research Laboratories, Eindhoven, The Netherlands.

III.4 Specific heat

Specific-heat data are shown in figs. III.1, III.3 and III.4. The data have been corrected for the contributions from the empty calorimeter. No significant contributions are expected from the lattice waves or from the hyperfine interaction²).

Fig. III.1 shows the measured points on a semilog scale. For clarity, we have omitted the $p=0.4$ data. Fig. III.3 shows some of the data on a reduced temperature scale, compared to various model calculations. The critical behaviour is shown in more detail in fig. III.4.

After some theoretical preliminaries, we will first discuss the dependence of T_N on p , and some general properties of the measured curves will be investigated. Next we will discuss the critical region. In this connection the problem of the effect of random impurities on the critical behaviour arises.

III.4-1 General behaviour, theory

At *high* temperatures the spin-spin correlations extend over short distances only, and it is expected that the thermodynamic properties of the diluted system can be obtained from those of the undiluted system by a simple transformation with the appropriate concentration factor. For example, the Curie-Weiss Δ should transform¹⁴) according to $\Delta(p) = p\Delta(1)$. At low temperatures the long-range order parameter, *i.e.* the (sub)lattice spontaneous magnetization M_0 , may become non-zero at a certain temperature which we call the transition point $T_t(p)$. From intuitive reasoning, and from calculations on closed form approximations we expect the properties of the diluted and undiluted systems not to be simply related at *low* temperatures.

For random spin systems, exact results on the functional dependence of M_0 on p and T have been obtained in the form of inequalities only^{1, 15}). The expected general behaviour has been sketched by Brout¹⁶). In the case of n.n. interactions only, the spontaneous moment at $T=0$ will decrease on decreasing p , and it will become zero at a certain critical concentration $p_c \geq 0$, which depends on the number of nearest neighbours or coordination number z . Presumably, $p = 1/z$ will be a reasonable estimate. Because (weak) long-range interactions, such as the dipolar interaction, will become important at low T and p , it is expected that long-range order can be established in an infinite system at all finite p values, and that the full saturation moment is reached at $T=0$. If the long-range interactions dominate like in some metallic systems¹⁷), this behaviour will become more apparent. The long-range interactions may favour a different configuration of the magnetic moments in the ordered state compared to the short-range interactions. This may lead to unexpected magnetic behaviour at low p values and low temperatures.

Calculations on random spin systems^{18, 19}) have shown that non-analytical behaviour of $M_0(p, T)$ should be expected at $T_t(1)$ at all p . However, from our measurements and also from other measurements on metallic and ionic bonded diluted systems reported in the literature, there are no indications that this non-analyticity has an observable effect^{17, 20, 21, 22}).

Complete $T_t(\rho)$ curves have been obtained from closed form approximations, such as the BPW approximation or the effective hamiltonian approximation^{7,10}, and from series expansion methods^{8,9}. As usual, the effective field methods are rather insensitive to the details of the interaction. In most cases they yield qualitative information only.

The presence of interactions of different sign and/or range in the system can lead to irregular $T_t(\rho)$ behaviour, as shown by Elliot and Heap²³. However, for nearest neighbour interactions only, the $T_t(\rho)$ curve of the Ising model on simple lattices should not depend on the sign of the interaction²³.

It has been proven²⁴ that the n.n. Ising problem is equivalent to the percolation problem. Hence the critical percolation probability p_0 for the site problem on a lattice is equal to the critical concentration p_c for ferromagnetism in the random Ising system on the same lattice. This equivalence can not generally be valid for the corresponding Heisenberg problem, because in that case a non-zero long-range order parameter is predicted in two-dimensional Heisenberg systems in a certain range of ρ and T , which contradicts a theorem by Mermin and Wagner²⁵. However, in two-dimensional Heisenberg systems, series-expansion methods^{8,9} indicate singular behaviour of the susceptibility at a non-zero temperature T_t^* , which depends on concentration. This singularity should vanish at the critical percolation probability. Experimentally, the diluted Heisenberg system in two and three dimensions has been studied on some manganese compounds^{20,21,22}. Those measurements partially confirm the $T_t^*(\rho)$ calculations.

III.4-2 General behaviour, experiment

The results of the specific-heat measurements show a nice series of peaks at temperatures which decrease regularly on decreasing ρ (fig. III.1). We have identified $T_t(\rho)$ with the temperature $T_m^c(\rho)$, at which the specific heat reaches its maximum value. This identification is somewhat in doubt, because it has been stated that each derivative of the free energy with respect to the field in the diluted system becomes non-analytic at a different temperature, which also differs from the temperature of the energy singularity²⁶. In particular, in a diluted ferromagnetic system, the susceptibility may become infinite without long-range order being established, like in the undiluted 2-d Heisenberg model.

Another difficulty arises because of the rounding of the specific heat²⁷. As can be seen from figs. III.1 and III.4, the peaks remain relatively sharp and become more symmetric on lowering ρ , hence the error introduced by identifying the temperature of the specific-heat singularity T_N by T_m^c is largest at $\rho=1$, where it is about 1%². The error in the reduced temperature $t_N(\rho) \equiv T_m^c(\rho)/T_N(1)$ will be of this order or less.

The values of $t_N(\rho)$ versus ρ , obtained from fig. III.1 are shown in fig. III.2, together with the results of some model calculations. Curve a is the molecular field result, $t_N(\rho)=\rho$. Curve b₁ and b₂ show the result of an effective hamiltonian calculation by Oguchi and Obakata¹⁰:

$$J/kT_c = \log \left[\frac{\rho'(z-1)+1}{\rho'(z-1)-1} \right]$$

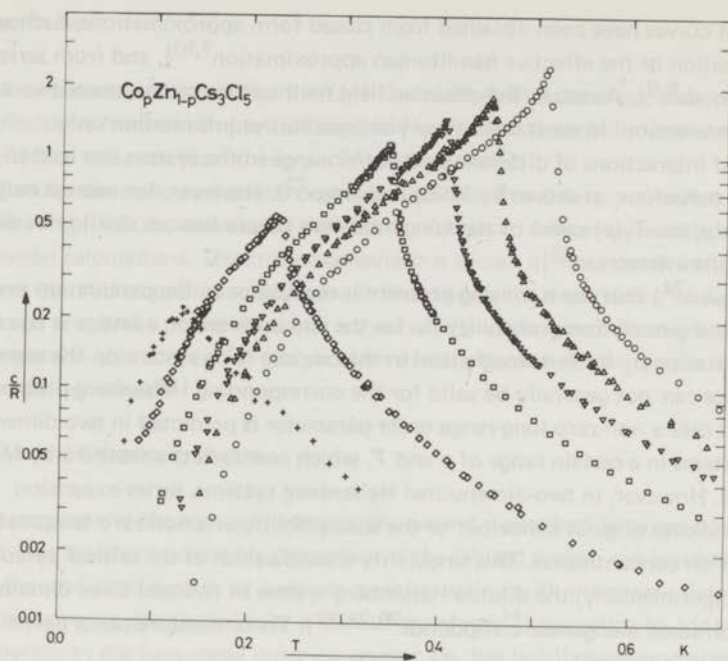


Fig. III.1. Specific-heat data of $\text{Co}_p\text{Zn}_{1-p}\text{Cs}_3\text{Cl}_5$ versus temperature on a semilogarithmic scale.
 $\circ: p=1; \triangle: p=0.9; \nabla: p=0.8; \square: p=0.7; \diamond: p=0.5; +: p=0.35.$

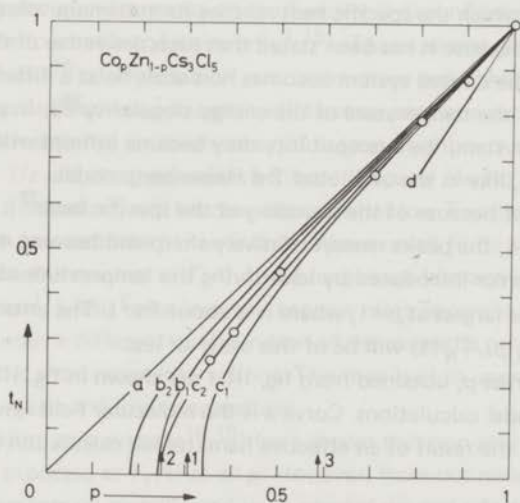


Fig. III.2. t_N versus p compared to model calculations. c_2 : b.c.c. Ising, ref. 9; other curves: see text.

where $p' = p[1 - (1-p)^z]$ and z is the coordination number (curve b_1 : $z=6$, curve b_2 : $z=8$). Curves c_1 and c_2 are obtained from series expansion calculations on the susceptibility by Heap for the s.c. and b.c.c. Ising model respectively⁹). The critical percolation probabilities p_0 for the site problem on the s.c. and b.c.c. lattices as calculated by Sykes and Essam²⁸) are indicated by the arrows 1 and 2.

As can be seen from the figure, the $t_N(p)$ data show regular behaviour and fit very nicely to the b.c.c. Ising curve obtained from the series expansion calculations. An important feature is the initial slope $s = (dt_N/dp)_{p=1}$, which is model dependent. For example, the initial slope for the s.c. Heisenberg model⁹) is shown by curve d in fig. III.2. The observed slope, $s=1$, is in accordance with the quenched Ising system expectation.

Another feature of interest is the apparent critical concentration, which differs for different lattices and for different interaction ranges. The critical percolation probability for the square lattice²⁸) is indicated by arrow 3 in fig. III.2. Although p_0 is not a characteristic of the dimensionality, but varies with the number of nearest neighbours within a given dimension, the apparent low value of the critical concentration can only be explained assuming three-dimensional ordering, unless the interaction is of unexpectedly long range. From the crystal structure and the near equality $|J_A| \approx |J_B| \approx |J_C|$, s.c. behaviour is expected; the tendency to higher effective coordination number is probably due to distant neighbour interactions. The apparent b.c.c. behaviour of $t_N(p)$ is in accordance with the critical values of the energy and the entropy of the concentrated compound²).

The critical values of the energy and the entropy as a function of p are collected in table III.1. They have been obtained from the measured curves (fig. III.1) by numerical integration, applying suitable extrapolation procedures at high and at low temperature.

Table III.1. Critical values of the energy and the entropy.

	T_m	$(S_{\infty} - S_c)/R$	$(S_c - S_0)/R$	$(S_{\infty} - S_c)/pR \log 2$	$(E_c - E_0)/pRT_N$	$-E_c/pRT_N$	E_c/E_0
$\text{Co}_p\text{Zn}_{1-p}\text{Cl}_2$							
ρ							
1.0 ^{a)}	0.523	0.106	0.593	0.153	0.459	0.173	0.272
0.9	0.450	0.125	0.491	0.201	0.423	0.19	0.31
0.8	0.404	0.117	0.429	0.211	0.406	0.21	0.34
0.7	0.343	0.117	0.366	0.241	0.393	0.22	0.35
0.5	0.228	0.121	0.230	0.349	0.254	0.39	0.55
0.4	0.163	0.13	0.15	0.46	0.25	0.60	0.71
0.35	0.130	0.12	0.11	0.50	0.22	0.70	0.77
Ising b.c.c.		0.107	0.586	0.155	0.460	0.169	0.269
Ising s.c.		0.133	0.560	0.192	0.447	0.218	0.328
Ising sq.		0.387	0.306	0.557	0.275	0.549	0.706

^{a)} Values from ref. 2. New measurements on a $p=1$ powdered sample show a 2% lower value of T_m ($T_m(1)=0.511$).

At low T , a graphical extrapolation has been used, assuming an exponential decay of the specific heat.

At high T , the asymptotic behaviour of the short-range ordering specific heat is given by:

$$cT^2/R = (z/8)(\rho'J/k)^2 \equiv b_2(\rho) \quad (III.4-2.1)$$

Using $J/k = -0.24$ K and $z=6$, we get $b_2(\rho) = \rho'^2 \times 0.043$ K². It has been remarked already³), that the calculated $b_2(1)$ value from eq. (III.4-2.1) is in disagreement with the measured value from adiabatic susceptibility measurements, viz. $b_2(1) = 0.0196$ K². From our measurements, it appears that the lower the concentration, the better the asymptotic high-temperature specific-heat behaviour agrees with eq. (III.4-2.1). Whether this means that z in eq. (III.4-2.1) is a function of ρ , or that at high ρ eq. (III.4-2.1) is not a good approximation in the temperature range of the measurement needs further investigation.

The errors in the numbers of table III.1 mainly arise from the lack of accuracy in the high-temperature extrapolation, because for the samples having $1 > \rho > 0.5$ the behaviour of the specific heat did not obey the T^{-2} relation. The estimated error in the E_c values due to this extrapolation error is about 10%. The errors in the other numbers are about 2% in this concentration range. At the lowest ρ values, the main error arises from the inaccuracy of the c/R data and from the low-temperature extrapolation. The resulting error amounts to $\approx 5\%$. All thermodynamic quantities tabulated show monotonic behaviour on decreasing ρ . The total entropy values are in good agreement with the expected values, $S(\rho) = \rho R \log 2$. As can be seen from the table, there is a tendency to lower effective coordination number, which according to Oguchi²⁹) should be attributed to a lowering of the effective dimensionality of the ordering. According to this reference, two-dimensional values of the critical parameters should be obtained at $\rho^* = 0.55$ for a s.c. Ising ferromagnet. From table III.1 it is clear that the critical entropy and energy values are between 2-d and 3-d at this ρ value. A remarkable feature is the constancy of the short-range ordering entropy. Extrapolating this behaviour, all entropy would be short-range ordering entropy at $\rho = 0.175$, which seems a rather low estimate of the critical concentration.

The general shape of the specific-heat curve for some ρ values is compared to various model calculations in fig. III.3. There is no clear indication of a change from 3-d to 2-d behaviour, except for the relative increase of the short-range ordering specific heat.

According to ref. 10, the short-range ordering specific heat is given by:

$$c/R = (z\rho'^2/2)(J/kT)^2 \frac{\exp(-J/kT)}{[1 + \exp(-J/kT)]^2} \quad (III.4-2.2)$$

which shows a maximum at $|kT_m/J| \approx 0.4$. Assuming $J/k = -0.24$ K, we get $T_m \approx 0.1$ K, hence this maximum will not be observed, unless $T_N(\rho) < 0.1$ K. Eq. (III.4-2.2) describes the high-temperature specific-heat behaviour of the $\rho=0.4$ and $\rho=0.35$ samples reasonably well if one takes $z=6$. As could be expected from the afore-mentioned discrepancy between the calculated and the measured b_2 values, the measured specific-heat curves deviate from eq. (III.4-2.2) at higher ρ in the range of measurement.

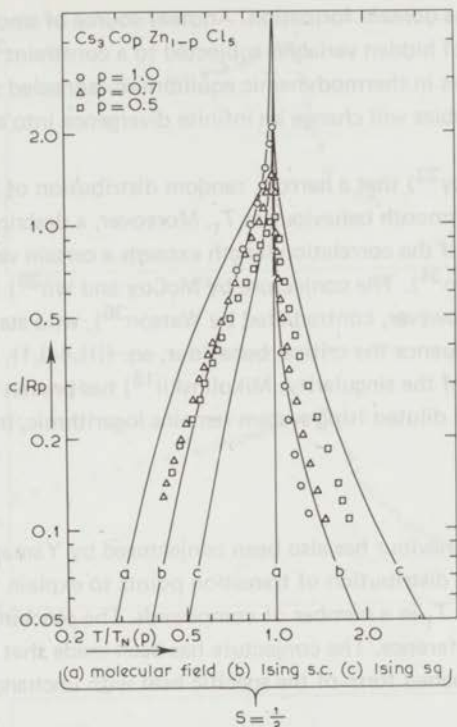


Fig. III.3. Normalized specific-heat data for some p values on a reduced temperature scale, compared to various model calculations.

III.4-3 Critical behaviour, theory

Singularities in the thermodynamic properties of ideal systems have been analysed in terms of critical exponents³⁰). For example, the specific-heat singularity of an ideal Ising system has an asymptotic behaviour according to:

$$c/R = Q_{\pm} + P_{\pm}(1 - \epsilon_{\pm}^{a_{\pm}})/a_{\pm} \quad (\text{III.4-3.1})$$

where $\epsilon_{\pm} = 1 - (T/T_c)^{\pm 1}$, and + and - denote the regions above and below T_c respectively. For 3-d Ising systems, $a_{\pm} \approx 1/8$ and for the 2-d Ising model the behaviour near T_c is logarithmic, which corresponds to $a_{\pm} = 0$.

Critical exponent analysis on real systems is hampered by the rounding of the specific-heat peak which is observed if measurements are performed with sufficiently large temperature resolution. This rounding is attributed to the non-ideality of the sample, for example its finite size and shape. Finite size effects are expected to be experimentally unobservable in specimens of macroscopic size³¹). However, there may be observable shape effects in ferro-

magnetic systems due to the domain formation. Another source of smoothing of the singularity is the presence of hidden variables subjected to a constraint³²), for example a fixed amount of impurities in thermodynamic equilibrium (annealed system). According to ref. 32 such hidden variables will change an infinite divergence into a finite, cusp-like singularity.

It has been shown by McCoy³³) that a narrow, random distribution of interaction constants in a 2-d Ising system causes smooth behaviour at T_t . Moreover, a description by critical exponents becomes invalid if the correlation length exceeds a certain value determined by the width of the distribution³⁴). The conjecture by McCoy and Wu³⁵) that random impurities cause rounding effects is, however, contradicted by Watson³⁶), who states that microscopic inhomogeneities do *not* influence the critical behaviour, eq. (III.4-3.1), except from diminishing the amplitude of the singularity. Mikulinskii¹⁸) has proven that the specific heat of the 2-d random quenched diluted Ising system remains logarithmic, but it is a 'pinched' logarithm:

$$c/R = \log [\epsilon_{\pm} + \delta(\rho)]$$

This pinched logarithmic behaviour has also been conjectured by Yamamoto *et al.*³⁷), in conjunction with a gaussian distribution of transition points to explain the observed rounding of the specific heat near T_t in a number of compounds. The pinching is ascribed to compressibility effects in this reference. The conjecture has been made that finite size effects also should give rise to a pinched form of the specific heat with unchanged critical exponents³¹).

Oguchi²⁹) has used the Padé approximant method to analyse the series expansions of Morgan and Rushbrooke⁸). This analysis yields a critical exponent γ , which depends on ρ . The rise of γ on decreasing ρ has been explained as a decrease of the effective dimensionality of the ordering phenomenon. Recently, the $\gamma(\rho)$ dependence has been called spurious³⁸).

III.4.4 Critical behaviour, experiment

The specific heat of $\text{Co}_\rho\text{Zn}_{1-\rho}\text{Cs}_3\text{Cl}_5$ near T_N with $\rho=1, 0.7$ and 0.5 is shown in fig. III.4. The $\rho=1$ data have been taken from ref. 2. They have been reanalysed in ref. 24. This analysis yields experimental values of a_{\pm} which are in reasonable agreement with the expected ones.

As can be seen from fig. III.4, the singularity weakens on decreasing ρ , but it shows a tendency to become *less* rounded. Hence randomly frozen-in impurities can not be the main cause of the rounding of the specific-heat peak of CoCs_3Cl_5 . We propose that the rounding has to be attributed to a distribution of interaction constants which narrows on decreasing the Co concentration.

There are too many parameters in the fit to yield an accurate numerical result on the critical

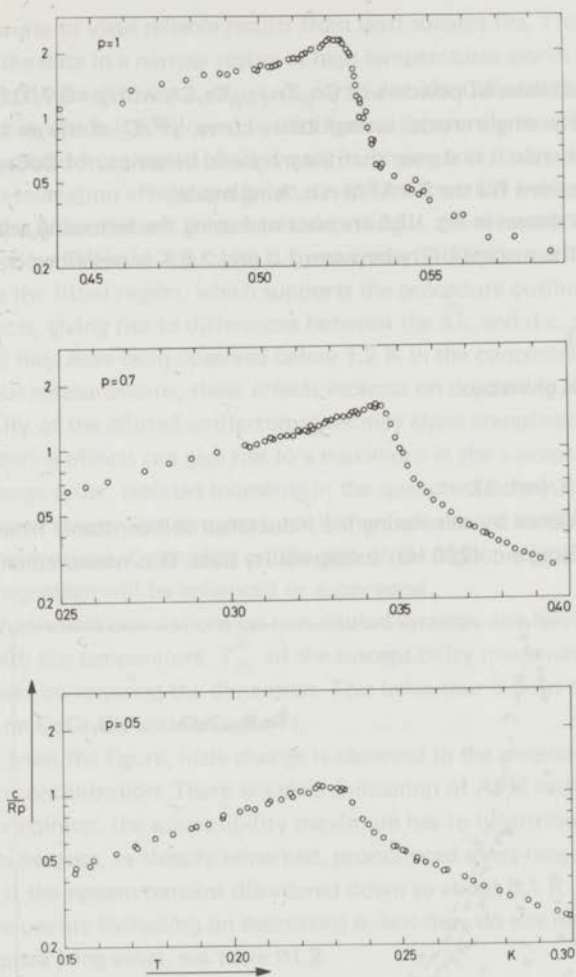


Fig. III.4. Behaviour of the specific heat near $T_N(p)$ for some p values.

exponents, but from fig. III.4 we infer a tendency to cusp-like behaviour at low p , which implies a change into negative α values.

It should be remarked that strong broadening of the peak upon diminishing p is observed in some hydrated ionic compounds, *e.g.* $\text{La}_2\text{Ni}_3\text{Mg}_3(1-p)(\text{NO}_3)_{12} \cdot 24\text{H}_2\text{O}$ ³⁹ and $\text{Dy}_p\text{Y}_{1-p}\text{Cl}_3 \cdot 6\text{H}_2\text{O}$ ⁴⁰). In our opinion, this effect has to be attributed to deviations from the random spin model, for example by a non-random distribution of impurities due to preferential growth in the aqueous solutions, and/or by an effect on the interactions among the magnetic moments, different from breaking the bonds only.

III.5 Susceptibility

The ballistic susceptibilities of powders of $\text{Co}_p\text{Zn}_{1-p}\text{Cs}_3\text{Cl}_5$ with $p=0.7, 0.5$ and 0.35 are shown in fig. III.5. The single crystal susceptibility curve, χ^{zz}/C , of the $p=1$ sample has been taken from ref. 3, wherein it is shown that the magnetic behaviour of CoCs_3Cl_5 is in agreement with the predictions for the 3-d AFM n.n. Ising model.

The measured points shown in fig. III.5 are obtained using the following assumptions:

a) The behaviour of the susceptibility between 1.3 and 2.8 K is described by a Curie-Weiss (CW) relation:

$$\chi/C(p) = 1/[T - \Delta(p)] \quad (\text{III.5.1})$$

b) The CW constant is given by:

$$\Delta(p) = p\Delta(1) \quad (\text{III.5.2})$$

where $\Delta(1) = -0.24$ K (ref. 3).

Values of χ/C are obtained by calculating the inductance coil constants from least squares fits on eq. (III.5.1), using a.c. (260 Hz) susceptibility data. D.c. measurements were found

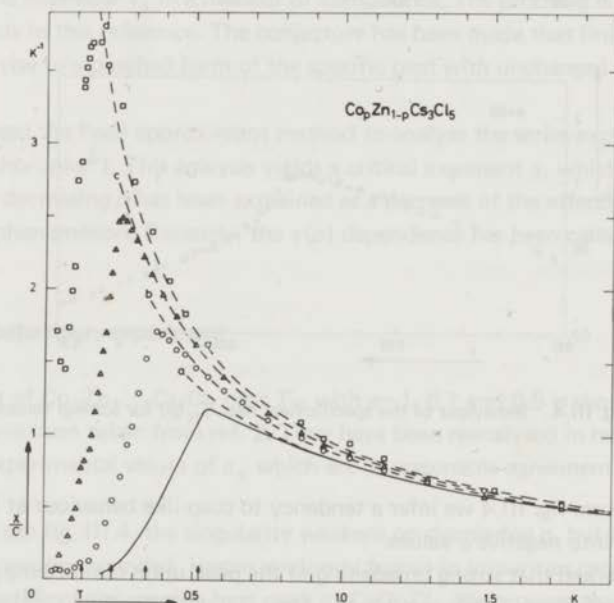


Fig. III.5. Susceptibility data versus temperature for some p values. Full curve: $p=1$; \circ : $p=0.7$; \triangle : $p=0.5$; \square : $p=0.35$. The corresponding transition points obtained from the specific-heat measurements are shown as arrows on the T axis. The dashed curves are Curie-Weiss relations: a: $\Delta=-0.24$ K; b: $\Delta=-0.17$ K; c: $\Delta=-0.12$ K; d: $\Delta=-0.084$ K.

to be too inaccurate to yield reliable results from least squares fits. The procedure of fitting eq. (III.5.1) to the data in a narrow region at high temperatures works well in the case $\rho > 0.5$, but is in doubt at lower ρ values. In particular, the CW constant obtained from least squares fits in which it is allowed to vary has an apparently much larger negative value than the one obtained from eq. (III.5.2) if data belonging to a low ρ value are used. We attribute this to relaxation effects and/or to deviations from CW behaviour in the temperature range of the measurement. Somewhat surprisingly, the measured d.c. susceptibilities approximately show CW behaviour with Δ given by eq. (III.5.2) over a large temperature interval outside the fitted region, which supports the procedure outlined above. Relaxation effects, giving rise to differences between the a.c. and d.c. susceptibilities even at zero external field have been observed below 1.2 K in the concentrated compound³). According to our measurements, these effects increase on decreasing ρ . The susceptibility of the diluted antiferromagnet may show complicated behaviour^{7,41}). Short-range ordering effects can give rise to a maximum in the susceptibility without the onset of long-range order. Isolated moments in the quenched system can react paramagnetically down to very low temperatures if there are nearest neighbour interactions only (parasitic paramagnetism). Depending on the sign of the higher neighbour interactions the parasitic paramagnetism will be enhanced or suppressed. According to theoretical calculations on non-diluted systems, the Néel temperature T_N does not coincide with the temperature T_m^X of the susceptibility maximum^{42,43}). The value of T_m^X/T_N increases on lowering the dimension. This behaviour is born out by susceptibility measurements on CoCs_3Cl_5 and CoCs_3Br_5 ³). As can be seen from the figure, little change is observed in the general behaviour upon decreasing the Co concentration. There is a clear indication of AFM ordering at all measured ρ values. In our opinion, the susceptibility maximum has to be attributed to long-range ordering effects because, as already remarked, pronounced short-range ordering effects are expected only if the system remains disordered down to about 0.1 K. The T_m^X/T_N values are increasing on decreasing ρ , but they do not reach to the two-dimensional square Ising value, see table III.2.

Table III.2

ρ	T_m^X/T_N
1	1.06 ^a)
0.7	1.08
0.5	1.13
0.35	1.31
s.c. Ising	1.06 ^b)
sq. Ising	1.537 ^b)

^a) ref. 3.

^b) ref. 43.

There is an indication of parasitic paramagnetism becoming important at $p=0.35$ at very low temperatures. However, there are strong relaxation effects observed at these temperatures, hence it is doubtful whether the low T data correspond to true thermodynamic equilibrium states. The dipolar interaction favours the AFM (layered) configuration (III.1), hence we expect the parasitic paramagnetism to be suppressed, unless strong ferromagnetic exchange interactions among distant neighbours are present¹²). The absence of pronounced changes from AFM to FM behaviour in the measurements seems to rule out the presence of such interactions.

III.6 Conclusions

Measurements on the specific heat and the susceptibility of the magnetically diluted system $\text{Co}_p\text{Zn}_{1-p}\text{Cs}_3\text{Cl}_5$ with $1 \geq p \geq 0.35$ are in agreement with the quenched Ising model expectations. From the $T_N(p)$ behaviour we conclude that the ordering is described by the three-dimensional Ising model, with predominantly nearest neighbour interactions (effective coordination number $z \approx 8$). The susceptibility data show the ordering to be antiferromagnetic at all $p \geq 0.35$. No strong enhancement effects on the susceptibility from parasitic paramagnetism have been observed down to $p=0.35$, which indicates that the long-range forces favour antiferromagnetic ordering. This could have been anticipated if it is assumed that the long-range forces are only from dipolar origin.

The critical behaviour weakens on decreasing p , but we believe that this can not be described simply by a lowering of the effective dimension. The relative sharpness of the specific-heat peak at low p implies that the rounding of the specific-heat curve of CoCs_3Cl_5 can not be attributed to randomly frozen-in impurities.

Similar experiments on the isomorphous compounds CoRb_3Cl_5 and CoCs_3Br_5 will be useful. CoRb_3Cl_5 orders at higher temperature ($T_N=1.14 \text{ K}^{44}$), which makes it easier to study the critical properties at low p and (relatively) low temperature. CoCs_3Br_5 has two-dimensional features^{2,3}), which should show up clearly in the behaviour of the diluted samples, in particular in the $T_N(p)$ curve.

References

- 1) Griffiths, R.B. and Lebowitz, J.L., *J. Math. Phys.* **9** (1968) 1284.
- 2) Wielinga, R.F., Blöte, H.W.J., Roest, J.A. and Huiskamp, W.J., *Physica* **34** (1967) 223; Wielinga, R.F., thesis, Leiden (1968).
- 3) Mess, K.W., Lagendijk, E., Curtiss, D.A. and Huiskamp, W.J., *Physica* **34** (1967) 126; Mess, K.W., thesis, Leiden (1969).
- 4) Van Stapele, R.P., Beljers, H.G., Bongers, P.F. and Zijlstra, H., *J. Chem. Phys.* **44** (1966) 3719.
- 5) Van Stapele, R.P., Henning, J.C.M., Hardeman, G.E.G. and Bongers, P.F., *Phys. Rev.* **150** (1966) 310.
- 6) Samokhvalov, A.A., Volkenshtein, N.V., Bamburov, V.G., Zotov, T.D., Ivakin, A.A., Morozov, Y.N. and Simonava, M.I., *Fizika Tverdogo Tela* **9** (1967) 706 (transl. *Sov. Phys. Solid State* **9** (1967) 555).
- 7) Sato, H., Arrott, A. and Kikuchi, R., *J. Phys. Chem. Sol.* **10** (1959) 19.
- 8) Rushbrooke, G.S., and Morgan, D.J., *Mol. Phys.* **4** (1961) 1; Morgan, D.J. and Rushbrooke, G.S., *Mol Phys.* **4** (1961) 291, **6** (1963) 477.
- 9) Heap, B.R., *Proc. Phys. Soc. (London)* **82** (1963) 252.
- 10) Oguchi, T. and Obokata, T., *J. Phys. Soc. Japan* **27** (1969) 1111.
- 11) Luttinger, J.M. and Tisza, L., *Phys. Rev.* **70** (1946) 954.
- 12) Hammann, J., *Physica* **43** (1969) 277.
- 13) See Appendix.
- 14) Blocker, T.G. and West, F.G., *Phys. Letters* **28A** (1969) 487.
- 15) Galavotti, G., *J. Math. Phys.* **11** (1970) 141.
- 16) Brout, R., *Phys. Rev.* **115** (1959) 824.
- 17) See for example Violet, C.E. and Borg, R.J., *Phys. Rev.* **149** (1966) 540.
- 18) Mikulinskii, M.A., *Zh. Eksperim. i Teor. Fiz.* **53** (1967) 1071 (transl. *Sov. Phys. JETP* **26** (1968) 637).
- 19) Griffiths, R.B., *Phys. Rev. Letters* **23** (1969) 17.
- 20) Baker, J.M., Lourens, J.A.J. and Stevenson, R.W., *Proc. Phys. Soc. (London)* **77** (1961) 1038; see also ref. 23.
- 21) Breed, D.J., Gilijamse, K., Sterkenburg, J.W.E. and Miedema, A.R., *J. Appl. Phys.* **41** (1970) 1267.
- 22) Takeda, K., Matsuura, M. and Haseda, T., *J. Phys. Soc. Japan* **28** (1970) 29.
- 23) Elliot, R.J. and Heap, B.R., *Proc. Roy. Soc. (London)* **A265** (1962) 264.
- 24) Kasteleyn, P.W. and Fortuin, C.M., *J. Phys. Soc. Japan* **26** (suppl.) (1969) 11; Fortuin, C.M., thesis, Leiden (1971).
- 25) Mermin, N.D. and Wagner, H., *Phys. Rev. Letters* **17** (1966) 1133.
- 26) Watson, P.G., *J. Phys. (London)* **C 3** (1970) 125.
- 27) Wielinga, R.F., *Comm. Solid State Phys.* **3** (1970) 59.
- 28) Sykes, M.F. and Essam, J.W., *Phys. Rev.* **133** (1964) A310.
- 29) Oguchi, T., *J. Phys. Soc. Japan* **26** (1969) 580; see also ref. 10.
- 30) Fisher, M.E., *Rep. Progr. Phys.* **30** (1967) 615.
- 31) Fisher, M.E. and Ferdinand, A.E., *Phys. Rev. Letters* **19** (1967) 169.
- 32) Fisher, M.E., *Phys. Rev.* **176** (1968) 257.
- 33) McCoy, B.M., *Phys. Rev.* **B 2** (1970) 2795.
- 34) McCoy, B.M., *Phys. Rev. Letters* **23** (1969) 383.
- 35) McCoy, B.M. and Wu, T.T., *Phys. Rev. Letters* **21** (1968) 549.
- 36) Watson, P.G., *J. Phys. (London)* **C 2** (1969) 948.
- 37) Yamamoto, T., Tanimoto, O., Yasuda, Y. and Okada, K., in 'Critical Phenomena', eds. M.S. Green and J.V. Sengers (N.B.S., Washington, D.C., 1966) p. 86.
- 38) Rapaport, D.C., *Phys. Letters* **37A** (1971) 15.

- 39) Mess, K.W., Lagendijk, E., Zimmerman, N.J., Van Duyneveldt, A.J., Giessen, J.J. and Huiskamp, W.J., *Physica* **43** (1969) 165.
- 40) See chapter II.
- 41) Katsura, S. and Tsujijama, B., ref. 37, p. 219.
- 42) Fisher, M.E., *Physica* **25** (1959) 521.
- 43) Sykes, M.F. and Fisher, M.E., *Physica* **28** (1962) 919, 939.
- 44) Blöte, H.W.J. and Huiskamp, W.J., *Phys. Letters* **29A** (1969) 304.

CHAPTER IV

NUCLEAR ORIENTATION STUDY ON THE BEHAVIOUR OF 3d TRANSITION METAL ELEMENTS DISSOLVED IN A NON-MAGNETIC METAL (THE KONDO PROBLEM)

Synopsis

Results of nuclear orientation measurements on ^{51}Cr , ^{54}Mn , and ^{60}Co in gold and ^{54}Mn in zinc with very low concentrations of the transition metal elements are presented. The behaviour of ^{51}Cr and ^{54}Mn in gold can be described by a free spin slow relaxation model in the range of measurement, $1 < 1/T < 60 \text{ K}^{-1}$ and $0 < H < 5 \text{ kOe}$. The other alloys can not be described by a free spin model, which is attributed to the effects of the s - d interaction (the Kondo effect).

IV.1 Introduction

The behaviour of dilute alloys, consisting of a non-magnetic metal in which a small number of transition element atoms is dissolved, has received active interest in recent years, both from theoretical and experimental side¹⁻⁵). Most of the theoretical work has started from the assumption of a *magnetic* impurity (a localized moment) interacting with the sea of conduction electrons through the s - d exchange interaction:

$$\mathcal{H}_{s-d} = J s \cdot S \quad (\text{IV.1.1})$$

where S is the impurity spin angular momentum and s is the conduction electron spin angular momentum density at the impurity site. Presumably, the s - d exchange interaction model is a good approximation for those alloys which are classified as (strongly) magnetic in the Blandin-Friedel scheme²), for example Cr, Mn, and Fe in the noble metal hosts. However, it has become clear that the formation of a local moment on the impurity can not be treated separately from its interactions with the surroundings. Hence the concept of a localized spin fluctuation (LSF) has arisen. The main characteristic of a LSF is its lifetime τ_{sf} . The extent of the validity of the two models, the s - d exchange model and the localized spin fluctuation model, and the relations between them are currently investigated. It has been shown by Rivier and Zuckerman⁶) that the two models lead to similar behaviour of a number of physical properties at low temperatures, such as the susceptibility and the electrical resistivity, in spite of the different mechanisms involved (non-magnetic behaviour due to the formation of a 'quasi bound state' versus slowing down of thermal fluctuations compared to spin fluctuations).

The properties of the hamiltonian eq. (IV.1.1) have been reviewed recently^{3,4,5}). Although simple in principle, the interaction has a true many body character and no exact solutions are known at present, except for some special cases. If $J < 0$, anomalous behaviour is expected at low temperatures from perturbation calculations, in accordance with experiment. Because we consider the effect of a single impurity spin, the number of degrees of freedom is low, and smooth behaviour is expected, instead of a sharp transition. Moreover, the effects of the interaction may spread out over many decades in temperature, due to thermal fluctuations. Hence, unlike the case of superconductivity, 'transition' temperatures far outside the range of measurement have been predicted. From each of the various anomalies observed in the thermodynamic and transport properties (X), characteristic temperatures T_{KT}^X may be derived, by fitting the experimental data to different theoretical expressions (T). At present, no unifying theory exists which describes the properties of all quantities of interest at all temperature and field values. Therefore the T_{KT}^X generally differ, according to the quantity measured and the approximation used. In high-temperature perturbation calculations, however, the anomalous part of many of the physical properties can be expressed within the limits of the s - d exchange model by terms containing powers of $J \log(T/T_{KA})$, where $kT_{KA} = D \exp(1/N(0)J)$. k is Boltzmann's constant, D is the width of the conduction band and $N(0)$ is the density of states of the conduction electrons at the Fermi level. T_{KA} is called the Kondo (Abrikosov) temperature⁷); due to its exponential dependence on J , widely varying T_{KA} values are obtained upon modest changes of J .

If the nucleus of the impurity carries a spin, and correspondingly a magnetic moment, it will be coupled to the electronic spin via hyperfine interaction. As long as this interaction is only a weak perturbation, the nucleus may be used to probe the electronic state of the impurity. Consequently, the behaviour of the magnetic field on the nucleus of a paramagnetic impurity in a metallic host has been measured using a variety of techniques, which have been applied in investigations on magnetic ions in ionic solids. Among those methods, Mössbauer effect (ME) measurements and nuclear orientation (NO) measurements are closely related. Both methods exploit the properties of radioactive nuclei, which allows very low impurity concentrations, hence interaction effects are expected to be absent down to ultra low temperatures.

We have performed NO measurements on ⁵⁴Mn parent nuclei dissolved in Au and Zn, studying the anisotropy of the emitted gamma radiation from the ⁵⁴Cr daughter nuclei. Based on the experience of NO measurements in a large variety of metallic and non-metallic samples, one expects that the alignment of the daughter nuclei is entirely determined by the alignment of the parent nuclei.

Our measurements indicate that Mn dissolved in very low concentration in Au behaves paramagnetically down to 20 mK in fields as low as 200 Oe. We have assumed slow relaxation, *i.e.* the relaxation time of the impurity spin to a heat bath is long compared to the nuclear precession time. It will be shown from an analysis of the dynamical behaviour that this assumption is reasonable.

Mn in Zn behaves differently and presumably the results can not be described by a free spin,

either in a slow or in a fast relaxation model. Our results on ZnMn do not agree with those obtained by other investigators. The differences may be due to metallurgical problems. A more elaborate study is necessary to obtain definite conclusions with respect to the impurity state in this alloy. Preliminary results on AuCo and AuCr will also be presented. The alloys have been chosen such that the NO measurements are expected to lie in different regimes of the Kondo effect. From plots of the Kondo temperatures *versus* the transition element impurity for various hosts (Schrieffer plots) we expect²⁾:
 $T_K(\text{AuMn}) \approx 0.01 \text{ K} < T_K(\text{AuCr}) \approx 1 \text{ K} < T_K(\text{AuCo}) \approx 300 \text{ K}$, and
 $T_K(\text{AuMn}) \approx 0.01 \text{ K} < T_K(\text{ZnMn}) \approx 1 \text{ K}$, T_K being a 'mean' T_{KT}^X value.

IV.2 Hyperfine interaction

In the isotropic case, the magnetic hyperfine interaction can be written:

$$\mathcal{H}_{\text{hf}} = AI \cdot S \quad (\text{IV.2.1})$$

where I is the nuclear spin and A is the hyperfine constant which is related to the saturation hyperfine field by:

$$H_{\text{hf}}^{\text{sat}} = AS/g_n \mu_n$$

g_n is the nuclear g factor and μ_n is the nuclear magneton.

Three contributions to the magnetic hyperfine interaction between electrons and nuclei can be discerned⁸⁾: a contact part which is non-zero for s electrons only, an orbital part and a spin dipolar part, the last two being non-zero for non- s electrons only. If there are no unpaired s electrons and if the orbital and spin dipolar parts vanish, *e.g.* due to spherical symmetry in S -states such as is the case in the Mn^{2+} ion, one-electron theory predicts the hyperfine field to be zero. However, a large hyperfine field ($\approx 700 \text{ kOe}$) is observed at the Mn^{2+} nucleus in ionic solids. This is explained by the effects of the d -shell on the inner core electrons belonging to s -shells (core polarization). For $3d$ transition metal ions, the hyperfine field due to core polarization amounts to $H_{\text{cp}}/2S \approx -125 \text{ kOe}$.

According to Hirst⁹⁾, the hyperfine coupling of a $3d$ dipositive transition metal ion in a non-magnetic metallic host should be affected by the *direct s-d* exchange interaction, which is positive and causes a lowering of the hyperfine field due to 'dynamic' spin polarization of the conduction electrons. As shown by measurements of the saturation hyperfine field this effect amounts to $H_{\text{dp}}/2S \approx +60 \text{ kOe}$. It should be emphasized that the *direct* exchange is involved and not the 'effective' exchange from the covalent admixture which is negative and mainly uses the $l=2$ channel¹⁰⁾. The direct exchange is expected to have a temperature- and, for $3d$ impurities in noble metals, also a host-independent effect. The temperature independence of the effect on the hyperfine constant is confirmed by experiments on CuFe, which show that the ratio of the impurity hyperfine field and the total impurity magnetization remains the same above and below T_K . However, as pointed out by Campbell¹¹⁾ there is

a striking systematic variation of the ratio $H_{\text{hf}}^{\text{sat}}/2S$ which diminishes when T_K increases. According to this reference, such a behaviour arises from the combined effect of the direct and the mixing terms of the s - d interaction.

In the following we will assume the hyperfine coupling A to be a constant, *i.e.* independent of temperature and applied field. A is determined from the saturation hyperfine field which is the *effective hyperfine* field at the nucleus if the applied external field is sufficiently large. Some of the measured values of $H_{\text{hf}}^{\text{sat}}$ are tabulated in table IV.1. The corresponding A values for ^{51}Cr and ^{54}Mn in Au are shown in table IV.2.

IV.3 Nuclear orientation, slow and fast relaxation

Presumably, a good approximation of the total hamiltonian of the systems under consideration is given by:

$$\mathcal{H} = g\mu_B H S_z + g_n \mu_n H I_z + A I \cdot S + JS \cdot s \quad (\text{IV.3.1})$$

which contains the electronic and nuclear Zeeman terms, the hyperfine interaction and the s - d exchange interaction. The nuclear orientation resulting from this spin hamiltonian can be calculated once the statistical averages $\langle I_z^k \rangle$ are known. Here k is a positive integer, and, as usual, $\langle A \rangle$ means $\text{Tr} \rho A / \text{Tr} \rho$ where ρ is the matrix density.

We have performed NO measurements by counting of the gamma quanta emitted by the nuclei in a direction parallel and perpendicular to an applied field as a function of temperature. The measured gamma-ray intensities will be denoted by $W(0)$ and $W(\pi/2)$ respectively and are normalized to 1 at high temperatures. The intensities for the systems investigated in this chapter are given by¹²⁾:

$$W(\varphi) = 1 + A_2 f_2 P_2(\cos\varphi) + A_4 f_4 P_4(\cos\varphi)$$

The A_k are constants determined by gamma decay characteristics and are tabulated in table IV.3, while f_2 and f_4 are given by:

$$f_2 = (1/I^2) [\langle I_z^2 \rangle - \frac{1}{3} I(I+1)]$$

$$f_4 = (1/I^4) [\langle I_z^4 \rangle - \frac{1}{7} (6I^2 + 6I - 5) \langle I_z^2 \rangle + \frac{3}{35} I(I-1)(I+1)(I+2)]$$

(The P_k are Legendre polynomials.)

One can calculate the statistical averages by diagonalizing the hamiltonian eq. (IV.3.1) and determining the quantum mechanical and Boltzmann averages from the calculated eigenvalues and eigenvectors. This method assumes that the electronic and nuclear spins are only weakly coupled to a heat bath (*e.g.* the conduction electron spin system or the lattice), so that the nuclear spin interacts with the instantaneous value of the electron spin. Hence the nuclear precession time should be short compared to the impurity electron spin relaxation times. This limit is called the slow relaxation model. The other extreme is to assume that the electron spin relaxation time is short compared to the nuclear precession time (fast

relaxation model). In that case the nuclear spin interacts effectively with the averaged electronic spin $\langle S_z \rangle$ which is related to the magnetization M_z according to:
 $M_z = N\mu_{\text{sat}} \langle S_z \rangle / S$. Then the measured NO would correspond to an effective hyperfine field:

$$H_{\text{hf}}^{\text{eff}} = H_{\text{hf}}^{\text{sat}} M_z / N\mu_{\text{sat}}$$

and can be determined easily once $W(0)$ and $W(\pi/2)$ are known as a function of $\Delta E/kT$ where $\Delta E = |g_n \mu_n (H_{\text{hf}}^{\text{eff}} \pm H)|$ is the energy separation of the nuclear magnetic sub-levels. T is the temperature of the heat bath which is the lattice temperature in a static experiment such as NO in view of the shortness of the spin-lattice relaxation times in metallic systems compared to the time of measurement. In fig. IV.1, $W(0)$ and $W(\pi/2)$ are shown calculated as a function of $\Delta E/kT$ in the case of ^{51}Cr , ^{54}Mn , and ^{60}Co . It is clear from the figure that large

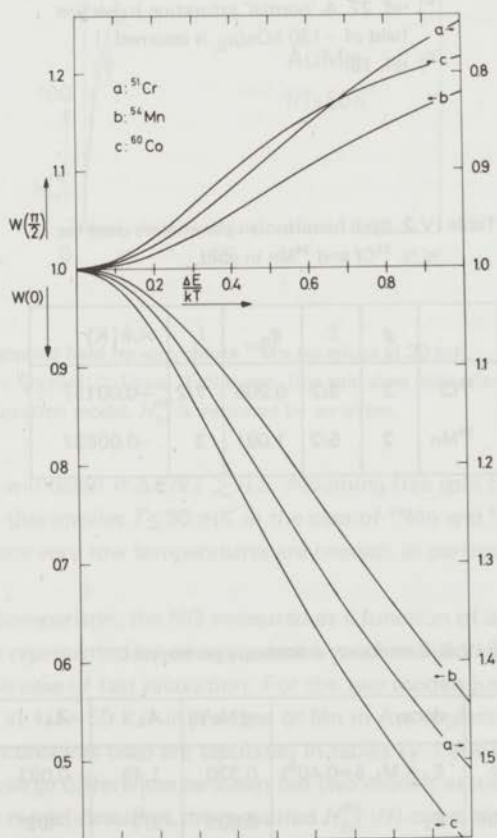


Fig. IV.1. Normalized gamma ray intensities in directions parallel ($W(0)$) and perpendicular ($W(\pi/2)$) to the field at the nucleus, as a function of $\Delta E/kT$, where ΔE is the (equidistant) nuclear magnetic sub-level splitting.

Table IV.1. Saturation hyperfine field and Kondo temperature data.

	$-H_{\text{hf}}^{\text{sat}}$ [kOe]	T_{K}^{NO} [K]
AuCr	$242 \pm 13^{\text{a}}$	< 0.1
AuMn	400 ± 10	< 0.01
AuCo		≥ 1
ZnMn	≈ 200	≈ 0.17
	188^{c}	0.26^{c}

a) ref. 21.

b) ref. 22. A 'normal' saturation hyperfine field of $-130 \text{ kOe}/\mu_{\text{B}}$ is assumed.

c) ref. 19.

Table IV.2. Spin hamiltonian parameters used for ^{51}Cr and ^{54}Mn in gold.

	g	S	g_{n}	l	A/k [K]
^{51}Cr	2	3/2	0.266	7/2	-0.00157
^{54}Mn	2	5/2	1.091	3	-0.00637

Table IV.3. Gamma-ray anisotropy parameters.

	decay	γ [MeV]	A_2	A_4
^{51}Cr	$E_2 + M_1, \delta=0.40^{\text{a}}$	0.320	1.49	0.093
^{54}Mn	E_2	0.835	-9/7	-9/2
^{60}Co	E_2	1.17 1.33	-1.190	-2.48

a) Mixing ratio.

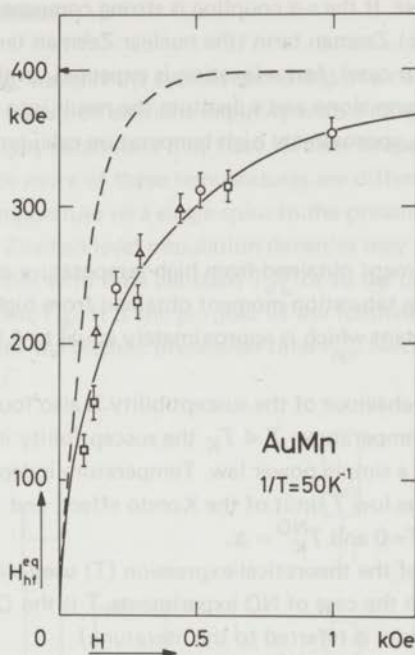


Fig. IV.2. H_{hf}^{eq} versus applied field for very dilute ^{54}Mn -Au alloys at 20 mK.

○: Leiden; △: Oxford; □: Orsay. Full curve: free spin slow relaxation model; dashed curve: free spin fast relaxation model. H_{hf}^{sat} is indicated by an arrow.

gamma anisotropies will occur if $\Delta E/kT \gtrsim 0.5$. Assuming free spin behaviour and a saturated spin value $\langle S_z \rangle = S$, this implies $T \lesssim 30$ mK in the case of ^{54}Mn and ^{60}Co , and $T \lesssim 10$ mK in the case of ^{51}Cr . Hence very low temperatures are needed, in particular in experiments on ^{51}Cr .

For the purpose of comparison, the NO measured as a function of applied field at a certain temperature may be represented by an equivalent hyperfine field H_{hf}^{eq} , which is the effective hyperfine field in the case of fast relaxation. For the two models just outlined, fig. IV.2 shows H_{hf}^{eq} versus H at $1/T = 50 \text{ K}^{-1}$ in the case of Mn in Au, neglecting the effects of the s - d interaction. The constants used are tabulated in tables IV.1 and IV.2. It is clear from the figure that there are large differences between the two models at low applied fields. The free spin slow relaxation model describes the measured $H_{hf}^{eq}(H)$ curve at $1/T = 50 \text{ K}^{-1}$ very well in the case of AuMn. Fast relaxation is expected at higher temperatures. Because most ME measurements have been performed at temperatures above 1 K, a fast relaxation model may be appropriate in this case.

Exact calculations of the NO from the hamiltonian eq. (IV.3.1) including the s - d interaction

have not been performed as yet. If the s - d coupling is strong compared to the hyperfine interaction and the (electronic) Zeeman term (the nuclear Zeeman term may be neglected for all practical purposes in our case), fast relaxation is expected. In that case we may calculate $\langle S_z \rangle$ from the s - d term alone and substitute the result into the remaining part of the hamiltonian. In low fields, approximate high-temperature calculations yield:

$$H_{\text{hf}}^{\text{eq}} = \frac{H_{\text{hf}}^{\text{sat}}}{\mu_{\text{sat}}} \frac{\mu_{\text{eff}}^2}{3k(T+\Delta)} H \quad (\text{IV.3.2})$$

where μ_{eff} is the magnetic moment obtained from high-temperature and low-field susceptibility measurements, μ_{sat} is the saturation moment obtained from high-field magnetization measurements, and Δ is a constant which is approximately equal to $4.5 T_{\text{KA}}$ if $7 < T/T_{\text{KA}} < 100$.

Experimentally, Curie-Weiss behaviour of the susceptibility is also found in a certain region below T_{K} , with $\Delta \approx T_{\text{K}}$. At temperatures $T \ll T_{\text{K}}$ the susceptibility is expected to approach a constant value, according to a simple power law. Temperature independent behaviour of $H_{\text{hf}}^{\text{eq}}$ has been interpreted as the low T limit of the Kondo effect, and T_{K}^{NO} has been obtained from eq. (IV.3.2) by putting $T=0$ and $T_{\text{K}}^{\text{NO}} = \Delta$.

(From now on, an indication of the theoretical expression (T) used will be omitted from the Kondo temperature symbol. In the case of NO experiments, T is the Curie-Weiss relation (IV.3.2). In other cases the reader is referred to the literature.)

Concludingly, NO measurements yield T_{K}^{NO} from low-field measurements and $H_{\text{hf}}^{\text{sat}}$ from high-field measurements once saturation is observed. NO experiments on a number of alloys which are known to have Kondo-like anomalies at low temperatures have been analysed in this way, yielding results which are in reasonable agreement with results from other experiments, see refs. 13 to 26.

If the s - d coupling is weak compared to the other interactions, NO measurements may decide which of either model, fast or slow relaxation adequately describes the system. Because NO measurements are relatively inaccurate due to the unavoidable statistical errors, minor deviations from paramagnetic behaviour can not be detected.

It should be kept in mind that the two models represent extremes. To our knowledge, no calculations on intermediate relaxation models have been published up to now. However, we expect the results of calculations on such a model to lie in-between the two extremes. Most NO data on systems which show low-temperature Kondo anomalies such as CuMn^{20} , AgMn^{18} and ZnMn (IV.9) lie below the free spin slow relaxation curve. Hence we expect that these measurements can not be explained by free spin intermediate relaxation behaviour. An applied magnetic field will slow down the impurity electron spin flip rate and accordingly may induce a transition from fast to slow relaxation²⁶). However, the two models give the same results in the limit of saturation of the electronic spin system.

Data on the relaxation times are necessary to decide which model is appropriate in a specific case. However, as pointed out in the next section, the few data available are amenable to criticism.

IV.4 The relaxation problem

Assuming weak coupling, we split the system consisting of a non-magnetic metallic host which contains a single transition element impurity with a localized moment into subsystems as shown in fig. IV.3. Every subsystem may have its own temperature, and relaxation processes occur if two or more of these temperatures are different. Strictly speaking, we can not assign a spin temperature to a single spin. In the presence of a magnetic field, however, the local moment Zeeman level population densities may define a Zeeman temperature which relaxes to the lattice with time constant T_{dL} or to the conduction electron spin system with time constant T_{ds} . It is the purpose of the following discussion to compare these time constants with the nuclear precession time τ_{np} . Nuclear relaxation processes will also be shortly reviewed.

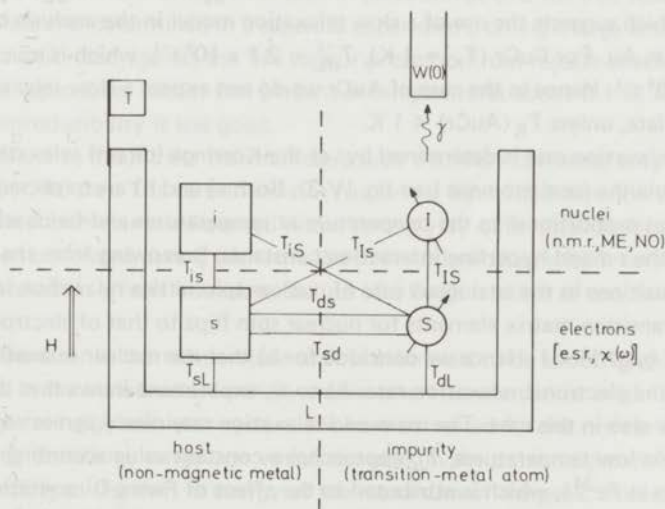


Fig. IV.3. Schematic view of a dilute magnetic alloy in the weak coupling limit. Relaxation processes which presumably are effective in the nuclear orientation measurement time (1-30 min.) are indicated by full lines. Applied field (H), thermometer (T), and counter are also included in the figure.

In the paramagnetic (unbound and unordered) region the lower (electronic) part of the diagram shown in fig. IV.3 is fairly well understood²⁷⁻³³). The assumption of an exchange coupled conduction electron spin-impurity spin system leads to a Korringa-like relaxation rate $T_{ds}^{-1} = aT s^{-1}$, where $a = 1.7 \times 10^9$ in the case of CuMn³²). Presumably, this number will be smaller in the case of AuMn because $J(\text{AuMn}) < J(\text{CuMn})$. Due to the limited heat capacity of the electrons at the Fermi surface, bottleneck effects may occur^{27,28}). The direct relaxation rate T_{dL}^{-1} may be attributed to admixture of conduction-band electron wave

functions into the localized $3d$ impurity wave function, which allows the localized d spins to relax to the lattice via distant impurities³¹). This mechanism gives rise to a temperature independent relaxation time. Accordingly, we expect T_{dL}^{-1} to decrease the more localized the impurity wave function is, hence the lower T_K . Thus we expect $T_{dL}^{-1}(\text{AuMn}) < T_{dL}^{-1}(\text{CuMn}) = 2.9 \times 10^8 \text{ s}^{-1}$ (ref. 32). The determination of T_{dL}^{-1} is based on the observation of a residual line width^{29,30}) at $T=0$ from e.s.r. measurements at relatively high temperatures ($T > 1 \text{ K}$). However, it is not excluded from these measurements that the extrapolated residual line-width is (partly) due to inhomogeneous broadening. Although the measurements can be satisfactorily described by a temperature independent T_{dL}^{-1} , the possibility of temperature dependence, in particular below T_K , is not excluded³³). In view of the foregoing, the quoted T_{dL}^{-1} values should be considered with care. Probably they are upper limits which, however, stresses our argument.

In conclusion, at temperatures below 0.1 K we expect $T_{ds}^{-1}(\text{AuMn}) < T_{dL}^{-1}(\text{AuMn}) < \tau_{np}^{-1} = 3 \times 10^8 \text{ s}^{-1}$, which suggests the use of a slow relaxation model in the analysis of NO experiments on Mn in Au. For CuCr ($T_K \approx 1 \text{ K}$), $T_{dL}^{-1} = 2.1 \times 10^9 \text{ s}^{-1}$, which is much larger than $\tau_{np}^{-1} = 0.5 \times 10^8 \text{ s}^{-1}$. Hence in the case of AuCr we do not expect a slow relaxation model to be appropriate, unless $T_K(\text{AuCr}) \ll 1 \text{ K}$.

The nuclear relaxation rate is determined by: a) the Korringa (direct) relaxation rate T_{Is}^{-1} and b) relaxation via the local moment (see fig. IV.3). Both a) and b) are expected to yield relaxation rates proportional to the temperature at temperatures and fields which are high compared to the s - d and hyperfine interaction constants. Borrowing from the knowledge on forbidden transitions in the analogous case of nuclear spin lattice relaxation in ionic solids, the ratio of transition matrix elements for nuclear spin flips to that of electronic spin flips is given by $(A/g\mu_B H)^2 \ll 1$. Hence we conclude for b) that the nuclear relaxation rate is small compared to the electronic relaxation rate. As to a), experiment shows that the relaxation is relatively slow also in this case. The measured relaxation rate nicely agrees with theoretical calculations. At low temperatures, T_{Is} approaches a constant value according to measurements on ^{60}Co in Fe^{34}), which is attributed to the effect of Fermi-Dirac statistics. At low fields, the nuclear spin is coupled to the electron spin such as to yield a single relaxation rate, which presumably is of the order of the high-field electron spin relaxation rate. Of course, if the local moment is compensated or decoupled, only the direct relaxation a) remains. Concludingly, we expect that the nuclear relaxation times of the impurity at very low temperatures and at fields above several hundred Oersteds are in the millisecond range, which is long compared to the electronic relaxation times and the nuclear precession time but short compared to the time scale of the NO measurement. Hence thermal equilibrium may be presupposed in the calculations (compare IV.3).

IV.5 Experimental

The equipment has been described extensively before³⁵). Adiabatic demagnetization of a CrK alum slurry enables us to reach temperatures in the sample down to 15 mK . Fields up

to 5 kOe can be applied at these temperatures using a Helmholtz coil outside the cryostat. NaI counters are mounted along directions parallel and perpendicular to the applied field. The thermometer used is a cerium magnesium nitrate (CMN) thermometer which is constructed by moulding molten CMN into a teflon cylinder containing a copper brush. The cylinder has diameter equal to height, such as to make demagnetization corrections negligible³⁶). The susceptibility of the CMN thermometer is measured using a Hartshorn bridge with lock-in detection at 260 Hz, and temperatures are derived from the bridge readings by application of Curie's law. The CMN thermometer is calibrated above 0.1 K against a previously calibrated carbon resistor thermometer which consists of a small slab of carbon cutted from a Speer 220 Ω 1/2 W carbon resistor. Heat contact is made using Apiezon N grease and coil foil; electrical contacts are made using silver paint. In this way we avoid that the resistance becomes unduly large at very low temperatures. The resistance is measured using a Wheatstone bridge with lock-in detection at 675 Hz. The resistance *versus* temperature relation is determined in a separate experiment, taking a large amount of CMN which in turn is calibrated against the ⁴He vapour pressure. From regular checks it appeared that the resistor reproduces within one percent at temperatures above 0.1 K. At lower temperatures reproducibility is less good.

Care has been taken to mount the thermometers such that they can sense only small magnetic fields (< 40 Oe). The carbon resistor has only a weak field dependence³⁷). However, the CMN thermometer is influenced rather strongly by quite small fields (\approx 10 Oe), hence it has been calibrated during each run. We have no indications from carbon resistor readings that saturation effects invalidate the use of a Curie relation at very low temperatures.

Concludingly, the error in the temperature scale is estimated to be about 5%.

The main errors in the measured anisotropy values arise from statistical origin and from drift in the counter-pulse height analyser system. We have corrected for the drift in first approximation, by shifting the energy range over which the peak in the pulse height spectrum is integrated according to the shift in energy of the maximum of the peak. This correction amounts to a few percent of the measured effect at most. It is especially important in the case of AuCr where long counting times have been taken to get sufficient statistics. Conical lead collimators have been utilized in some cases to minimize the influence of Compton scattering at the walls of the cryostat and at the magnet. Background and solid angle corrections appeared to be negligible.

The errors indicated in the figures are the statistical errors only.

IV.6 Preparation of the samples

Samples of AuMn, AuCr, AuCo, ZnMn, and CdMn have been prepared by the metallurgical department of the laboratory*. Mn and Cr are well soluble in gold (> 10% at room temper-

* We thank Mr. C.E. Snel, Mr. H.J. Tan, Mr. T.J. Gortemulder and Dr. B. Knook for the preparation of the samples. Code numbers are: 6902, 7029 (AuMn); 6994 (AuCr); 69106 (AuCo); uncoded (ZnMn); 7081 (CdMn).

ature), but Co in gold and Mn in zinc and in cadmium have a small solubility ($< 0.5\%$ at r.t.), see ref. 38. Because of the low concentrations of the magnetic atoms ($\lesssim 1$ ppm) no precipitation and/or clustering effects were expected on cooling down from the molten solution to room temperature and below, irrespective of the cooling rate.

Solutions of radioactive transition metal chlorides were deposited on the host metal (99.999% purity, containing less than 4 ppm Fe as the most abundant magnetic impurity). After careful drying, the chlorides are reduced in a hydrogen atmosphere at temperatures below the melting point of the host metal and thereafter the samples are molten, and cooled down to room temperature in about nine hours.

After cold rolling, the samples were investigated on surface effects by grinding the surfaces carefully and measuring the loss of activity per unit loss of weight. This analysis showed the Mn activity of the Cd alloy to be almost exclusively at the surface. We ascribe this to insufficient reduction at a comparatively low reduction temperature, which was restricted by the low melting point of Cd.

The experiments on CdMn have not been pursued further. In the other alloys a true volume activity was found, hence we conclude that the transition element was in solution. One AuMn alloy has been prepared by diffusion of Mn at about 1000°C during 20 hours. Subsequent analysis revealed that the activity was not homogeneously distributed over the sample. Apparently, the diffusion time should have been taken much longer. We have not performed NO measurements on this sample. Compton *et al.*¹⁴) report good agreement between the measured anisotropies of diffused and molten samples of Mn in noble metal hosts.

From the activities, ^{54}Mn and ^{60}Co concentrations of much less than one ppm are derived ($c \approx 10^{-8}$). The CrCl_3 solution was not carrierfree, hence a higher concentration of Cr was present in the AuCr alloy (≈ 1 ppm). In view of the concentration dependence of the transition point T_t in more concentrated alloys, T_t/c being 1-50 K per at %, interaction effects among the impurities will be negligible in our samples, unless clustering occurs. The effects of clustering can be very important because clusters can be strongly magnetic even if the single atoms are not, for example in the AuCo system³⁹). Conversely, clusters may behave non-magnetically while isolated atoms have a local moment, *e.g.* V in Au⁴⁰).

IV.7 AuMn

Mn in the noble metal hosts (Cu, Ag, Au) is strongly magnetic as shown by susceptibility measurements^{41,42}). Those measurements indicate that Mn has a spin value in these hosts which is close to the free ion value $S=5/2$. Because the corresponding Mn^{2+} ion is in an S state no quenching mechanism has to be invoked and presumably the *s-d* model is a very good approximation. Numerous studies on the properties of these alloys can be found in the literature. Optical, susceptibility, specific-heat and resistivity data have been reviewed by Smith and Smith⁴³), showing that the behaviour is analogous to classical Kondo systems

like CuCr and CuFe with very low values of T_K ($\lesssim 0.1$ K). In the case of AgMn, $T_K^{\text{opt}} \approx T_K^x \approx 5$ mK, which value is also found from NO measurements. However, the Kondo temperature derived from resistivity measurements is 6 orders of magnitude smaller, $T_K^p = 1.7 \times 10^{-9}$ K. According to (IV.1), such an enormous difference in T_K^x values corresponds to only modest changes of the s - d exchange integral. Schrieffer plots indicate that $T_K(\text{AuMn}) < T_K(\text{AgMn})$, hence we expect $T_K(\text{AuMn})$ to be in the milli-degree range or below, which is confirmed by measurements on the susceptibility and the resistivity⁴⁴). However, at ultra low temperatures the Kondo effect may be quenched due to other interactions such as the hyperfine interaction, eq. (IV.2.1).

The dynamical problem has been reviewed in IV.4, where it has been conjectured that AuMn obeys a slow relaxation model.

Our nuclear orientation data on AuMn are shown in fig. IV.4. The full curves have been calculated applying the theory outlined in IV.3 assuming slow relaxation. The hyperfine coupling constant A which is the only adjustable parameter can be chosen such that excellent agreement of the calculated curves with the measured data is obtained at all temperature and field values in the range of measurement, see fig. IV.4. The corresponding hyperfine constant and the saturation hf field are tabulated in tables IV.2 and IV.1. Curves calculated on the assumption of fast relaxation inserting this value of the saturation hf field are in definite disagreement with the measured data at low fields, see fig. IV.4. The value of $H_{\text{hf}}^{\text{sat}}$ is in accordance with the value obtained from NO measurements by Cameron *et al.*¹³). Data

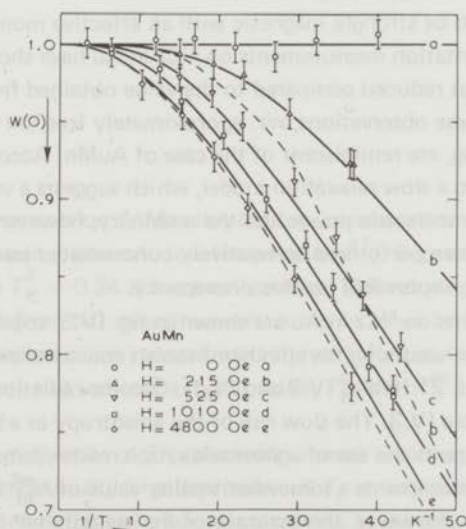


Fig. IV.4. Gamma-ray anisotropy $W(0)$ versus reciprocal temperature of oriented ^{54}Mn in gold for various field strengths.

Full curves: free spin slow relaxation model; dashed curves: free spin fast relaxation model.

See also fig. IV.2.

from different groups are collected in fig. IV.2, which partly has been taken from ref. 26. There is nice agreement, which may be considered as an argument in favour of the consistency of the experimental procedures, in particular with respect to thermometry. The measured gamma-ray anisotropies have been explained in ref. 14 on the assumption of fast relaxation and a randomly oriented hyperfine field. However, as pointed out in IV.4, fast relaxation is unlikely in AuMn below 0.1 K, and no mechanism has been devised which can disorient the hyperfine field in these very dilute alloys.

In conclusion, there are no indications from our nuclear orientation measurements in applied fields larger than 200 Oe and at temperatures above 20 mK that a Kondo bound state is formed in very dilute AuMn alloys. As can be seen from fig. IV.4, the AuMn system is a suitable radioactive thermometer in the millidegree range, in particular if the free spin behaviour pertains to lower temperatures. The sensitivity of this thermometer can be adjusted by varying the external field.

IV.8 AuCr

The Cr^{3+} ion has $g=1.98$ in ligand fields of various symmetries and strengths which suggests a nearly quenched orbital momentum. The free ion spin value is $S=3/2$. The hyperfine interaction is isotropic and originates mainly from core polarization⁴⁵). Hence the spin hamiltonian eq. (IV.3.1) should be a good approximation.

Cr in Au has been found to be strongly magnetic with an effective moment which corresponds to $S \approx 3/2$ ⁴⁶). Nuclear orientation measurements on ^{51}Cr in Au have shown that the saturation hyperfine field is somewhat reduced compared to the value obtained from the ionic ($3d^3$) hyperfine constant²¹). These observations, *viz.* approximately free ion spin value and reduced hyperfine coupling, are reminiscent of the case of AuMn. According to ref. 21, also AuCr should correspond to a slow relaxation model, which suggests a very low T_K^{NO} value. Measurements on the thermoelectric power and the resistivity, however, indicate $T_K \approx 1$ K. Since these measurements are performed on relatively concentrated samples ($c \geq 200$ ppm), interaction effects may be responsible for this discrepancy.

Results of NO measurements on ^{51}Cr in Au are shown in fig. IV.5, together with the calculated free spin behaviour, assuming the spin hamiltonian constants and the corresponding saturation hf field from ref. 21 (tables IV.2 and IV.1). Gamma-radiation anisotropy parameters are tabulated in table IV.3. The slow rise of the anisotropy as a function of applied field (fig. IV.5) clearly suggests the use of a slow relaxation model, hence a low value of T_K^{NO} is expected. From our measurements a somewhat smaller value of $H_{\text{hf}}^{\text{sat}}$ is inferred than the one used in the calculation. However, the accuracy of the measurement is too low and the range of the measurement is too small to yield a reasonably precise value of $H_{\text{hf}}^{\text{sat}}$. The extent of the validity of the free spin slow relaxation model and the values of the constants in the hamiltonian should be obtained from more elaborate measurements. As in the case of AuMn, dilute AuCr alloys are promising nuclear orientation thermometers in the millikelvin range.

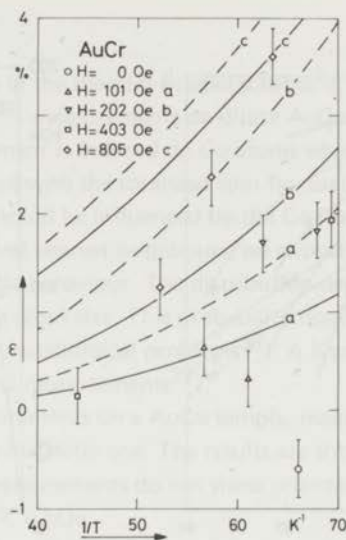


Fig. IV.5. Gamma-ray anisotropy $\epsilon = W(0) - W(\pi/2)$ versus reciprocal temperature of oriented ^{51}Cr in gold for various field strengths.

Full curves: free spin slow relaxation model; dashed curves: free spin fast relaxation model.

IV.9 ZnMn

Susceptibility measurements on ZnMn alloys at low concentrations of Mn (10-1000 ppm) show Curie-Weiss behaviour down to low temperatures⁴⁷). From the Curie-Weiss constant a Kondo temperature $T_K^X = 0.24$ K has been derived. This value agrees with the value obtained by Marsh¹⁹) from NO measurements. A higher value (≈ 2 K) has been reported from susceptibility data on more concentrated alloys²). Resistivity data at very low concentrations (< 10 ppm) also indicate a higher value, $T_K^R \approx 1$ K⁴⁸). All measurements agree on a spin value $S \approx 3/2$.

The superconductive properties of Zn containing a small amount of Mn impurities have been studied⁴⁹), showing an unusually large depression of T_c on increasing the impurity content, which is attributed to the effect of a bound state lying in the gap. The superconductivity is destroyed if a field larger than 50 Oe is applied.

Different heat treatments may have a large effect on the resistivity behaviour⁵⁰). Even at quite low concentrations ($c \approx 10$ ppm), interaction effects have been observed⁴⁸) at low temperatures.

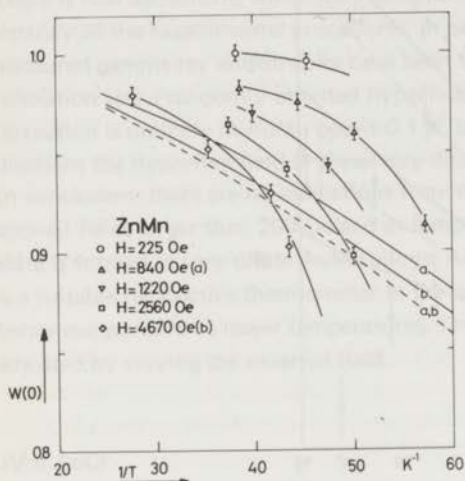


Fig. IV.6

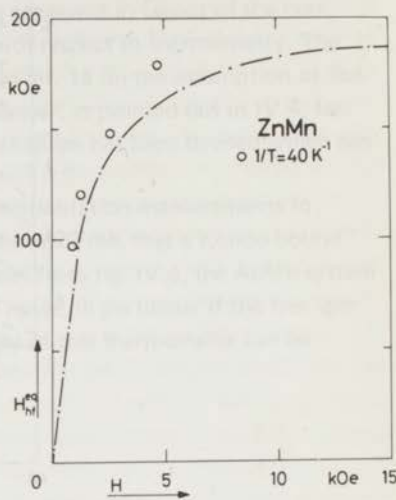


Fig. IV.7

Fig. IV.6. Gamma-ray anisotropy $W(0)$ versus reciprocal temperature of oriented ^{54}Mn in zinc for various field strengths. Curves are fitted to the points. Note the unusually fast decrease of $W(0)$. (Labelled) full curves: free spin slow relaxation model; dashed curves: free spin fast relaxation model. $H_{\text{hf}}^{\text{sat}} = 188 \text{ kOe}$ has been used¹⁹).

Fig. IV.7. $H_{\text{hf}}^{\text{eq}}$ versus applied field for very dilute ^{54}Mn -Zn alloys at 25 mK. Dash-dotted curve: measurements of ref. 21 ($T = 10\text{-}20 \text{ mK}$).

Our NO data are shown in fig. IV.6. The equivalent hyperfine field $H_{\text{hf}}^{\text{eq}}$ as a function of applied field H at $1/T = 40 \text{ K}^{-1}$ is shown in fig. IV.7. According to Marsh, $H_{\text{hf}}^{\text{eq}}$ is independent of temperature between 10 and 20 mK which suggests a temperature-independent susceptibility in this range. Moreover, the data can not be fitted by a free spin model. Hence the NO measurements presumably lie in the sub-Kondo region and the Kondo temperature may be derived according to eq. (IV.3.2). The result of Marsh is also shown in fig. IV.7. The two measurements clearly disagree, our data indicating a larger value of the saturation hf field. A rough estimate yields $H_{\text{hf}}^{\text{sat}} = 200 \text{ kOe}$ from which we derive $\Delta \equiv T_{\text{K}}^{\text{NO}} \approx 0.17 \text{ K}$, applying eq. (IV.3.2). More measurements are needed to solve the discrepancies regarding the hf saturation field. In particular, the effect of different heat treatments should be investigated.

IV.10 AuCo

This alloy is a borderline case in the Blandin-Friedel scheme²). Resistivity⁵¹), magnetization^{52, 53}) and specific-heat³⁹) measurements on dilute AuCo alloys have been interpreted assuming that a magnetic moment is induced on Co atoms which have Co nearest neighbours. This behaviour is in accordance with the localized spin fluctuation model, because the mean spin fluctuation lifetime τ_{sf} should be influenced by the Co-Co interactions. Hence, depending on the number of (effective) nearest neighbours, we expect a spectrum of transitions from magnetic to non-magnetic behaviour. The distribution depends on the probability of the formation of a cluster of a given size. This probability does not generally correspond to a random dilution because of metallurgical problems³⁸). A Kondo temperature as low as $T_K^{NO} \approx 30$ K is derived from NO measurements²²).

We have performed NO measurements on a AuCo sample, mainly to verify the classification of this alloy as a (nearly) non-magnetic one. The results are shown in fig. IV.8. Within the experimental accuracy, the measurements do not show orientation effects in the ranges $0 < 1/T < 50$ K⁻¹ and $0 < H < 5$ kOe.

Concludingly, if a transition from magnetic to non-magnetic behaviour occurs in our sample, it is expected to be at temperatures well above 1 K.

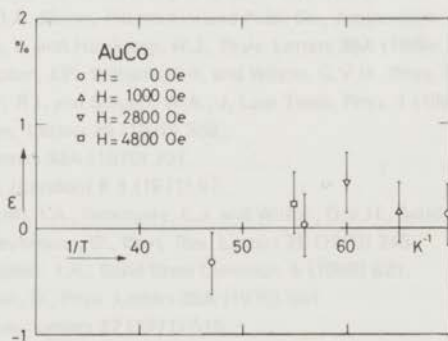


Fig. IV.8. Gamma-ray anisotropy $\epsilon = W(\pi/2) - W(0)$ versus reciprocal temperature of oriented ⁶⁰Co in gold for various field strengths.

IV.11 Concluding remarks

The results of our measurements have been summarized in table IV.1.

From nuclear orientation experiments on very dilute alloys, reasonably precise values of the saturation hyperfine fields can be obtained. Information on the *s-d* interaction effects from NO measurements should be considered as imprecise. However, the NO method provides useful additional data, in particular on the very low concentration limit. The

influence of the s - d interaction can be better delineated if theoretical calculations become available on the low temperature ($T \lesssim T_K$) and low field ($g\mu_B H \ll kT_K$) limit. As pointed out in this chapter, dynamical effects are important in the interpretation of static NO data. AuMn, and presumably also AuCr, have several advantages compared to other nuclear orientation thermometers^{17, 54}), because:

- from the measured anisotropy, the temperature can be obtained using the *calculated* curve derived from the free spin slow relaxation model,
- the sensitivity can be adjusted by varying the external field, and
- in ultra low temperature applications, only a small external field (≈ 100 Oe) is needed.

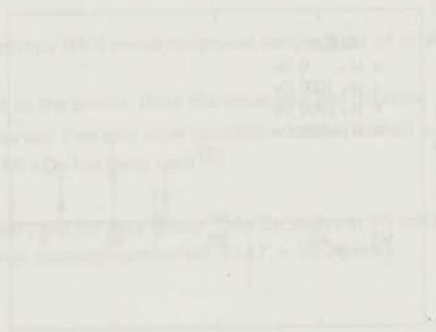


Fig. 1.6. Anisotropy of the ^{199}Au nuclear orientation in AuMn as a function of temperature. The anisotropy is measured at a constant external field of 100 Oe. The temperature is measured in Kelvin. The curve shows a sharp increase in anisotropy as the temperature decreases below approximately 100 K. The y-axis is labeled 'Anisotropy' and the x-axis is labeled 'Temperature (K)'. A vertical line is drawn at 100 K, and a horizontal line is drawn from the curve at that temperature to the y-axis. The text '100 Oe' is written near the x-axis.

References

- 1) Van den Berg, G.J., in 'Progress in Low Temperature Physics', ed. C.J. Gorter (North Holland Publ. Co., Amsterdam, 1964) vol. IV, ch. 4.
- 2) Daybell, M.D. and Steyert, W.A., *Rev. Mod. Phys.* **40** (1968) 380.
- 3) Heeger, A.J., in 'Solid State Physics', eds. F. Seitz, D. Turnbull and H. Ehrenreich (Academic Press, New York, 1969) vol. 23, p. 283.
- 4) Kondo, J., ref. 3, p. 183.
- 5) Fischer, K., in 'Springer Tracts in Modern Physics', ed. G. Höhler (Springer Verlag, Berlin, 1970) vol. 54, p. 1.
- 6) Rivier, N. and Zuckerman, M.J., *Phys. Rev. Letters* **21** (1968) 904.
- 7) Abrikosov, A., *Physics* **2** (1965) 5.
- 8) Freeman, A.J. and Watson, R.E., in 'Magnetism', eds. G.T. Rado and H. Suhl (Academic Press, New York, 1965) vol. IIA, ch. 4.
- 9) Hirst, L.L., *Z. Physik* **245** (1971) 378.
- 10) Schrieffer, J.R., *J. Appl. Phys.* **38** (1967) 1143.
- 11) Campbell, I.A., *Solid State Commun.* **9** (1971) 301.
- 12) De Groot, S.R., Tolhoek, H.A. and Huiskamp, W.J., in 'Alpha-, Beta- and Gamma ray Spectroscopy', ed. K. Siegbahn (North Holland Publ. Co., Amsterdam, 1965) p. 1199.
- 13) Cameron, J.A., Campbell, I.A., Compton, J.P., Lines, R.A.G. and Wilson, G.V.H., *Phys. Letters* **20** (1966) 569.
- 14) Compton, J.P., Williams, I.R. and Wilson, G.V.H., in 'Hyperfine Structure and Nuclear Radiations', eds. E. Matthias and D.A. Shirley (North Holland Publ. Co., Amsterdam, 1968) p. 793.
- 15) Legendijk, E., Niesen, L. and Huiskamp, W.J., *Phys. Letters* **30A** (1969) 326.
- 16) Campbell, I.A., Compton, J.P., Williams, I.R. and Wilson, G.V.H., *Phys. Rev. Letters* **19** (1967) 1319.
- 17) Pratt, W.P., Schermer, R.I. and Steyert, W.A., *J. Low Temp. Phys.* **1** (1969) 469.
- 18) Flouquet, J., *Phys. Rev. Letters* **25** (1970) 288.
- 19) Marsh, J.D., *Phys. Letters* **33A** (1970) 207.
- 20) Flouquet, J., *J. Phys. (London)* **F 1** (1971) 87.
- 21) Williams, I.R., Campbell, I.A., Sanctuary, C.J. and Wilson, G.V.H., *Solid State Commun.* **8** (1970) 125.
- 22) Holliday, R.J. and Weyhmann, W., *Phys. Rev. Letters* **25** (1970) 243.
- 23) Gallop, J.C. and Campbell, I.A., *Solid State Commun.* **6** (1968) 831.
- 24) Flouquet, J. and Marsh, D., *Phys. Letters* **32A** (1970) 501.
- 25) Flouquet, J., *Phys. Rev. Letters* **27** (1971) 515.
- 26) Flouquet, J., thesis, Orsay (1971).
We thank dr. Flouquet for providing us with a copy of his thesis.
- 27) Hasegawa, H., *Progr. Theor. Phys. (Kyoto)* **21** (1959) 4.
- 28) Gossard, A.C., Heeger, A.J. and Wernick, J.H., *J. Appl. Phys.* **38** (1967) 1251.
- 29) Schultz, S., Shanabarger, M.R. and Platzman, P.M., *Phys. Rev. Letters* **19** (1967) 749.
- 30) Monod, P. and Schultz, S., *Phys. Rev.* **173** (1968) 645.
- 31) McElroy, J.A. and Heeger, A.J., *Phys. Rev. Letters* **20** (1968) 1481.
- 32) Nakamura, A. and Kinoshita, N., *J. Phys. Soc. Japan* **26** (1969) 48.
- 33) Menyhard, N., Solyom, F. and Zawadowski, A., *Phys. Rev. B* **3** (1971) 113.
- 34) Brewer, W.D., Shirley, D.A. and Templeton, J.E., *Phys. Rev. Letters* **27A** (1968) 81.
- 35) Niesen, L. and Huiskamp, W.J., *Physica* **50** (1970) 259; **57** (1972) 1.
- 36) Wheatley, J.C., in 'Progress in Low Temperature Physics', ed. C.J. Gorter (North Holland Publ. Co., Amsterdam, 1970) vol. VI, p. 132.
- 37) Haasbroek, J.N., thesis, Leiden (1971); see also the appendix.

- 38) Hansen, M., 'Constitution of Binary Alloys' (McGraw-Hill Book Company Inc., New York, 1958) and Elliot, R.P., *ibidem*, First Supplement (1965).
- 39) Costa Ribeiro, P., Souletie, J. and Thoulouze, D., Phys. Rev. Letters **24** (1970) 900.
- 40) Narath, A. and Gossard, A.C., Phys. Rev. **183** (1969) 391.
- 41) Owen, J., Browne, M.E., Arp, V. and Kip, A.E., J. Phys. Chem. Sol. **2** (1957) 85.
- 42) Shaltiel, D. and Wernick, J.H., Phys. Rev. **136** (1964) A245.
- 43) Smith, D.A. and Smith, G.B., Phys. Rev. **B 4** (1971) 191.
- 44) Loram, J.W., Whall, T.E. and Ford, P.J., Phys. Rev. **B 3** (1971) 953.
- 45) Abragam, A. and Bleaney, B., 'Electron Paramagnetic Resonance of Transition Ions' (Clarendon Press, Oxford, 1970) p. 430.
- 46) Lutes, O.S. and Smith, J.L., Phys. Rev. **134** (1964) A676.
- 47) Newrock, R.S., Serin, B., Vig, J. and Boato, G., J. Low Temp. Phys. **5** (1971) 701.
- 48) Ford, P.J., Rizutto, C., Salamoni, E. and Zani, P., J. Phys. (Paris) **32** (1971) c1-221.
- 49) Smith, E.W., J. Low Temp. Phys. **5** (1971) 683.
- 50) Wassermann, E.F., Falke, H. and Jablonski, H.P., Solid State Commun. **9** (1971) 1171.
- 51) Loram, J.W., Ford, P.J. and Whall, T.E., J. Phys. Chem. Sol. **31** (1970) 763.
- 52) Bancraft, M.H., Phys. Rev. **B 2** (1970) 2597.
- 53) Boucai, E., Lecoanet, B., Pilon, J., Tholence, J.L. and Tournier, R., Phys. Rev. **B 3** (1971) 3834.
- 54) Berglund, P.M., Collan, H.K., Ehnholm, G.J., Gylling, R.G. and Lounasmaa, O.V., J. Low Temp. Phys. **6** (1972) 357.

APPENDIX

CARBON RESISTANCE THERMOMETRY BELOW 1 K

Synopsis

A multiparameter equation is given, which fits the resistance vs temperature data of Speer carbon resistors with an accuracy of 0.5% of the temperature over the range 0.03-2 K.

A low parameter equation and the possibility of its use for extrapolation from the liquid helium region to lower temperatures are discussed. The reproducibility of the thermometers for temperatures above 0.08 K is shown to be within 0.5% after cycling to room temperature. Some applications of carbon resistance thermometry are discussed.

A.1 Introduction

The use of carbon resistors for thermometry below 1 K has been described several times in the literature^{1,2,3}). We have used Speer 220 Ω 1/2 W carbon resistors for accurate relative temperature measurements in calorimetric experiments between 0.08 and 1 K. The advantages of carbon resistor thermometers over magnetic susceptibility thermometers are: a) small heat capacity, b) simplicity of measurement, c) small size, d) quick response, and e) small magnetic field dependence^{2,4}). The disadvantages are: a) the necessity of calibration over the whole temperature range, because no theoretical resistance vs temperature ($R-T$) relation is known which can be used for extrapolation with sufficient accuracy, b) irreproducibility after thermal cycling to room temperature, and c) the sensitivity for electromagnetic stray fields, especially at high resistances and correspondingly low temperatures⁵). It is the purpose of the following discussion to show that there exist series expansions such as

$$f_0(Y) = \sum_{i=1}^m c_i [f_i(X)]^{i-1} \quad (\text{A.1.1})$$

where $10 \leq m \leq 15$, and (X, Y) corresponding to (R, T) or (T, R) , which fit the resistance vs temperature relation within 0.5% over the range 0.03-2 K; further, it is shown that the resistance is reproducible in the range 0.08-2 K with the same accuracy. It can be

demonstrated that the function

$$\log(R/R_0) = c/T^s \quad (\text{A.1.2})$$

describes the R - T relation within a few percent of the temperature between 0.3 and 2 K, where $s=0.55$, R_0 is the resistance at room temperature, and c is determined by a single calibration point in the liquid helium region.

A.2 Calibration

As already mentioned, the resistors used are 220 Ω 1/2 W Speer resistors. Part of the insulation is removed, and thermal contact is made with a copper brush using Apiezon N grease. The resistance is measured by an a.c. Wheatstone bridge with lock-in detection, operating at 675 Hz. The heat input due to the measuring current into the thermometer is kept below 10^{-12} W. The primary thermometer is a slab of cerium magnesium nitrate (CMN) glued between copper plates with Apiezon N for thermal contact, or a cylinder filled with molten CMN which crystallizes around a copper brush. The cylinder has a diameter equal to its height, which form is chosen such as to make the demagnetization correction negligible⁶). The susceptibility of the CMN sample is measured by a Hartshorn bridge with lock-in detection operating at 225 Hz. The parameters necessary to obtain the magnetic temperature T^* from the reading n of the magnetic bridge are the slope of the n vs $1/T$ relation and the empty coil correction. They are determined by calibration against the vapour pressure of the ^4He bath above 1 K with an estimated accuracy of 0.5%, hence the accuracy in the temperature values obtained by extrapolation of the Curie-Weiss behaviour is about 1%. The validity of this extrapolation is based upon the temperature scale of CMN, T^* (T), which has been a controversial subject in the past few years⁶). At temperatures above 10 mK, however, the susceptibility of CMN obeys a Curie Weiss relation with an intrinsic Curie-Weiss constant as small as 0.3 mK. If necessary, demagnetization corrections have been made, approximating the shape of the CMN sample by an ellipsoid. These corrections are of the order of 1 mK.

Care has to be taken to shield and ground the carbon resistor correctly, otherwise stray r.f. fields and/or line frequency effects will influence the resistance at low temperatures in an irreproducible fashion. We have not used capacitor shunting of the resistor, because sufficient precautions were taken with respect to shielding to keep stray field effects negligible down to 40 mK. Besides, the effect of ground loops are apparently more harmful (effects up to 50% of the resistance have been observed at 80 mK). In all experiments, the noise and hum level measured over the resistor was below 50 μV .

The adiabatic demagnetization apparatus used has been described before⁷). Its principal parts are shown in fig. A.1. Temperatures between 0.03 and 3 K can be obtained quite easily, if contact is made with the cooling salt and no large heat capacities and/or long relaxation times are present in the system. The resistance variation of the carbon resistor in this range is from 300 to 0.5 k Ω approximately.

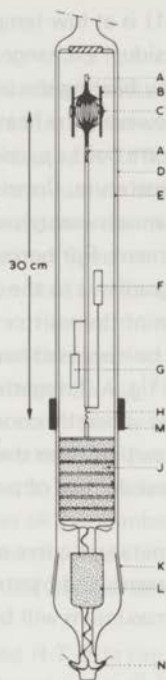


Fig. A.1. The apparatus.

- | | | |
|---------------------------|-------------------------|-------------------------|
| A: copper bundle | E: glass thermal shield | J: cooling salt |
| B: perspex plates | F: heater | K: glass ground joint |
| C: CeMgN sphere | G: carbon resistor | L: guard cylinder |
| D: high vacuum glass tube | H: thermal switch | M: superconducting coil |
| | | N: Pt-glass seals |

Not shown in the figure are the susceptibility coils at the sample (C).

As long as the temperature is kept below the ^4He bath temperature (about 1 K), equilibrium can be obtained for the whole inner system, consisting of the cooling salt, heater and thermometers, with low or zero heat input. The equilibrium time decreased typically from a few minutes at 30 mK to less than a second at 100 mK. The estimated relative accuracy of the temperature and of the resistance measurement is $1:10^4$ in the range 0.1 to 1 K. At very low temperatures ($T < 0.05$ K), the carbon resistors were found to be very sensitive to switching pulses in the laboratory surroundings, so as to preclude accurate measurements, especially in calorimetric experiments with low heat capacities. Moreover, the resistance and the sensitivity of our thermometer become disturbingly high and the reproducibility is poor. Therefore the carbon resistor has been used below 0.05 K for monitoring purposes only.

As long as the cooling pill (L in fig. A.1) is at low temperature, it is a buffer for heat conduction to the bath and it keeps residual exchange gas adsorbed, hence it is possible to reach temperatures above 1 K simply by heating the inner part of the apparatus without changing the ^4He bath temperature. However, the heat input necessary quickly rises with temperature, so temperature gradients are built up, and the sensitivity of the magnetic thermometer becomes low at high temperature. Concludingly, the accuracy at very low temperatures is restricted by the resistance measurement and at high temperatures it is restricted by the temperature measurement. For better accuracy, and to avoid a non-equilibrium situation by temperature gradients in the system, the R - T relation used at high temperatures is obtained by calibration of the resistor against the ^4He vapour pressure directly. These measurements will not be discussed here.

A typical calibration curve is shown in fig. A.2, together with the sensitivity of the thermometer, $\alpha = (-1/R) \times (dR/dT)$. α can be varied by choosing the appropriate nominal resistance, or by removing part of the carbon from the resistor. Generally, 50 to 100 calibration points are taken, with the largest density of points on the $\log T$ scale in the range 0.1-1 K.

The flattening of the resistance vs temperature curve at the lowest temperatures is probably due to heat input by the measuring current, and by stray r.f. fields. It is not clear from our experiments if ultimately an intrinsic maximum will be reached⁸).

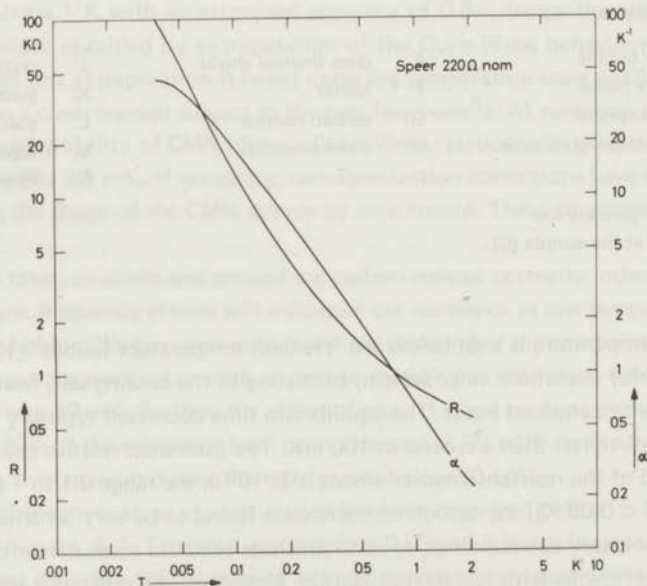


Fig. A.2. Resistance vs temperature curve (R) and sensitivity vs temperature curve (α).

A.3 Numerical procedures

In order to obtain temperatures from measured resistances, which are different from the calibration values, an interpolation procedure can be used, or an analytical formula can be sought which fits the experimental R - T data with sufficient accuracy. A good deal of work in fitting R - T data has been done for germanium resistance thermometers, and Allen-Bradley and some home-made carbon resistance thermometers, especially in the range 1-100 K^{3,9}). Relatively little is known about Speer carbon resistors^{10,11}).

As usual, a least squares method has been used in fitting the data. The use of orthogonal polynomials is preferable if the number of terms in the expansion becomes high, see refs 11 and 12. We have also applied a matrix inversion method for solving the normal equations, according to a procedure of Banachiewicz¹³). This procedure has the advantage that the coefficients and the error in the coefficients, due to measuring errors in the dependent variable, can be calculated simultaneously, which is useful if some physical significance can be given to the coefficients. There were no essential differences between the results of the two methods for low values of the number of terms in the expansion ($m < 10$), but at high values of m , the method of matrix inversion fails, as could be expected^{11,12}). All calculations have been done on the IBM 360/50 computer of the Centraal Reken Instituut of the University of Leiden.

The formulas used in fitting the measured R - T data can be divided into low parameter formulae, suggested by theories on semiconductivity^{8,14}), which are useful for extrapolation purposes, and into multi parameter formulae, mostly series expansions such as eq. (A.1.1). In general, no physical information can be obtained from such long term expansions and they can be used for interpolation purposes only. Oscillations between the fitted points must be avoided, and this limits the number of terms in the series expansion. Another upper limit for the number of terms is set by the propagation of rounding errors with increasing m , which makes the fit impossible if a matrix inversion method is used and causes the standard deviation to pass through a minimum if one uses the method of orthogonal polynomials. To improve the fit, a weighting factor can be assigned to every point. Generally this is a function of X and/or Y . The simplest functions are step functions, excluding some temperature or resistance ranges from the fit or giving extra weight to others in a discontinuous way. If in formula (A.1.1) unit weight is attributed to every point, the minimized quantity is

$$\epsilon_{f_0} = \sum_{i=1}^N (\Delta f_0^i)^2$$
 (N is the number of fitted points and Δf_0^i is the difference between the calculated and observed values of f_0 in the i -th point). However, the quantity which has to be minimized is $\epsilon_Y^{\text{abs}} = \sum_{i=1}^N (\Delta Y^i)^2$. So the inverse of the derivative squared, $(df_0/dY)^{-2}$, has

to be inserted as a weighting factor. Usually, in low temperature phenomena, the relative temperature scale is of more fundamental importance than the absolute scale. Then the

quantity to be minimized should be $\epsilon_Y^{\text{rel}} = \sum_{i=1}^N ((\Delta Y/Y)^i)^2$, and $(Y \times (df_0/dY))^{-2}$ enters as a weighting factor.

A.4 Low parameter fit

A three parameter formula has been proposed by Balcombe *et al.*¹¹):

$$T = A/(\log R - B)^p \quad (\text{A.4.1})$$

This formula fits the behaviour of a Speer 470 Ω 1/2 W resistor with an accuracy of 0.3% over the temperature range 0.6-4.2 K. The constants A , B , and p were calculated from three calibration points. Inversion of formula (A.4.1) gives:

$$\log R = c_1 + c_2/T^s, \quad (\text{A.4.2})$$

where $c_1=B$, $c_2=A^{1/p}$ and $s=1/p$. The formula had already been suggested by Clement and Quinell in this form¹⁴).

Another three parameter formula for Speer resistors in the range 0.2-3 K has been proposed by Hetzler *et al.*¹⁰):

$$1/T = A + BR + CR^n$$

with $n=1/4$ or $1/2$. In this case, the maximum difference between the calculated and measured temperatures was 1%. A , B , and C were obtained from a least squares fit.

We have applied formula (A.4.2) to carry out some calculations on the calibration data of a Speer 220 Ω 1/2 W carbon resistor (fig. A.2). About 100 points were used between 0.03 and 2 K, distributed with approximately equal density on the $\log T$ scale. The constants c_1 , c_2 , and s can be calculated from three calibration points. We have chosen two fixed points between 1 and 2 K, and we have varied the third point between 0.03 and 1.5 K. Now the variation of c_1 , c_2 , and s will show in which temperature range formula (A.4.2) gives a reasonable description of the function $R(T)$. Although the calculated values of s depend somewhat on the fixed points chosen, stabilization is observed for $T > 0.5$ K for different choices of fixed points. Next, linear least squares fits in the range $0.5 < T < 2$ K using s as a variable parameter have been made. The value of s which minimizes the sum ϵ of the squares of the differences between the calculated and measured values of $\log R$, and the corresponding values of c_1 and c_2 are $s=0.551$, $c_1=-1.386$, $c_2=1.202$ (R is expressed in $k\Omega$). A deviation plot, $\Delta T/T$ vs T , is shown in fig. A.3.

Statistically acceptable values of ϵ are those with $(\epsilon - \epsilon_{\text{min}}) \leq \epsilon_{\text{min}}/\sqrt{N}$, where N is the number of points in the fit. In our case, where $\epsilon_{\text{min}} \times 10^4 = 5.27$, and $N \approx 100$, the corresponding ranges of s , c_1 , and c_2 -values are: $0.546 < s < 0.557$, $-1.398 < c_1 < -1.373$, and $1.214 > c_2 > 1.188$.

It can be remarked that in reasonable approximation, $c_1 \approx \log R_0$, where R_0 is the measured

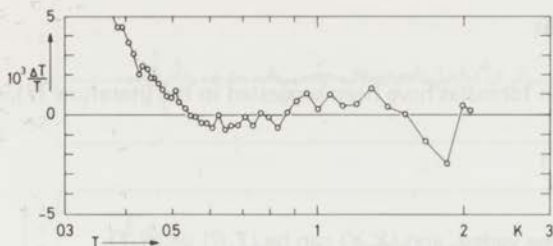


Fig. A.3. Deviation plot, see text.

room temperature resistance of the thermometer. Furthermore, the value $s=0.55$ gives $\rho=1.82$ in (A.4.1), which is in reasonable agreement with the value of Balcombe *et al.* for a 470Ω Speer resistor. Assuming this value to be universal for all Speer resistors, only one point at low temperature has to be measured to fix the remaining constant. Then an extrapolation can be made, which fits the $R(T)$ behaviour within a few percent down to 0.3 K , see fig. A.4.

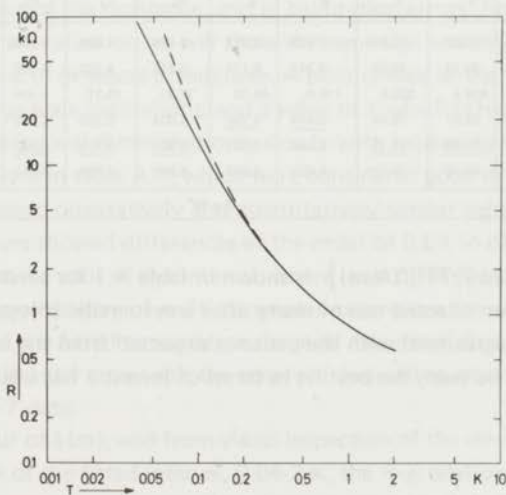


Fig. A.4. Extrapolation of eq. (A.4.2) (dashed curve) compared to experimental curve (full curve).

Formula (A.4.2) has been used for calculating some points in the region $4\text{--}10 \text{ K}$ by extrapolation, to improve multi parameter fits (A.5) at the high-temperature side of the interval.

A.5 Multi parameter fit

Several series expansion formulas have been suggested in the literature^{3,9}). Generally we can write:

$$f_0(Y) = \sum_{i=1}^m c_i [f_1(X)]^{i-1} \quad (\text{A.1.1})$$

Now f_0 , f_1 , and m can be varied, and (X, Y) can be (T, R) or (R, T) .

Although it is not clear from the experimental or theoretical data whether the resistance is singular at $T=0$ or not⁸), the steep ascent of the resistance at low temperature suggests the use of functions f_0 and f_1 , which have a singularity at the origin, for example the inverse function, and the logarithmic function. A fit can be labeled by $\{f_0(Y)[f_1(X)], g(X, Y), m\}$, where the symbols f_0 , f_1 , and m refer to equation (A.1.1), and g denotes the weight-function.

Table A.1. $\delta = \sqrt{(\sum(\Delta T/T)^2)/(N-m)}$ as a function of m for six expansions $\{f_0(Y)[f_1(X)], g(X, Y), m\}$. The minimum value of δ in a column is underlined.

	$m=5$	6	7	8	9	10	11	12	13	14	15
$\{1/T[\log R], T^2, m\}$	61.44	30.60	13.26	7.139	5.397	4.659	4.606	4.496	4.389	4.151	4.024
$\{\log T[\log R], 1, m\}$	120.2	39.73	20.94	8.347	6.171	5.211	4.352	4.308	4.073	3.930	3.889
$\{T[\log R], T^{-2}, m\}$	761.4	406.4	220.8	115.6	59.05	32.30	15.71	9.594	5.205	4.399	<u>3.790</u>
$\{1/R[\log T], R^2, m\}$	167.7	39.57	18.54	<u>5.444</u>	<u>4.786</u>	4.904	5.103	4.228	3.950	3.872	3.866
$\{R(1/T), R^{-2}, m\}$	<u>24.37</u>	<u>11.86</u>	<u>11.18</u>	6.849	6.777	<u>3.905</u>	<u>4.025</u>	<u>3.801</u>	<u>3.833</u>	<u>3.846</u>	3.800
$\{\log R[\log T], 1, m\}$	85.20	43.74	15.11	5.826	4.922	4.890	4.925	5.011	5.009	4.554	4.481
$\delta \times 10^4$											

The variance $\delta = \sqrt{\{\sum(\Delta T/T)^2/(N-m)\}}$ is shown in table A.1 for several fits as a function of m . These fits have been selected out of many after a systematic investigation, because the value of δ reached is in agreement with the variance expected from the errors in the calibration data. As can be seen, the best fit in terms of lowest δ has been obtained using an expansion:

$$R = \sum_{i=1}^m c_i (1/T)^{i-1} \quad (\text{A.5.1})$$

where δ stabilizes for $m > 10$, and R^{-2} is the weightfunction. Fits on other calibration data have shown that the formula:

$$\log R = \sum_{i=1}^m c_i (\log T)^{i-1} \quad (\text{A.5.2})$$

($m \approx 10$, unit weightfunction) is preferable in many cases, especially if the calibration data

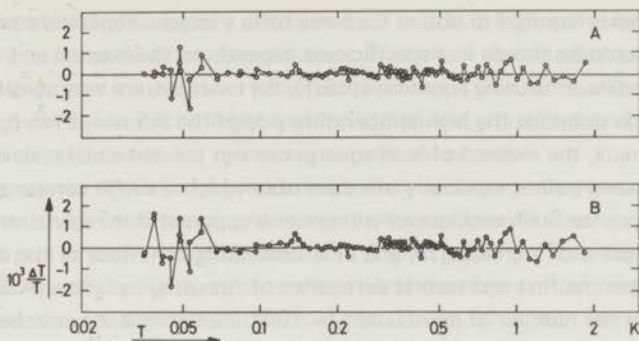


Fig. A.5. Deviation plots. A: fit on eq. (A.5.1), B: fit on eq. (A.5.2), $m=12$ in both cases.

are not very accurate. Both formulas have the disadvantage that T cannot be obtained from a measured R value directly. To calculate T values from measured R values, a root of equation (A.5.1) or (A.5.2) has to be calculated in the appropriate range.

Deviation plots for $m = 12$ are shown in fig. A.5. The deviations between measured and calculated temperatures are due to a) inadequateness of the formula to describe the functional behaviour of the resistance, and b) calibration errors. For a given formula, deviations due to calibration errors will show the same sign and magnitude for increasing m , starting from a value of m where δ stabilizes. A poor choice of the functions in the expansion will show up in large scale oscillations, and a value of δ which is high compared to the experimental accuracy and diminishes only slowly with increasing m .

For all the expansions in table A.1, which were considered good in terms of low δ , the deviation plots showed qualitatively and quantitatively similar behaviour. Comparison of the calculated derivatives showed differences of the order of 0.5% in dR/dT and of 1% in d^2R/dT^2 , except at the ends of the interval, where large differences occurred. This emphasizes the inapplicability of multi parameter expansions for extrapolation purposes. In the inner part of the fitted temperature range all calculated first and second derivatives agree within experimental error with the observed derivatives, obtained by numerical differentiation of the R - T data.

From the behaviour of $\delta(m)$, and from visual inspection of the deviation plots, we conclude that in the interior of the fitted interval, 0.04-2 K, the R - T relation of our Speer resistor can be fitted satisfactory to any one of the formulas in table A.1. Computer experiments on the calibration data of Speer carbon resistor thermometers of other nominal resistance value and/or different construction give the same results⁴). The interval can easily be extended to higher temperatures, by adding points obtained from a calibration against the ^4He vapour pressure or from extrapolation of formula (A.4.2), without the fit becoming worse. Calibration points at lower temperatures, however, may worsen the fit over the whole temperature interval, although successful fits have been made down to 0.02 K. Generally, a higher

degree polynomial is required to obtain the same fit in a larger temperature range. Which formula should be chosen in a specific case depends on the interval and the precision of the calibration data. Fits using equation (A.5.1), for example, are very sensitive to less accurate calibration points at the high-temperature side of the interval. Even for a good choice of the formula, the method of least squares can not prevent small scale oscillations between the measured points, especially at values of m which are high compared to the number of fitted points. Such oscillations will become apparent if the deviation plot qualitatively changes with increasing m , and in an oscillating behaviour of the derivatives. We have investigated the first and second derivatives of fits using equation (A.5.2), as a function of m . For the number of points used (≈ 100), oscillating behaviour between the fitted points starts at an m value of the order of 20, as shown by changes of sign of the second derivative in the fitted temperature range. This is about the value of m , where δ passes through a minimum ($\delta_{\min} \times 10^4 = 3.839$ at $m = 19$).

A.6 Reproducibility

In earlier investigations, it was reported that the Speer resistor seemed to be reproducible within 0.5% for temperatures above 0.1 K²). This is within the absolute accuracy of the calibration, which is also of the order of 0.5%, due to errors in the determination of the characteristics of the magnetic thermometer. After a two years use of Speer resistors, with periods of about one month between two calibrations, and about 8 cycles to room temperature per month, this statement now seems to be true under the following restrictions:

a) a slight shift is sometimes observed ($\Delta R \approx -0.1 \Omega$) after cycling to room temperature,

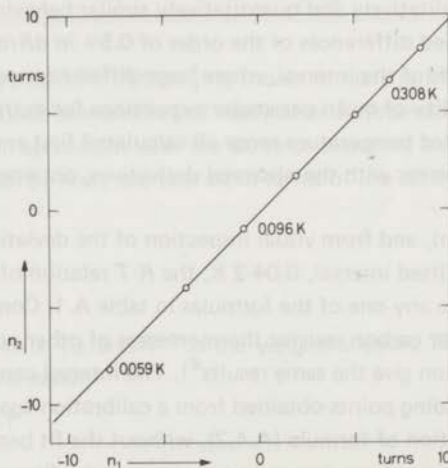


Fig. A.6. Test of reproducibility, see text.

b) stray fields and/or line frequency effects and, of course, a higher measuring input cause a decrease of the resistance at low temperatures. We believe that the flattening of the resistance vs temperature curve at very low temperatures is due to the effect of heat input by electromagnetic fields. Accordingly, good shielding and grounding, and a low and unchanging heat input due to the measuring current are essential. There is a nice way to check the reproducibility directly, namely by comparing the readings of the magnetic bridge in different calibrations at the same resistances, say $n_1(R)$ and $n_2(R)$ (fig. A.6). If a plot of $n_1(R)$ vs $n_2(R)$ for various R gives a straight line, this proves reproducibility and the slope of the line is equal to the ratio of the slopes of the magnetic thermometer. (A correction for the shift of the resistance during cycling can be made by comparing the readings at liquid helium temperatures.)

A.7 Use of the carbon resistor

The carbon resistor has been used for:

- a) Very accurate specific heat measurements near the phase transition of a magnetic system ($|T - T_c|/T_c > 10^{-4}$), see ref. 15. The carbon resistor offers an advantage above the magnetic thermometer because of greater ease of measurement. (For instance it is difficult to trim our magnetic bridge, which is of the Hartshorn type, with an absolute accuracy of 0.001 turn.)
- b) Susceptibility measurements. Magnetic thermometry in this case would require two coil systems and two magnetic bridges (although one bridge may be sufficient if an interpolation technique can be used).
- c) Measurements of temperatures in a magnetic field. The carbon resistor is not very sensitive to magnetic fields, contrary to a magnetic thermometer. The following empirical relation, due to Haasbroek⁴, was found to represent the magnetic field effect $\Delta R(R, H)$ on the resistance rather well:
$$\Delta R/R = -0.10 (H/kOe)(R/k\Omega)^{1-0.02(H/kOe)}$$
- d) Monitoring. Carbon resistors are in general use now for monitoring very low temperature devices. We have used carbon resistors as monitors in nuclear orientation experiments, see refs. 16 and 17. The reproducibility and relatively low field dependence of the carbon resistor at higher temperatures ($T > 0.1$ K) was used to calibrate the magnetic thermometer attached to the sample.

A.8 Conclusions

Carbon resistors of the Speer type can be used for accurate thermometry in the temperature range 0.08-3 K. The resistance vs temperature relation can be fitted to a polynomial within

the accuracy of our calibration data. The best results have been obtained using expansions:

$$\log R = \sum_{i=1}^m c_i (\log T)^{i-1},$$

with m about 10, and 1 as weighting factor.

For use at higher temperatures (> 0.5 K), a low parameter fit can be used, e.g.

$$\log R = c_1 + c_2/T^s,$$

with $s=0.55$ and $c_1 \approx \log R_0$ (s seems to be independent of the nominal resistance value, and R_0 denotes the room temperature resistance value).

The reproducibility is better than 0.5% in the range 0.08-3 K. At temperatures below 0.05 K, stray fields and measuring current effects become predominant, so that the carbon resistor is not reliable in this region, unless very great care is taken with respect to heat input, shielding, and grounding.

References

- 1) Black, W.C., Roach, W.R. and Wheatley, J.C., *Rev. Sci. Instr.* **35** (1964) 587.
- 2) Edelstein, A.S. and Mess, K.W., *Physica* **31** (1965) 1707.
- 3) Rubin, L.G., *Cryogenics* **10** (1970) 14. Contains many references.
- 4) Haasbroek, J.N., thesis, Leiden (1971).
- 5) Ambler, E. and Plumb, H., *Rev. Sci. Instr.* **31** (1960) 656.
- 6) Wheatley, J.C., in 'Progress in Low Temperature Physics', ed. C.J. Gorter (North Holland Publishing Co., Amsterdam, 1970) vol VI, p. 132.
- 7) Miedema, A.R. and Mess, K.W., *Physica* **30** (1964) 1849.
- 8) Friedberg, S.A., in 'Temperature, its Measurement and Control in Science and Industry' (Reinhold Publishing Corporation, New York, 1956) vol. II, p. 370.
- 9) Blakemore, J.S., Winstel, J. and Edwards, R.V., *Rev. Sci. Instr.* **41** (1970) 835.
- 10) Hetzler, M.C. and Walton, D., *Rev. Sci. Instr.* **39** (1968) 1656.
- 11) Balcombe, R.J., Emerson, D.J. and Potton, R.J., *J. Sci. Instr.* **3** (1970) 43.
The algorithm used has been taken from 'Fortran in the Physical Sciences', IBM Student Text.
- 12) Forsythe, G.E., *J. Soc. Industr. Appl. Math.* **5** (1957) 74.
- 13) Faddeeva, V.N., 'Computational Methods in Linear Algebra' (Dover Publications Inc., New York, 1959) p. 81. The algorithm has been programmed by dr. A. Ollongren of the Centraal Reken Instituut of the University of Leiden.
- 14) Clement, J.R. and Quinzel, E.H., *Rev. Sci. Instr.* **23** (1952) 213.
- 15) Lagendijk, E., Wielinga, R.F. and Huiskamp, W.J., *Phys. Letters* **31A** (1971) 375; chapter II.
- 16) Lagendijk, E., Niesen, L. and Huiskamp, W.J., *Phys. Letters* **30A** (1969) 326; chapter IV.
- 17) Niesen, L., thesis, Leiden (1971).

11. G. W. Hill, *Proc. Roy. Soc. London*, **10**, 413 (1902).
 12. G. W. Hill, *Proc. Roy. Soc. London*, **10**, 426 (1902).
 13. G. W. Hill, *Proc. Roy. Soc. London*, **10**, 441 (1902).
 14. G. W. Hill, *Proc. Roy. Soc. London*, **10**, 456 (1902).
 15. G. W. Hill, *Proc. Roy. Soc. London*, **10**, 471 (1902).
 16. G. W. Hill, *Proc. Roy. Soc. London*, **10**, 486 (1902).
 17. G. W. Hill, *Proc. Roy. Soc. London*, **10**, 501 (1902).
 18. G. W. Hill, *Proc. Roy. Soc. London*, **10**, 516 (1902).
 19. G. W. Hill, *Proc. Roy. Soc. London*, **10**, 531 (1902).
 20. G. W. Hill, *Proc. Roy. Soc. London*, **10**, 546 (1902).
 21. G. W. Hill, *Proc. Roy. Soc. London*, **10**, 561 (1902).
 22. G. W. Hill, *Proc. Roy. Soc. London*, **10**, 576 (1902).
 23. G. W. Hill, *Proc. Roy. Soc. London*, **10**, 591 (1902).
 24. G. W. Hill, *Proc. Roy. Soc. London*, **10**, 606 (1902).
 25. G. W. Hill, *Proc. Roy. Soc. London*, **10**, 621 (1902).
 26. G. W. Hill, *Proc. Roy. Soc. London*, **10**, 636 (1902).
 27. G. W. Hill, *Proc. Roy. Soc. London*, **10**, 651 (1902).
 28. G. W. Hill, *Proc. Roy. Soc. London*, **10**, 666 (1902).
 29. G. W. Hill, *Proc. Roy. Soc. London*, **10**, 681 (1902).
 30. G. W. Hill, *Proc. Roy. Soc. London*, **10**, 696 (1902).
 31. G. W. Hill, *Proc. Roy. Soc. London*, **10**, 711 (1902).
 32. G. W. Hill, *Proc. Roy. Soc. London*, **10**, 726 (1902).
 33. G. W. Hill, *Proc. Roy. Soc. London*, **10**, 741 (1902).
 34. G. W. Hill, *Proc. Roy. Soc. London*, **10**, 756 (1902).
 35. G. W. Hill, *Proc. Roy. Soc. London*, **10**, 771 (1902).
 36. G. W. Hill, *Proc. Roy. Soc. London*, **10**, 786 (1902).
 37. G. W. Hill, *Proc. Roy. Soc. London*, **10**, 801 (1902).
 38. G. W. Hill, *Proc. Roy. Soc. London*, **10**, 816 (1902).
 39. G. W. Hill, *Proc. Roy. Soc. London*, **10**, 831 (1902).
 40. G. W. Hill, *Proc. Roy. Soc. London*, **10**, 846 (1902).
 41. G. W. Hill, *Proc. Roy. Soc. London*, **10**, 861 (1902).
 42. G. W. Hill, *Proc. Roy. Soc. London*, **10**, 876 (1902).
 43. G. W. Hill, *Proc. Roy. Soc. London*, **10**, 891 (1902).
 44. G. W. Hill, *Proc. Roy. Soc. London*, **10**, 906 (1902).
 45. G. W. Hill, *Proc. Roy. Soc. London*, **10**, 921 (1902).
 46. G. W. Hill, *Proc. Roy. Soc. London*, **10**, 936 (1902).
 47. G. W. Hill, *Proc. Roy. Soc. London*, **10**, 951 (1902).
 48. G. W. Hill, *Proc. Roy. Soc. London*, **10**, 966 (1902).
 49. G. W. Hill, *Proc. Roy. Soc. London*, **10**, 981 (1902).
 50. G. W. Hill, *Proc. Roy. Soc. London*, **10**, 996 (1902).

VERANTWOORDING:

Aan de vervaardiging van dit proefschrift is door een groot aantal instanties en personen bijgedragen. Veel steun kreeg ik van de centrale diensten van het Kamerlingh Onnes Laboratorium en van de leden van de werkgroep kernfysica en magnetisme (FOM KIV). J.J. Bosman, D.L. de Jong, F.J. van Steenwijk, J. van der Waals en J. van Weesel hebben gedurende geruime tijd dagelijks aan het onderzoek meegewerkt.

CURRICULUM VITAE van Erik Lagendijk, geboren 10 augustus 1942 te Amsterdam.

Na het eindexamen middelbare school te hebben afgelegd aan het Barlaeus Gymnasium te Amsterdam begon ik in 1960 met mijn studie in de natuurkunde te Leiden. Het kandidaats-examen natuur- en wiskunde met sterrenkunde (a') werd afgelegd in februari 1964. Daarna bereidde ik mij voor op het doctoraal examen experimentele en theoretische natuurkunde met wiskunde (gemengde richting). Voor dit examen werden tentamens afgelegd in klassieke mechanica, statistische mechanica, quantum mechanica, elektromagnetisme, neutronen diffractie, groepentheorie, functietheorie, magnetische ruimtgroepen en theorie van de vaste stof bij de hoogleraren dr. J.A.M. Cox, dr. P. Mazur, dr. P.W. Kasteleyn, dr. J.A. Goedkoop, wijlen dr. H.D. Kloosterman, dr. C. Visser en dr. W. Opechowski (Vancouver). Het experimentele werk voor het doctoraal examen, begonnen in 1965, stond onder leiding van de hoogleraren dr. W.J. Huiskamp en dr. C.J. Gorter en werd verricht in de werkgroep kernfysica en magnetisme van het Kamerlingh Onnes Laboratorium van de Rijksuniversiteit Leiden waarin opgenomen de werkgroep KIV van de Stichting voor Fundamenteel Onderzoek der Materie (FOM). Het doctoraal examen legde ik af in maart 1967 waarna ik het onderzoek aan magnetische ordeningsverschijnselen bij zeer lage temperaturen met behulp van calorische en kernoriëntatie technieken voortzette. In december 1967 trad ik in dienst van de stichting FOM als wetenschappelijk medewerker. Bij het onderzoek werd intensief gebruik gemaakt van de computer van het Centraal Reken Instituut van de universiteit zowel voor data reductie als voor theoretische berekeningen. Vanaf 1965 heb ik geassisteerd bij het onderwijs aan voor-kandidaats studenten, aanvankelijk als assistent bij dr. J. de Nobel en later als hoofdassistent bij prof.dr. J.J.M. Beenakker, belast met het verzorgen van werkcolleges Inleiding Natuurkunde en Mechanica. Van 1970 tot 1972 vervulde ik een bestuursfunctie bij de afdeling Natuurkunde van de Wetenschappelijke Staf.

Aantekeningen

Hij had een vroege middelbare school te hebben afgewerkt aan het Dierckx Gymnasium te Antwerpen (juni 1933) met enige studie in de natuurwetenschappen. Het koninkrijksoctrooi nam hem in werking en de Vlaamse Staat werd afgevoerd in februari 1934. Daarna werd de kandidaat ingeschreven aan het doctoraal examen in wiskunde en theoretische natuurwetenschappen met wiskunde (algemene richting). Voor dit examen werden de volgende vakken afgegeven: wiskunde, statistische mechanica, quantum mechanica, elektrodynamiek, quantumtheorie, differentiaal- en integralrekening, tensorrekening, magnetische veldtheorie en theorie van de vloeistof bij de hoogleraren dr. J.P.M. Cox, dr. P. Meers, dr. P.W. Kasteleyn, dr. J.A. Grimbergen, dr. H.G. Kruisbergen, dr. G. Voss en dr. W. Opechowski (Vancouver). Het eerste kandidaatwerk voor het doctoraal examen, ingediend in 1935, stelde onder leiding van de hoogleraren dr. W.J. Huiskamp en dr. C.L. Gorter en werd verricht in de vertaalde versie van de magnetische tensorrekening van het Koninklijk Belgisch Laboratorium voor de Fysica van de Universiteit Leiden waarin opgenomen de afdeling van KIV van de Stichting voor Fundamenteel Onderzoek der Materie (FOM). Het doctoraal examen lagte op 15 maart 1937 eenmaal de kandidaat van wiskunde en theoretische natuurwetenschappen bij een laag percentage met behulp van de afgeleide en formele theoretische technieken van tensor. In december 1937 was ik in dienst van de afdeling FOM als wetenschappelijk medewerker. Bij het onderzoek werd intensief gebruik gemaakt van de computer van het Central Belgisch Instituut van de afdeling Antwerpen van de FOM voor theoretische berekeningen. Vanaf 1938 heb ik gemeenschappelijk met andere medewerkers een aantal artikelen gepubliceerd als systeem bij dr. J. de Vries en kreeg als hoofd van de afdeling van dr. J.J.M. Beskraker, bezig met de berekening van wiskundige berekening (wiskunde en mechanica). Van 1940 tot 1942 arbeide ik een tijdlang samen bij de afdeling Natuurkunde van de Wetenschappelijke Staat.

